

Universiteit
Leiden
The Netherlands

Shedding light on surface-assembled photosynthetic systems

Magis, J.G.

Citation
Magis, J. G. (2012, May 1). *Shedding light on surface-assembled photosynthetic systems*. *Casimir PhD Series*. Retrieved from https://hdl.handle.net/1887/18810

Version:	Corrected Publisher's Version
License:	Licence agreement concerning inclusion of doctoral thesis in the Institutional Repository of the University of Leiden
Downloaded from:	https://hdl.handle.net/1887/18810

Note: To cite this publication please use the final published version (if applicable).

Cover Page



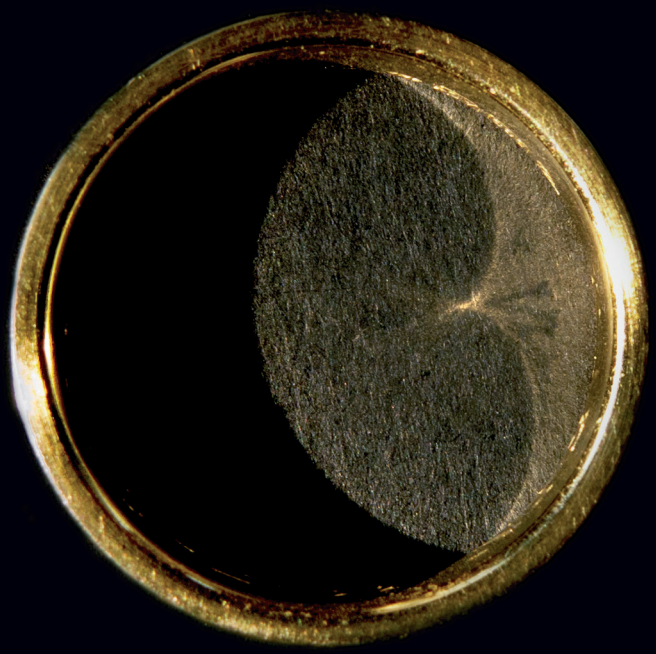
Universiteit Leiden



The handle http://hdl.handle.net/1887/18810 holds various files of this Leiden University dissertation.

Author: Magis, Johan Gerhard
Title: Shedding light on surface-assembled photosynthetic systems
Date: 2012-05-01

Shedding Light on Surface-Assembled Photosynthetic Systems



Gerhard Magis

Shedding light on surface-assembled photosynthetic systems

Proefschrift
ter verkrijging van
de graad van Doctor aan de Universiteit Leiden,
op gezag van Rector Magnificus prof.mr. P.F. van der Heijden,
volgens besluit van het College voor Promoties
te verdedigen op dinsdag 1 mei 2012
klokke 11:15 uur

door

Johan Gerhard Magis
geboren te Winterswijk
in 1978

Promotiecommissie:

Promotor:	Prof. Dr. T.J. Aartsma	Universiteit Leiden
Co-Promotor:	Dr. R.N. Frese	Vrije Universiteit, Amsterdam
Overige leden:	Prof. Dr. C.N. Hunter	University of Sheffield (UK)
	Dr. M.R. Jones	University of Bristol (UK)
	Prof. Dr. H.J.M. de Groot	Universiteit Leiden
	Dr. H.J. van Gorkom	Universiteit Leiden
	Prof. Dr. E.R. Eliel	Universiteit Leiden

ISBN 978-90-8593-112-6
Casimir PhD series, Delft-Leiden 2012-1

Voor Daniël,
Het stralende middelpunt van mijn universum.

Contents

Chapter 1. Introduction **7**
1.1 Photosynthesis 8
1.1.1 Bacterial photosynthesis 8
1.1.2 Light-harvesting complex 2 (LH2) from *Rhodobacter sphaeroides* 11
1.1.3 Light-harvesting complex 1 (LH1) from *Rhodobacter sphaeroides* 12
1.1.4 Reaction Center (RC) from *Rhodobacter sphaeroides* 13
1.1.5 Energy transfer, interactions and coupling between pigments 15
1.1.6 Bacteriochlorophyll vibronic states and the photoprotective role of carotenoids in light-harvesting complexes 16
1.1.7 Fluorescence quenching 18
1.2 Experimental techniques 18
1.2.1 Fluorescence spectroscopy 18
1.2.2 Confocal microscopy – resolution and excitation rate of photosynthetic complexes 21
1.2.3 Absorpton / emission in fluid 22
1.2.4 Photoelectrochemistry 23
1.2.5 Atomic Force Microscopy 24

Chapter 2. Light harvesting, energy transfer and electron cycling of a native photosynthetic membrane adsorbed onto a gold-surface **31**
2.1 Introduction 32
2.2 Materials and Methods 33
2.2.1 Biological membranes 33
2.2.2 RCLH1 membranes 34
2.2.3 Isolated photosynthetic complexes 34
2.2.4 Gold surface preparation 34
2.2.5 Protein immobilization for spectroscopy 35
2.2.6 Atomic Force Microscopy 35
2.2.7 Spectroscopy 35
2.2.8 Photostability measurements 36
2.2.9 Electrochemistry 36
2.3 Results and Discussioin 37
2.3.1 Adsorption of membranes onto a gold surface 37
2.3.2 Electron-transfers of photosynthetic membranes adsorbed onto a gold-electrode 39
2.3.3 Energy-transfer and photostability of photosynthetic membranes adsorbed onto a gold surface 42
2.3.4 Photostability of isolated light-harvesting complexes 46
2.3.5 The function of LH2 and LH1 within membranes 47
2.4 Conclusion 49

Chapter 3. Enhanced photocurrent generation by photosynthetic bacterial reaction centers through molecular relays, light-harvesting complexes and direct protein-gold interactions **53**
3.1 Introduction 54
3.2 Materials and Methods 58
3.2.1 Photosynthetic complexes 58
3.2.2 Adhesion protocol 59

3.2.3 Self-assembled monolayers 59
3.2.4 Experimental apparatus 59
3.3 Results 60
3.3.1 Characteristics of RCs adhered to a bare-gold electrode 60
3.3.2 Comparisons with photocurrent generation by RCs adhered to an electrode coated with a SAM 62
3.3.3 The mechanism of photocurrent generation 63
3.3.4 Comparison of photocurrent generation by pre-adhered RCs and RCs in solution 66
3.3.5 Photocurrent generation by RC-LH1 complexes 68
3.4 Discussion 72
3.4.1 Is it possible to dispense with a SAM for adherence of RCs to a gold electrode? 72
3.4.2 How do RCs and RC-LH1 complexes adhere to a bare-gold electrode? 73
3.4.3 Is it necessary to adhere RCs to the working electrode to achieve high photocurrents? 74
3.4.4 Microamp photocurrents obtained from RC-LH1 complexes adhered to a working electrode 77
3.5 Conclusions 75

Chapter 4. Use of engineered unique cysteine residues to facilitate oriented coupling of proteins directely to a gold substrate 83
4.1 Introduction 84
4.2 Materials and Methods 87
4.2.1 Site-directed mutagenesis 87
4.2.2 Preparation of samples 87
4.2.3 Preparation of surfaces 87
4.2.4 Protein immobilization 88
4.2.5 Spectroscopy of surface-immobilized proteins 89
4.2.6 Photostability assessment of immobilized proteins 90
4.2.7 Atomic Force Microscopy 90
4.3 Results and Discussion 90
4.4 Conclusion 97

Summary 101

Samenvatting 105

Curriculum Vitae 109

Nawoord 111

Chapter 1

Introduction

Photosynthetic pigment-protein complexes are highly optimized in terms of chromophore density and energy transfer efficiency and are therefore a paradigm for technological applications, for instance in bio-organic solar cells. The major challenges for such potential applications are firstly, the intrinsic instability of the proteins under ambient conditions and secondly the ability to obtain uniformly oriented and organized complexes.

In this thesis, the results are presented of room temperature fluorescence spectroscopy (fluorescence excitation and emission) and electrochemistry experiments on surface immobilized isolated photosynthetic complexes and photosynthetic membranes. The intrinsic chromophores of these complexes act as local molecular reporters of the integrity of the proteins, and allow us to address the functionality and energy transferring capabilities of proteins interfaced to solid supports.

In Chapter 2, native photosynthetic membranes are interfaced onto a gold surface. The results demonstrate that the membranes retain their optical activity and energy transforming capabilities. Furthermore, they are shown to be remarkably photostable even under ambient conditions, without oxygen scavengers, to light intensities well above that of direct solar irradiation. Illuminating native membranes adhered onto a gold-electrode show the highest photo-induced currents generated to date and demonstrate a remarkable durability. These findings present a major advancement, facilitating the characterization of supramolecular biological and artificial energy transducing mechanisms.

An electrochemistry study on photosynthetic bacterial reaction center (RC) and reaction center-light harvesting 1 (RCLH1) complexes deposited onto a bare gold-electrode is presented in Chapter 3. The results show that the capability for electron transfer reactions between RCs and electrode are retained despite the absence of a protective layer or engineered linker molecules to mediate between the surface and the tethered RCs.

In Chapter 4 the stability and functionality of isolated light-harvesting complex 1 and 2 immobilized on various surfaces is assessed. Two different approaches are used to assemble the complexes on a surface. A self assembled monolayer (SAM) creates a surface with defined chemistry on a substrate, in this case gold, which facilitates the immobilization of the protein in a specific orientation. The second approach uses direct

assembly of a genetically engineered protein that has surface exposed cysteine residues to enable direct covalent binding to a gold surface.

The data shows that light-harvesting complexes can be immobilized directly on a gold surface and on various SAM surfaces whilst still retaining their full optical functionality. All energy transferring reactions still take place and are similar to those observed for the detergent solubilized proteins. Furthermore it is shown that LH1 exhibits a remarkable photostability, even under ambient conditions. These findings demonstrate the possibility of interfacing a fully functional energy transferring protein complex to a conducting substrate in the presence of oxygen.

In section 1.1 of this introduction, an overview is provided of the major constituents in bacterial photosynthesis, regarding their structural and functional signatures. In section 1.2, the experimental techniques are presented that have been employed in this research.

1.1 Photosynthesis

Nearly all life on earth depends on photosynthesis, the conversion of solar energy into chemical energy. The process starts with the capture of light by chromophores that are held in precise arrangements by the protein skeleton that surrounds them. This captured energy is transferred very rapidly to the reaction center (RC) and results in a photon-induced charge separation and charge stabilization (Blankenship, 2002).

The process of photosynthesis can be performed by higher plants, phytoplankton, algae and photosynthetic bacteria. The latter (figure 1) have the most simple organization of their photosynthetic apparatus and can therefore be considered a model system for photosynthesis. Extensive studies over the past decades of the bacterial photosynthetic unit and the consituent proteins have provided a wealth of information and insight in the underlying processes of energy capture, energy transfer and the general organization of the photosynthetic membrane (Bahatyrova et al., 2004a;Cogdell et al., 1996;Cogdell et al., 2006;Papiz et al., 1996;van Grondelle and Novoderezhkin, 2006).

1.1.1 Bacterial photosynthesis

The photosynthetic machinery of bacteria is embedded in specialized parts of the cytoplasmic membrane and consists, for most purple bacteria, of two distinct light-harvesting antenna complexes (LH1 and LH2) and a reaction center (RC). The RC is surrounded by the LH1 complex and the LH2 complexes are arranged around the RC-LH1

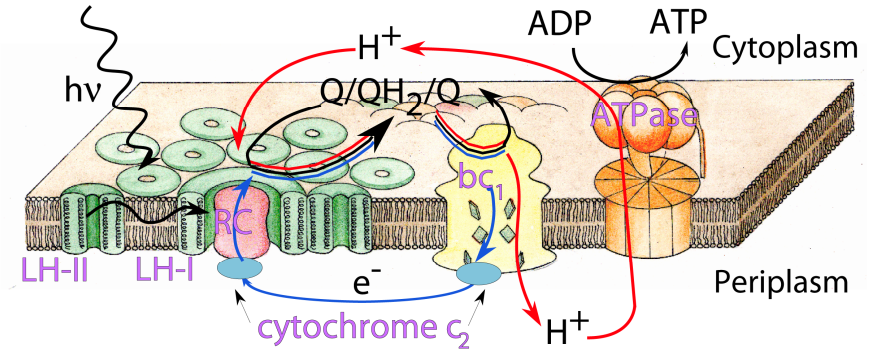


Figure 1. A schematic representation of the photosynthetic membrane of purple bacteria. The redox reactions in the RC (electron transfer through the complex) produce a proton gradient across the membrane that drives the synthesis of ATP from ADP by ATPase. Charge transfer in the RC is discussed in more detail in section 1.1.4 of this introduction. The picture was reproduced, with permission, from Hu et al (Hu et al., 2002).

core complex (Bahatyrova et al., 2004a;Cogdell et al., 1996;Cogdell et al., 2006;Frese et al., 2004;Hu et al., 1998;Jungas et al., 1999;Miller, 1982;Papiz et al., 1996;Roszak et al., 2003;Siebert et al., 2004;Sundstrom et al., 1999). The reaction center (RC) is the terminal acceptor of excited-state energy delivered by the surrounding light-harvesting complexes in the photosynthetic membrane. The RC also has intrinsic light-absorbing pigments and can absorb photons by itself. However, exposed to direct sunlight this only results in a photon absorption every 0.1 - 10 seconds (Borisov and Godik, 1973) which is well below the RC turnover time (1 millisecond). The purpose of the antenna is therefore to increase the energy collection efficiency under low light intensities by harvesting incoming sunlight and transferring this energy to the reaction centers (Papiz et al., 1996), thereby optimizing the rate of photosynthetic energy conversion in the RC. This is achieved by the close contact and the inter-complex energy gradient between adjacent LH2/RCLH1 complexes, facilitating the rapid and efficient transfer of excitation energy towards the RC (Bahatyrova et al., 2004a;Hess et al., 1995;Nagarajan and Parson, 1997;Sundstrom et al., 1986;Visscher et al., 1989;Zhang et al., 1992). The ultimate result is the conversion of sunlight into chemical energy in the form of ATP (adenosine triphosphate) (Blankenship, 2002).

The bacterial photosynthetic species that was chosen for the research presented in this thesis is *Rhodobacter sphaeroides*. There are several reasons for this. First of all, the availability of structural models of the constituent protein complexes (Allen et al., 1987a;Allen et al., 1987b;Qian et al., 2005;Qian et al., 2008;Walz et al., 1998). Secondly,

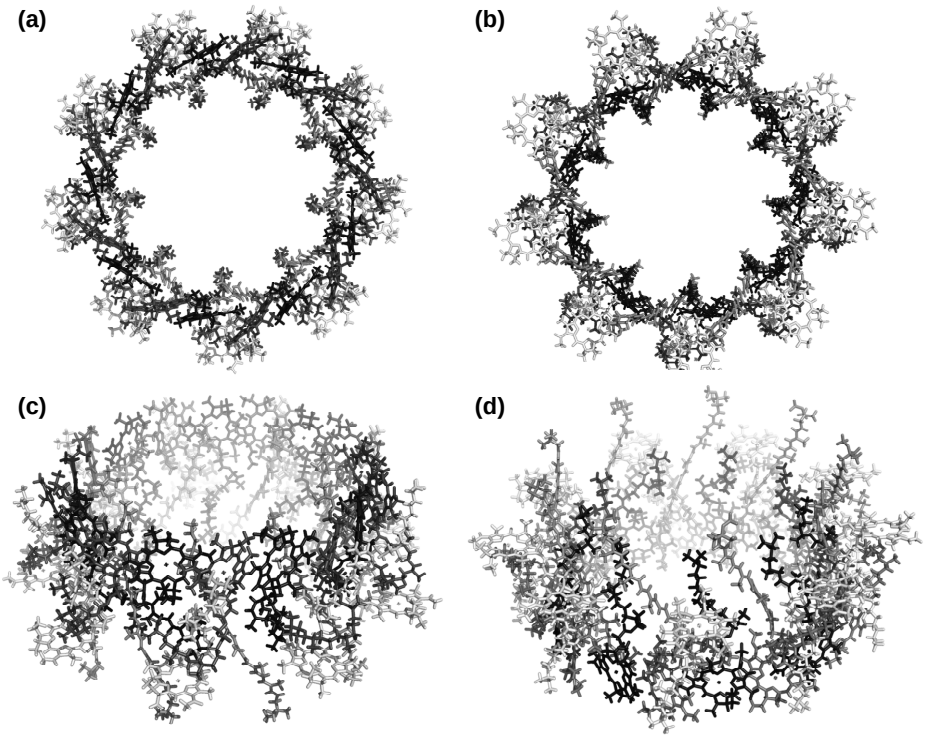


Figure 2. Structure and organization of the pigments in LH2.
Color code: B800 BChls are black, B850 BChls are in light-grey, and the carotenoids are in dark-grey.
(A) view from the periplasmic side of the photosynthetic membrane. The relative orientation of the 18 B850 pigments can be clearly seen. They have their molecular planes perpendicular to the membrane and are organized like the blades on a turbine.
(B) view from the cytoplasmic side of the membrane, showing the 9 B800 pigments that have their molecular planes perpendicular to the symmetry axis of the protein (along the direction of the membrane).
(C) side view of the complex with the B850 ring on top.
(D) side view of the complex with the B800 ring on top. The model of LH2 from *Rhodobacter sphaeroides* was kindly provided by Klaus Schulten. Great thanks to John Olsen for producing the figures.

functional and organizational information is available since this species has been studied extensively in the past (Bahatyrova et al., 2004a;Bradforth et al., 1995;Clayton and Clayton, 1981;Hess et al., 1993;Jimenez et al., 1996;Jungas et al., 1999;Straley et al., 1973). But most important for this research is the fact that it is one of the few species that has a well developed mutagenesis system with well characterized deletion strains (Jones et al., 1992). This allows for the expression of membranes with varying composition (LH2-only, LH1-only, LH1RC-only, and native membranes). Mutations in the carotenoid biosynthetic pathway allow the expression of the LH complexes incorporating different carotenoids, e.g. neurosporene instead of spheroidene. Moreover, specific residues can be

changed with site-directed mutagenesis, creating surface exposed cysteines that allow for the covalent linking of the protein in a specific orientation on a surface (Escalante et al., 2008).

1.1.2 Light-harvesting complex 2 (LH2) from *Rhodobacter sphaeroides*

The LH2 complex has a nine-fold cyclic repetition of a subunit (Walz et al., 1998) that consists of two transmembrane polypeptides (α and β), three bacteriochlorophyll-*a* (BChl-*a*) molecules and one or two carotenoids (Kramer et al., 1984). The structure is likely to be very similar to the homologous LH2 complex from *Rhodopseudomonas acidophila* for which the crystal structure was first resolved by Cogdell and co-workers (McDermott et al., 1995).

The organization of LH2 results in a cylindrical assembly of 6 nm diameter and 5 nm high. The pigments that are used for absorbing sunlight are the BChl's which absorb mainly in the near-infrared. In addition the carotenoids absorb light in the green part of the spectrum (around 500 nm), hereby increasing the total cross-section for solar light capture of the complex. Besides their role in light harvesting, the carotenoids also have an important photoprotective function, which will be discussed in more detail in a subsequent paragraph, and they significantly contribute to the structural assembly and integrity of the LH2 complex (Prince et al., 1997).

The transmembrane pigment-protein complex is inserted in the photosynthetic membrane with the N-termini of the polypeptides exposed on the cytoplasmic face of the membrane and the C-termini on the periplasmic side of the membrane. Each subunit contains 3 BChl-*a* molecules of which one is ligated by the N-terminal methionine on the α-polypeptide and the other two are ligated by totally conserved histidine residues on both α and β polypeptides near the C-termini of both. The circular repetition of subunits in this nonamer results in two concentric rings of pigments along the normal of the membrane that are approximately 2 nm apart, see figure 2.

The absorption wavelength of the bacteriochlorophylls depends on pigment-pigment and pigment-protein interactions and is therefore sensitive to local changes in the surrounding protein matrix (Gall et al., 1997). In the case of LH2, the two rings of 9 BChls at the cytoplasmic side and 18 BChls near the periplasmic side of the protein complex have a characteristic near-infrared absorption of 800 nm and 850 nm respectively, and are therefore often referred to as the B800 and the B850 ring. The BChl's in the B800-ring have little interaction and the excitation energy here is localized on one or two pigments

(van Oijen et al., 1999). In the B850-ring, however, the 18 BChl's are closely coupled and as a result an excitation is delocalized over the entire B850-ring (Ketelaars et al., 2001;Pullerits et al., 1996). The light absorbed by the B800 ring is rapidly transferred to the B850 ring within 650 femtoseconds at room temperature (Hess et al., 1993;Monshouwer et al., 1995;Reddy et al., 1991;Shreve et al., 1991). Energy transfer between the B850 pigments occurs on an even faster timescale (Jimenez et al., 1996). Subsequently, light-energy absorbed by LH2 is transferred within approximately 3 picoseconds to a neighboring LH1 (Hess et al., 1995;Nagarajan and Parson, 1997;Zhang et al., 1992), which is well within the excited-state lifetime of 1 nanosecond (Monshouwer et al., 1997;Sundstrom et al., 1999).

1.1.3 Light-harvesting complex 1 (LH1) from *Rhodobacter sphaeroides*[1]

The LH1 protein of many purple bacteria is a cylindrical assembly of 12 nm diameter and 7 nm high consisting of 16 identical subunits (Qian et al., 2003). Each unit contains two transmembrane polypeptides (α and β) that bind two bacteriochlorophyll-*a* molecules and one or two carotenoids. In the photosynthetic membrane the N- and C-termini of the polypeptides face the cytoplasmic and the periplasmic side of the membrane, respectively. The two BChl's in each subunit are positioned near the C-terminus of both the alpha- and beta-polypeptide. The assembly of this pigment-protein complex results in a ring of 32 chlorophylls at the periplasmic side of the protein, which is often referred to as the B875 ring due to its characteristic near-infrared absorption around 875 nm. These pigments are strongly coupled which results in a delocalization of the excitation energy (Ketelaars et al., 2002;van Amerongen et al., 2000;van Grondelle et al., 1994). The B875-ring in LH1 and the B850-ring in LH2 are positioned in the same plane in the photosynthetic membrane, facilitating rapid energy transfer between adjacent LH2 and LH1 complexes (Jimenez et al., 1996;Monshouwer et al., 1995;Reddy et al., 1991). Ultimately, this energy is transferred from LH1 to the RC within 20-50 picoseconds (Sundstrom et al., 1986;Visscher et al., 1989).

In *Rb. sphaeroides* LH1 (figure 3) and the RC associate together with the small protein PufX, to form the core complex. Recently it has been established that the core complex of *Rb. sphaeroides* is not a closed ring structure but actually a double arc joining two RCs in a dimeric super-complex (Bahatyrova et al., 2004a;Jungas et al., 1999;Qian et al., 2005;Qian et al., 2008;Siebert et al., 2004).

[1] Even before the structure of LH2 was resolved (McDermott et al., 1995) it was revealed by Gosh et al that LH1 has a ring structure (Karrasch et al., 1995). Although the three dimensional structure of LH1 has not yet been solved with high resolution, atomic force microscopy and electron microscopy experiments (Bahatyrova et al., 2004b;Walz et al., 1998) have confirmed the ringlike structure of LH1.

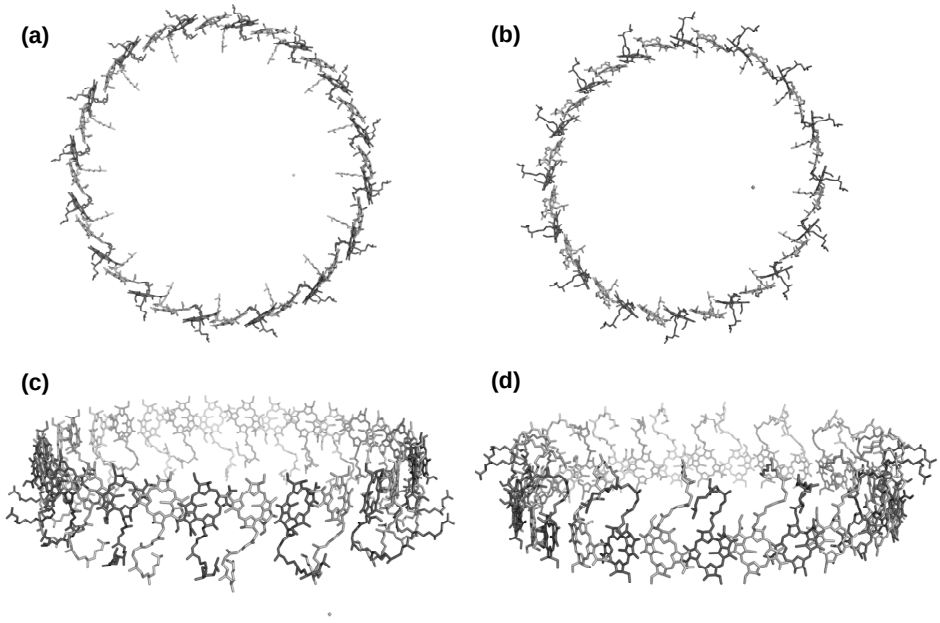


Figure 3. Structure and organization of the pigments in LH1.
The BChls ligated to the alpha and beta polypeptide are respectively light- and dark-grey. The model of LH1 from *Rhodobacter Sphaeroides* is used from Ansgar Phillipsen. Great thanks to John Olsen for producing the figures.
(A) view from the periplasmic side of the photosynthetic membrane. The relative orientation of the 32 pigments can be clearly seen. They have their molecular planes perpendicular to the membrane and are organized like the blades on a turbine.
(B) view from the cytoplasmic side of the membrane.
(C,D) side views of the complex.

1.1.4 Reaction Center (RC) from *Rhodobacter sphaeroides*

The RC was the first transmembrane protein complex for which the crystal structure was solved (Deisenhofer et al., 1984;Deisenhofer et al., 1985). For this accomplishment Deisenhofer, Huber and Michel were awarded the Nobel prize in chemistry in 1988. The structure of the RC from *Rhodobacter sphaeroides* was solved in 1986 (Allen et al., 1986). It consists of 3 subunits (L, M, H). The bulk of the H subunit is on the cytoplasmic side of the membrane, with a single membrane spanning helix. The L and M subunits each consist of 5 transmembrane polypeptides and both are confined to the membrane. They accommodate four bacteriochlorophyll-*a* (BChl-*a*) molecules, two bacteriopheophytin-*a* (BPh) molecules, one carotenoid, one tightly bound quinone (Q_A), one exchangeable quinone (Q_B) and an iron atom (Allen et al., 1987a;Allen et al., 1987b;Walz et al., 1998).

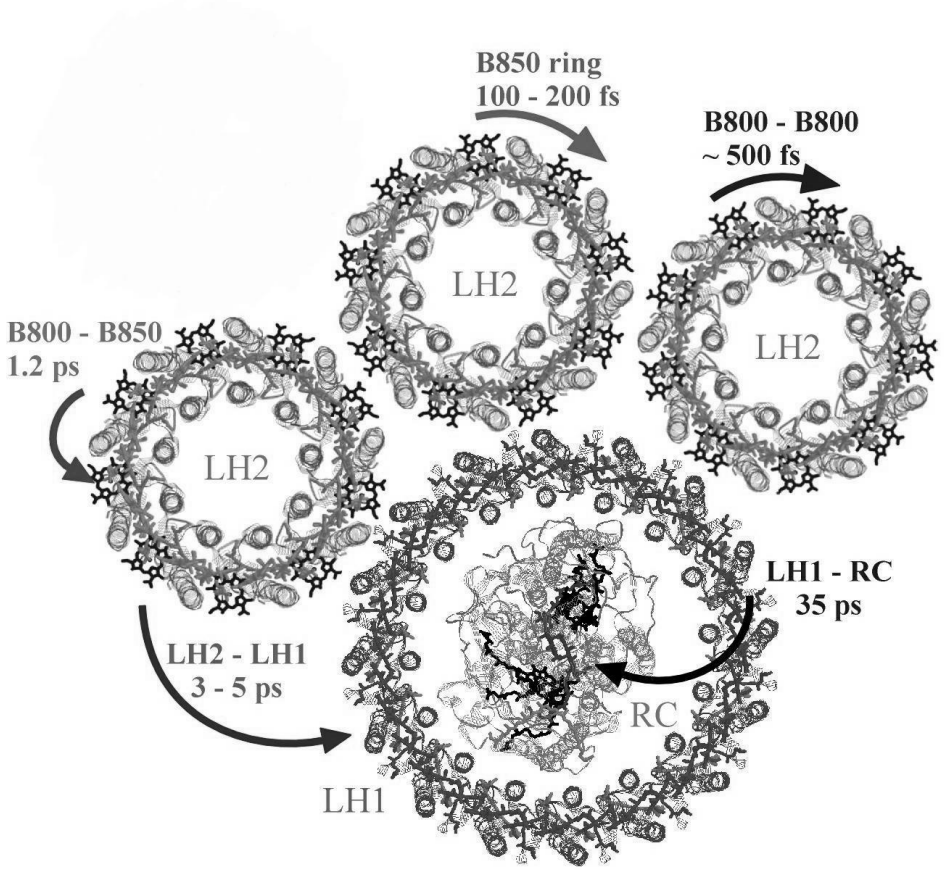


Figure 4. Schematic representation of the components in the bacterial photosynthetic unit and the energy transfer times involved. This figure was kindly provided by Rienk van Grondelle and Bruno Robert.

The primary electron transfer step is triggered when excitations reach the special pair P, which is a strongly coupled dimer of BChl's located near the periplasmic side of the RC, and an electron is ejected. Electron transfer subsequently takes place along the L subunit via a monomeric BChl (B_A) and a BPh (H_A) to the tightly bound quinone (Q_A). The electron is then transferred to the exchangeable quinone (Q_B) and the oxidized special pair, P^+, is reduced by a soluble cytochrome c_2 in the periplasmic space. After the special pair has turned over a second time and the second electron is transferred to Q_B, QH_2 is formed (Blankenship, 2002).

In vivo, the electrons return from the reduced quinones to the oxidized cytochrome c_2 via a separate protein, the cytochrome bc_1 complex. This is coupled to a translocation of protons

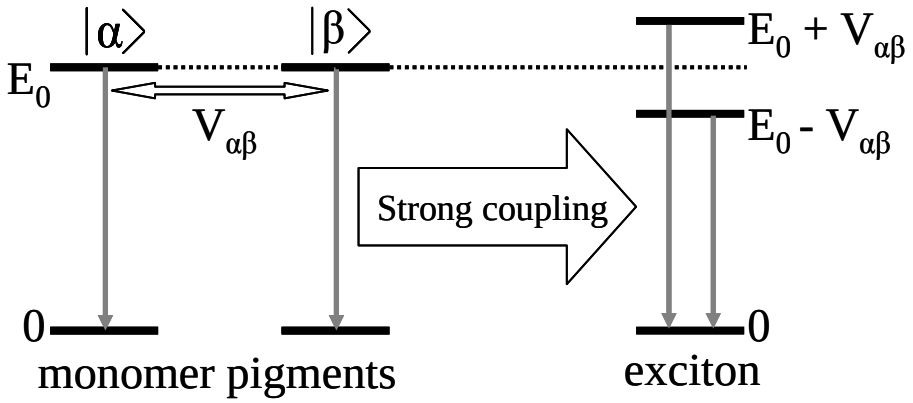


Figure 5. In weakly interacting pigments (alpha and beta), the excited states are localized on the individual molecules (left). Strong coupling between the two pigments results in an effective dimer on which the excitation is delocalized (right).

from the cytoplasmic to the periplasmic side of the membrane, which provides the driving force for ATP synthesis (figure 1). In the measurements described in this thesis, the light-induced electron transfer from cyt c_2 to quinone by RCs is used to generate a current between two electrodes.

1.1.5 Energy transfer, interactions and coupling between pigments

The excitation energy of a pigment (often referred to as site energy, E_0) depends on the local protein environment of the binding sites (e.g. specific hydrogen bonds between pigment and protein, relative orientation of the pigments, electrostatic interactions). As a result, any deformation of the protein or induced structural disorder has an effect on the intermolecular interactions and hence on the excitation energy of the pigments (often referred to as off-diagonal disorder). The amount of variation in site energies is reflected in the broadening of the absorption band.
In addition, the pigments themselves also interact electronically via Coulombic and exchange interactions. The former is the result of interactions between nuclei and electrons from one molecule with another (dipolar interaction), and the latter is due to overlapping molecular orbitals of neighboring pigments.

In the case of weak dipole-dipole interactions (as compared to the variation in site energies of the individual pigments), the excited states are mainly localized on each individual pigment (see left of figure 5). This situation is referred to as the weak coupling limit. In the case of strong coupling, the interactions are much larger then variations in site energies. This gives rise to the formation of a Frenkel-excition, where the excited state of the

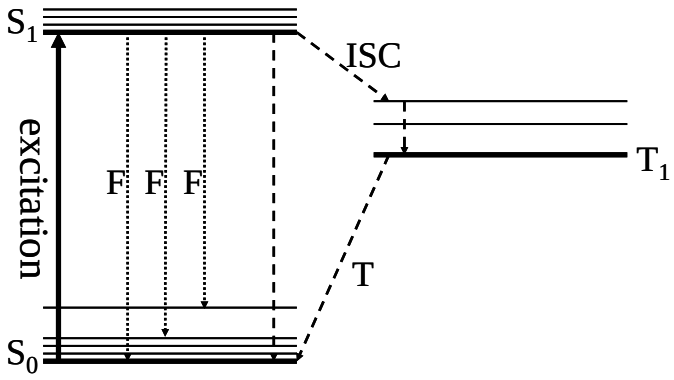


Figure 6. Jablonski diagram of a chlorophyll molecule. S_0, S_1 and T_1 denote respectively the ground state, singlet excited state and triplet state (thick lines). The thin lines indicate the vibronic states associated with each energy level. After excitation, the molecule is promoted from its ground state to its singlet excited state. The dotted lines indicate fluorescence (F), the dashed lines indicate non-radiative decay channels such as internal conversion and intersystem-crossing (ISC).

interacting pigments is a superposition of the individual states having two energy levels (Hu et al., 2002;van Amerongen et al., 2000;van Grondelle et al., 1994). How much oscillator strength (the quantity describing the strength of coupling between an electronic transition and radiation) each level gets depends on the orientation of the transition dipole moments of the pigments and hence on the degree of symmetry in the ring of pigments.

1.1.6 Bacteriochlorophyll vibronic states and the photoprotective role of carotenoids in light-harvesting complexes

After the initial capture of light the BChl is promoted from its ground state to the first excited state (^{1}BChl + hν → ^{1}BChl*). The ultimate goal is to direct the absorbed energy via a series of intra- and inter-complex energy transfer steps to the reaction center. However, this excitation energy can be lost either due to a process of non-radiative decay from the excited state to the ground state, or relaxation to the ground state whereby the energy is emitted in the form of a photon (^{1}BChl* → ^{1}BChl + hν). There is also a chance that a triplet BChl is formed (^{1}BChl* → ^{3}BChl*) via intersystem-crossing (ISC), which has a relatively long lifetime of tens of microseconds (figure 6). Although this transition is spin-forbidden, it can be induced by, e.g., spin-orbit coupling. The rate of ISC can vary from one molecule to another, but for BChl it is in the range of 0.2-0.3.

The BChl triplet is capable of interacting with oxygen (which is a triplet in its ground state) thereby generating singlet oxygen (^{3}BChl* + $^3O_2$ → ^{1}BChl + $^1O_2$*), a very reactive species that can damage biological molecules. Therefore, (single molecule) studies on LH

Bacteriochlorophyll:

$^1BChl + h\nu \rightarrow {}^1BChl^* \rightarrow ET$	intra- and intercomplex energy transfer (ET)
$\rightarrow {}^1BChl + h\nu$	fluorescence
$\rightarrow {}^3BChl^*$	triplet formation

Carotenoid:

$^1Car + h\nu \rightarrow {}^1Car^*$	absorption
$^1Car^* \rightarrow {}^1Car + h\nu$	fluorescence
$^1Car^* + {}^1BChl \rightarrow {}^1Car + {}^1BChl^*$	excitation transfer (singlet – singlet)

Singlet-oxygen formation:

$^3BChl^* + {}^3O_2 \rightarrow {}^1BChl + {}^1O_2^*$

BChl triplet quenching (triplet – triplet exchange):

$^3BChl^* + {}^1Car \rightarrow {}^1BChl + {}^3Car^* \rightarrow {}^1BChl + {}^1Car + heat$

Singlet oxygen scavenging:

$^1O_2^* + {}^1Car \rightarrow {}^3O_2 + {}^3Car^* \rightarrow {}^3O_2 + {}^1Car + heat$

Figure 7. Summary of energy pathways in photosynthetic light-harvesting complexes.

complexes are generally performed in the presence of oxygen scavengers to increase the time period a molecule can be studied. Without the presence of oxygen scavengers, photobleaching limits the observation of such single molecules to a few seconds at room temperature.

The carotenoid pigments have three major functions in photosynthesis. First of all, they contribute significantly to the structural assembly and integrity of the LH complexes (Prince et al., 1997). Secondly, they absorb light in the green part of the spectrum ($^1Car + h\nu \rightarrow {}^1Car^*$) and transfer the excitation energy to the BChl pigments ($^1Car^* + {}^1BChl \rightarrow {}^1Car + {}^1BChl^*$), thus increasing the total absorption cross-section for light of the complex. However, in the context of excitation energy transfer between BChls the main function of the carotenoid pigments is to protect the BChl's from photo-oxidation. This is achieved by preventing the formation of singlet oxygen species through quenching of its precursor, the triplet BChl via triplet-triplet exchange ($^3BChl^* + {}^1Car \rightarrow {}^1BChl + {}^3Car^* \rightarrow {}^1BChl + {}^1Car$), or by direct quenching of singlet oxygen ($^1O_2^* + {}^1Car \rightarrow {}^3O_2 + {}^3Car^* \rightarrow {}^3O_2 + {}^1Car$) (Borland et al., 1989;Cogdell et al., 1981;Cogdell et al., 2000;Cogdell and Frank, 1987;Limantara et al., 1998).

The triplet-triplet exchange reduces the lifetime of the BChl triplet state from 70 microseconds to 20 nanoseconds and significantly diminishes the probability of triplet BChl to react with singlet oxygen, which occurs on a timescale of tens of microseconds (Monger et al., 1976). Since the carotenoid triplet energy is lower than that of singlet oxygen, the carotenoid triplet cannot sensitize singlet oxygen by itself and ultimately decays to the ground state within 2 – 8 microseconds (Monger et al., 1976).

1.1.7 Fluorescence quenching

Fluorescence quenching is the general term to describe a decrease in fluorescence emission. There are several non-radiative decay channels for excited state energy of the bacteriochlorophylls that are responsible for this: intercomplex energy transfer, internal conversion (where energy is converted to heat), intersystem crossing (creating triplet states), photochemistry (photo-oxidized chlorophyll acts as an excitation trap) (Bopp et al., 1997;Liu et al., 2006), annihilation (dipolar interaction between nearby excited chlorophylls can cause one or both to return to the ground state non-radiatively) (van Grondelle, 1986), and finally singlet-triplet interactions (carotenoid triplet states are efficient traps for singlet excited chlorophyll)(Bradforth et al., 1995;Cogdell, 1985;Jimenez et al., 1996;Monger et al., 1976;Monger and Parson, 1977).

Since all of these mechanisms can reduce the fluorescence signal emitted from light-harvesting complexes, it is difficult to ascertain to what extent each one of them is responsible for an observed decrease in fluorescence emission.

1.2 Experimental techniques

In order to determine the functionality and photostability of surface immobilized pigment-protein complexes and membranes, the following experimental techniques are employed: fluorescence spectroscopy (light-absorption and energy transfer on a surface), light-induced electrochemistry (absorption and electron transfer on a surface), atomic force microscopy (to determine the distribution of complexes on the surface under investigation), and finally the absorption and emission of the detergent solubilized photosynthetic complexes (as a standard for the intrinsic photostability and functionality of the isolated complexes and membranes). These techniques will be described in more detail in the following sections.

1.2.1 Fluorescence spectroscopy

Both fluorescence emission and fluorescence excitation (fluorescence detected absorption) experiments on surface immobilized proteins were performed at room temperature using

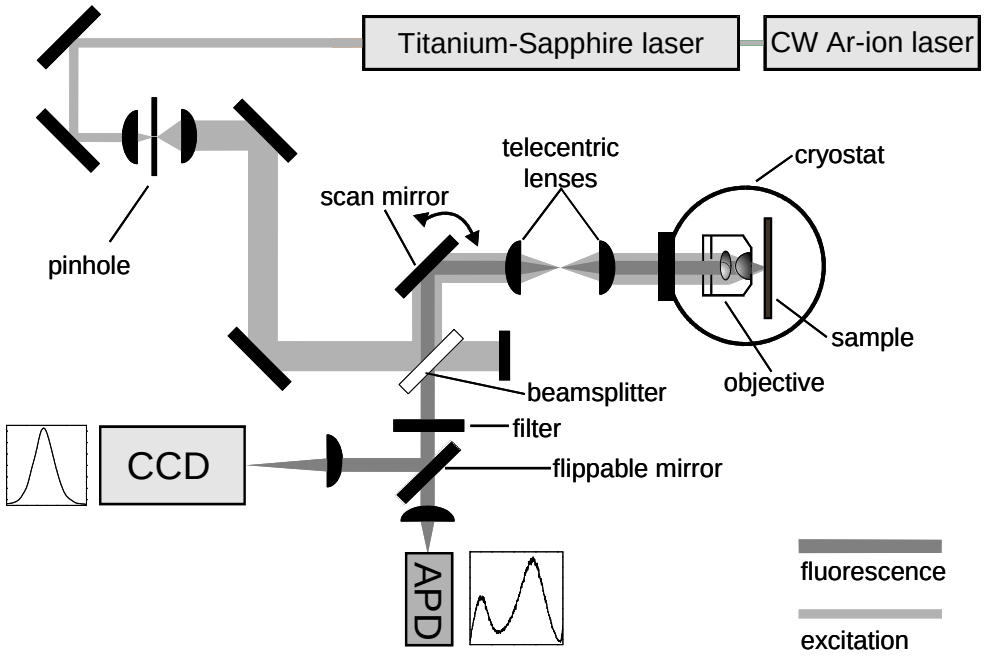


Figure 8. Schematic representation of the home-built confocal microscope setup used for fluorescence spectroscopy experiments on surface immobilized proteins.

the setup as schematically depicted in figure 8. The sample is mounted inside a cryostat, allowing these measurements also to be conducted in an oxygen free environment, by pumping the cryostat to vacuum. The sample is excited with a continuous-wave titanium sapphire (TiSa) laser (Spectra Physics 3900S), the wavelength of which can be tuned.

To assess the sample coverage, a scan mirror in conjunction with 2 telecentric lenses is incorporated in the setup, which allows movement of the focus laterally without losing the alignment with the confocal aperture. Homogeneity of the sample distribution on the surface was then checked by confocally scanning the laser over a wide-range (hundreds of micrometers) at a fixed wavelength (870 nm for LH1, 800 or 850 nm for LH2) and monitoring the fluorescence signal using an avalanche photodiode (APD, Perkin-Elmer SPCM-AQR-16).

Fluorescence emission spectra were recorded by exciting the sample at 800 nm. The fluorescence emission is then directed via a series of longpass filters with a transmission between 815 and 1015 nm (Hugo Anders, Germany), towards a blazed grating (Richardson Gratings) that disperses the collimated fluorescence. A lens is finally used to project the

dispersed beam onto a liquid-nitrogen-cooled CCD camera (Roper Scientific, USA). The excitation intensity used to record an emission spectrum was approximately 200 W cm^{-2}. Integration times were typically 60 seconds. The recorded spectra were all corrected for the sensitivity of the CCD camera.

Fluorescence excitation spectra were recorded in vacuum at room temperature. Appropriate bandpass filters were used to transmit the emission signal but remove most of the scatter and stray light (residual excitation light passing through the detection-filters). These filters are essential in order to be able to measure emission fluorescence in the presence of high back scattering from a reflective surface such as gold. A series of 3 identical interference bandpass filters were employed in the detection path; for LH1 and membranes a set with a transmission between 905 and 940 nm was utilised, and for LH2 a second set with a transmission between 875 and 910 nm. This scheme allows the detection of the red-most part of the fluorescence for both LH1 and LH2.
Fluorescence-excitation-spectra were then recorded by tuning the wavelength of the laser from 790 nm (lower limit of the laser) to either 870 or 900 nm, depending on which filter-set is used. The fluorescence was detected with the APD. In all cases linearly polarized light was used. The polarization dependence of the spectra can be investigated by rotating the polarization by means of a ½λ plate in conjunction with a linear polarizer in steps of 3.6° after each scan. The excitation spectra presented are the average of 100 consecutive spectra (during which the polarization changed by 360°). The total time of illumination was approximately 120 minutes. All fluorescence excitation spectra were corrected for both the sensitivity of the APD and the wavelength dependence of the excitation-energy.

To study the photostability of light-harvesting assemblies on a surface, we employ the scheme for fluorescence emission spectroscopy as outlined above but with the replacement of the long-pass filters for emission detection by a series of 3 identical interference bandpass filters (transmission between 875 and 910 nm for LH2, transmission between 905 and 940 nm for LH1). This limits the detection of the emission to the red-most part of the fluorescence. The main advantage of this scheme is that we can now excite at higher wavelengths where the LH complexes have more absorption. For all photostability measurements, the sample was illuminated with the same intensity: 75 W cm^{-2} at a wavelength of 870 nm for measurements on LH1, and 20 W cm^{-2} at 800 nm for measurements on LH2. The detected fluorescence signal was integrated for 60 seconds to improve the signal-to-noise ratio.

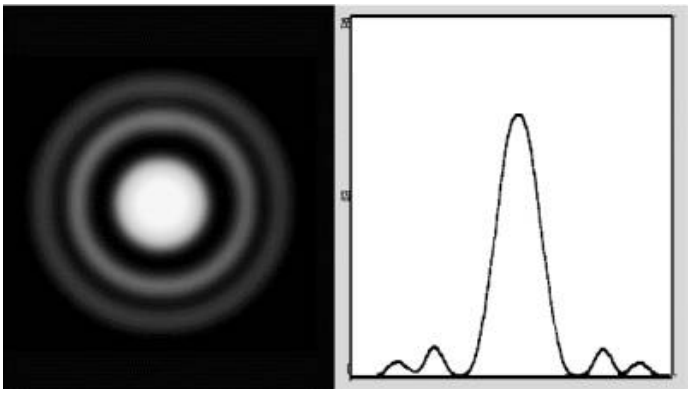


Figure 9. Diffraction pattern for a circular aperture (left) and cross-section (right)

1.2.2 Confocal microscopy – resolution and excitation rate of photosynthetic complexes

For an ideal microscope objective, the intensity profile in the focal plane has the shape of an Airy disk (Lauterborn et al., 1995). The full width at half maximum (FWHM) of this disk is determined by the numerical aperture (NA) of the microscope objective and the wavelength (λ) of the incident light. The FWHM of the Airy disk defines the spatial resolution (r) of the microscope, as derived from Fraunhofer diffraction of a circular aperture, and is equal to: $r = 0.61 \times \lambda / N.A.$

Our microscope objective has an N.A. of 0.9 (Microthek GmbH, Germany). In our experiments we typically employ wavelengths of 800, 850 and 875 nm. Values for the resolution, diameter and area of the diffraction limited spot are given in table 1.

λ [nm]	r [nm]	Diameter [μm]	Area [μm^2]
800	542	1.08	0.92
850	576	1.15	1.04
875	593	1.19	1.10

Table 1. The resolution (r), laser spot diameter and spot area with respect to the wavelength used.

Since the fluorescence experiments are conducted on surface immobilized isolated LH complexes and photosynthetic membranes, the number of light-harvesting complexes within the confocal volume of our laser is limited. In the case of a densely packed surface, we are restricted to a maximum of 32000 LH2 or 8000 LH1 complexes within the focal spot. However, the typical sample coverage in our experiments is much less and results in approximately 500 LH complexes within the focal spot of the laser.

The excitation rate (R), or number of photons absorbed per complex per second, depends on the photon density incident on the sample and the absorption cross-section of the complex for a given wavelength (σ): $R(\lambda) = \sigma(\lambda) \times$ photon density.
The photon density can be calculated by measuring the laser power incident on the sample and using the fact that 84% of all the light-intensity in the Airy-profile is located in the center spot. In our experiments the laser power ranges from 0.2 μW to 7 mW.
The absorption cross-section (σ) can be determined with the following formula: $\sigma(\lambda) = 2303 \times \varepsilon(\lambda) \times N_a^{-1}$, where Na is Avogadro's number and ε the extinction coefficient of the complex.

The absorption cross-sections can be calculated using the following values reported by Clayton (Clayton and Clayton, 1981) for the BChl extinction coefficients: 213, 184, and 126 per millimol BChl per cm for BChl-800, BChl-850, and BChl-875 respectively. The absorption cross-sections for the RC are calculated using the values reported by Straley et al. (Straley et al., 1973) for the RC molar extinction coefficient: $\varepsilon(802) = 2.88 \times 10^5\ M^{-1}\ cm^{-1}$ and $\varepsilon(865) = 1.28 \times 10^5\ M^{-1}\ cm^{-1}$.

This results in the following absorption cross-sections for LH2, LH1 and the RC:
LH2: $\sigma(800) = 7.33 \times 10^{-15}\ cm^2$, and $\sigma(850) = 1.27 \times 10^{-14}\ cm^2$.
LH1: $\sigma(875) = 1.54 \times 10^{-14}\ cm^2$.
RC: $\sigma(802) = 1.27 \times 10^{-15}\ cm^2$, and $\sigma(865) = 4.90 \times 10^{-16}\ cm^2$.

The absorption rates for a typical illumination intensity of 150 W cm^{-2} are listed in table 2.

λ [nm]	R (LH1)	R (LH2)	R (RC)
800		$6.5 \times 10^6\ s^{-1}$	$1.0 \times 10^6\ s^{-1}$
850		$7.5 \times 10^6\ s^{-1}$	
875	$4.9 \times 10^6\ s^{-1}$		$1.6 \times 10^5\ s^{-1}$

Table 2. Number of photons absorbed per second per complex for a typical illumination intensity of 150 W cm^{-2}.

1.2.3 Absorption / emission in fluid

In order to interpret the fluorescence experiments on surface immobilized photosynthetic assemblies, it is necessary to have a control value to which all data can be related. The most native and least harmful measurement environment for the photosynthetic components is a buffer solution. To assess the photophysical properties (absorption and emission spectroscopy) of detergent solubilized complexes and chromatophores in suspension, a home-built setup was used integrating a spectrophotometer (Ocean Optics,

QE6500), a halogen-lamp as light source, a sample cuvet (open to air) and appropriate filters. Long-term illumination (and excitation) with white light (400 – 1000 nm) was conducted through a 10 cm water-filter to minimize heating. For both types of measurement, the power of white-light illumination was 20 mW at the illumination window of the cuvet. The samples were continuously illuminated until no further reduction in absorption or emission was observed. For the fluorescence emission experiments, a cut-off filter transparent between 700 and 1000 nm was employed in the detection path, in conjunction with a filter transparent between 400 and 700 nm in the excitation path.

1.2.4 Photoelectrochemistry

Photon-induced electron transfer from bacterial reaction centers can be characterized with electrochemistry experiments. The experimental setup consisted of a standard three-electrode configuration, comprising a working electrode (gold disk from BAS, with an area of 3.14 mm^2) on which the photosynthetic assemblies are deposited, a counter electrode (platinum wire) to measure the current and a reference electrode (standard calomel electrode ; SCE) with fixed potential relative to which the potential is set. The potential applied to the working electrode is controlled by a commercial potentiostat (CHI-instruments).

The electrodes are inserted in a home-built electrochemical cell containing inlets for the electrodes, an illumination window and inlets and outlets for argon gas. The working electrode is inserted from the top, the incident light enters from the bottom. The reference and counter electrode are at an angle of ~40 degrees with the working electrode. The distance between the working electrode and the reference electrode is 3 mm. Two stainless steel tubes provide an argon inlet and outlet, which makes it possible to exclude oxygen from the measurement chamber.

Samples can be illuminated with Light Emitting Diodes (LEDS) with broad band excitation of approximately 50 nm FWHM, the output of a white-light illuminated monochromator, or with an Argon pumped titanium-sapphire (TiSa) laser (Coherent). Illumination powers employed are 20 and 15 mW cm^{-2}, for the LEDs and the monochromator respectively at highest output.

Light-response

After immersing the working electrode in the liquid cell and setting the desired potential, the whole system is left to equilibrate in the dark until the dark current reaches a typical value of a few nano-amperes. The light is switched on and the response in current is

measured, after which the light is switched off again. The light-induced current as a function of time has the shape of a rectangle superposed on a background current. The background in the *I-t* curve falls off in a non-linear way when the potential is applied, which becomes approximately linear or constant after equilibration.

Action spectra

Wavelength dependent action spectra are obtained by step-wise scanning of the monochromator with a computer controlled shutter and focusing the light on the working electrode. This enables the current to be measured in response to the wavelength of the incident light.

1.2.5 Atomic Force Microscopy

The AFM was invented by Binnig, Quate and Gerber in 1986 (Binnig et al., 1986). It uses a small very sharp tip, mounted on a flexible cantilever, that interacts with the sample under investigation. The cantilever deflects from its equilibrium position by the tip-sample interactions. A topographic image of the sample is formed by scanning the tip over the sample in a raster fashion and monitoring the force feedback signal that is needed to maintain a constant interaction force.

The small tip radius, typically a few nanometers, and low spring constant of the cantilever enable sub-nanometer resolution profiling of the surface and the possibility to do this with sensitive interactions between probe and sample. The latter is a prerequisite for probing delicate organic molecules (Bahatyrova et al., 2004a;Engel et al., 1997;Heymann et al., 1997;Muller and Engel, 1997).

In this research, AFM images of the samples were obtained in order to assess the presence and distribution of the protein assemblies, by using a commercial AFM (Nanoscope IIIa, Veeco, Santa Barbara, CA, USA). Tapping mode images in air were acquired with an E-scanner (14 μm range) and using Si probes with a resonance frequency of 75 kHz and a nominal spring constant of 2.8 N m^{-1}.

References

Allen, J. P., G. Feher, T. O. Yeates, H. Komiya, and D. C. Rees. 1987a. Structure of the Reaction Center from Rhodobacter-Sphaeroides R-26 - the Cofactors .1. *Proceedings of the National Academy of Sciences of the United States of America* 84:5730-5734.

Allen, J. P., G. Feher, T. O. Yeates, H. Komiya, and D. C. Rees. 1987b. Structure of the Reaction Center from Rhodobacter-Sphaeroides R-26 - the Protein Subunits. *Proceedings of the National Academy of Sciences of the United States of America* 84:6162-6166.

Allen, J. P., G. Feher, T. O. Yeates, D. C. Rees, J. Deisenhofer, H. Michel, and R. Huber. 1986. Structural Homology of Reaction Centers from Rhodopseudomonas-Sphaeroides and Rhodopseudomonas-Viridis As Determined by X-Ray-Diffraction. *Proceedings of the National Academy of Sciences of the United States of America* 83:8589-8593.

Bahatyrova, S., R. N. Frese, C. A. Siebert, J. D. Olsen, K. O. van der Werf, R. van Grondelle, R. A. Niederman, P. A. Bullough, C. Otto, and C. N. Hunter. 2004a. The native architecture of a photosynthetic membrane. *Nature* 430:1058-1062.

Bahatyrova, S., R. N. Frese, K. O. van der Werf, C. Otto, C. N. Hunter, and J. D. Olsen. 2004b. Flexibility and size heterogeneity of the LH1 light harvesting complex revealed by atomic force microscopy - Functional significance for bacterial photosynthesis. *Journal of Biological Chemistry* 279:21327-21333.

Binnig, G., C. F. Quate, and C. Gerber. 1986. Atomic Force Microscope. *Physical Review Letters* 56:930-933.

Blankenship, R. E. 2002. Molecular mechanisms of photosynthesis. Blackwell Science, Oxford..

Bopp, M. A., Y. W. Jia, L. Q. Li, R. J. Cogdell, and R. M. Hochstrasser. 1997. Fluorescence and photobleaching dynamics of single light-harvesting complexes. *Proceedings of the National Academy of Sciences of the United States of America* 94:10630-10635.

Borisov, A. Y. and V. I. Godik. 1973. Excitation-energy transfer in photosynthesis. *Biochimica et Biophysica Acta* 301:227-248.

Borland, C. F., R. J. Cogdell, E. J. Land, and T. G. Truscott. 1989. Bacteriochlorophyll Alpha-Triplet State and Its Interactions with Bacterial Carotenoids and Oxygen. *Journal of Photochemistry and Photobiology B-Biology* 3:237-245.

Bradforth, S. E., R. Jinenez, F. Vanmourik, R. Vangrondelle, and G. R. Fleming. 1995. Excitation Transfer in the Core Light-Harvesting Complex (Lh-1) of Rhodobacter-Sphaeroides - An Ultrafast Fluorescence Depolarization and Annihilation Study. *Journal of Physical Chemistry* 99:16179-16191.

Clayton, R. K. and B. J. Clayton. 1981. B850 Pigment-Protein Complex of Rhodopseudomonas-Sphaeroides - Extinction Coefficients, Circular-Dichroism, and the Reversible Binding of Bacteriochlorophyll. *Proceedings of the National Academy of Sciences of the United States of America-Biological Sciences* 78:5583-5587.

Cogdell, R. J. 1985. Carotenoids in Photosynthesis. *Pure and Applied Chemistry* 57:723-728.

Cogdell, R. J. and H. A. Frank. 1987. How Carotenoids Function in Photosynthetic Bacteria. *Biochimica et Biophysica Acta* 895:63-79.

Cogdell, R. J., P. K. Fyfe, S. J. Barrett, S. M. Prince, A. A. Freer, N. W. Isaacs, P. McGlynn, and C. N. Hunter. 1996. The purple bacterial photosynthetic unit. *Photosynthesis Research* 48:55-63.

Cogdell, R. J., A. Gall, and J. Kohler. 2006. The architecture and function of the light-harvesting apparatus of purple bacteria: from single molecules to in vivo membranes. *Quarterly Reviews of Biophysics* 39:227-324.

Cogdell, R. J., M. F. Hipkins, W. Macdonald, and T. G. Truscott. 1981. Energy-Transfer Between the Carotenoid and the Bacteriochlorophyll Within the B-800-850 Light-Harvesting Pigment-Protein Complex of Rhodopseudomonas-Sphaeroides. *Biochimica et Biophysica Acta* 634:191-202.

Cogdell, R. J., T. D. Howard, R. Bittl, E. Schlodder, I. Geisenheimer, and W. Lubitz. 2000. How carotenoids protect bacterial photosynthesis. *Philosophical Transactions of the Royal Society of London Series B-Biological Sciences* 355:1345-1349.

Deisenhofer, J., O. Epp, K. Miki, R. Huber, and H. Michel. 1984. X-Ray Structure-Analysis of A Membrane-Protein Complex - Electron-Density Map at 3A Resolution and A Model of the Chromophores of the Photosynthetic Reaction Center from Rhodopseudomonas-Viridis. *Journal of Molecular Biology* 180:385-398.

Deisenhofer, J., O. Epp, K. Miki, R. Huber, and H. Michel. 1985. Structure of the Protein Subunits in the Photosynthetic Reaction Center of Rhodopseudomonas-Viridis at 3A Resolution. *Nature* 318:618-624.

Engel, A., C. A. Schoenenberger, and D. J. Muller. 1997. High resolution imaging of native biological sample surfaces using scanning probe microscopy. *Current Opinion in Structural Biology* 7:279-284.

Escalante, M., Y. Zhao, M. J. W. Ludden, R. Vermeij, J. D. Olsen, E. Berenschot, C. N. Hunter, J. S. V. Huskens, and C. Otto. 2008. Nanometer arrays of functional light harvesting antenna complexes by nanoimprint lithography and host-guest interactions. *Journal of the American Chemical Society* 130:8892-8893.

Frese, R. N., C. A. Siebert, R. A. Niederman, C. N. Hunter, C. Otto, and R. van Grondelle. 2004. The long-range organization of a native photosynthetic membrane. *Proceedings of the National Academy of Sciences of the United States of America* 101:17994-17999.

Gall, A., G. J. S. Fowler, C. N. Hunter, and B. Robert. 1997. Influence of the protein binding site on the absorption properties of the monomeric bacteriochlorophyll in Rhodobacter sphaeroides LH2 complex. *Biochemistry* 36:16282-16287.

Hess, S., M. Chachisvilis, K. Timpmann, M. R. Jones, G. J. S. Fowler, C. N. Hunter, and V. Sundstrom. 1995. Temporally and spectrally resolved subpicosecond energy transfer within the peripheral antenna complex (LH2) and from LH2 to the core antenna complex in photosynthetic purple bacteria. *Proceedings of the National Academy of Sciences of the United States of America* 92:12333-12337.

Hess, S., F. Feldchtein, A. Babin, I. Nurgaleev, T. Pullerits, A. Sergeev, and V. Sundstrom. 1993. Femtosecond Energy-Transfer Within the Lh2 Peripheral Antenna of the Photosynthetic Purple Bacteria Rhodobacter-Sphaeroides and Rhodopseudomonas-Palustris Ll. *Chemical Physics Letters* 216:247-257.

Heymann, J. B., D. J. Muller, K. Mitsuoka, and A. Engel. 1997. Electron and atomic force microscopy of membrane proteins. *Current Opinion in Structural Biology* 7:543-549.

Hu, X. C., A. Damjanovic, T. Ritz, and K. Schulten. 1998. Architecture and mechanism of the light-harvesting apparatus of purple bacteria. *Proceedings of the National Academy of Sciences of the United States of America* 95:5935-5941.

Hu, X. C., T. Ritz, A. Damjanovic, F. Autenrieth, and K. Schulten. 2002. Photosynthetic apparatus of purple bacteria. *Quarterly Reviews of Biophysics* 35:1-62.

Jimenez, R., S. N. Dikshit, S. E. Bradforth, and G. R. Fleming. 1996. Electronic excitation transfer in the LH2 complex of Rhodobacter sphaeroides. *Journal of Physical Chemistry* 100:6825-6834.

Jones, M. R., G. J. S. Fowler, L. C. D. Gibson, G. G. Grief, J. D. Olsen, W. Crielaard, and C. N. Hunter. 1992. Mutants of Rhodobacter-Sphaeroides Lacking One Or More Pigment Protein Complexes and Complementation with Reaction-Center, Lh1, and Lh2 Genes. *Molecular Microbiology* 6:1173-1184.

Jungas, C., J. L. Ranck, J. L. Rigaud, P. Joliot, and A. Vermeglio. 1999. Supramolecular organization of the photosynthetic apparatus of Rhodobacter sphaeroides. *Embo Journal* 18:534-542.

Karrasch, S., P. A. Bullough, and R. Ghosh. 1995. The 8.5 A projection map of the light-harvesting complex I from *Rhodospirillum rubrum* reveals a ring composed of 16 subunits. *Embo Journal* 14:631-638.

Ketelaars, M., C. Hofmann, J. Kohler, T. D. Howard, R. J. Cogdell, J. Schmidt, and T. J. Aartsma. 2002. Spectroscopy on individual light-harvesting 1 complexes of Rhodopseudomonas acidophila. *Biophysical Journal* 83:1701-1715.

Ketelaars, M., A. M. van Oijen, M. Matsushita, J. Kohler, J. Schmidt, and T. J. Aartsma. 2001. Spectroscopy on the B850 band of individual light-harvesting 2 complexes of Rhodopseudomonas acidophila I. Experiments and Monte Carlo simulations. *Biophysical Journal* 80:1591-1603.

Kramer, H. J. M., R. Vangrondelle, C. N. Hunter, W. H. J. Westerhuis, and J. Amesz. 1984. Pigment Organization of the B800-850 Antenna Complex of Rhodopseudomonas-Sphaeroides. *Biochimica et Biophysica Acta* 765:156-165.

Lauterborn, W., T. Kurz, and M. Wiesenfeldt. 1995. Coherent Optics. Springer-Verlag. Berlin.

Limantara, L., R. Fujii, J. P. Zhang, T. Kakuno, H. Hara, A. Kawamori, T. Yagura, R. J. Cogdell, and Y. Koyama. 1998. Generation of triplet and cation-radical bacteriochlorophyll a in carotenoidless LH1 and LH2 antenna complexes from Rhodobacter sphaeroides. *Biochemistry* 37:17469-17486.

Liu, W. M., Y. D. Lu, Y. Liu, K. J. Liu, Y. L. Yan, J. L. Kong, C. H. Xu, and S. X. Qian. 2006. Effect of the in situ electrochemical oxidation on the pigment-protein arrangement and energy transfer in light-harvesting complex from Rhodobacter sphaeroides 601. *Biochemical and Biophysical Research Communications* 340:505-511.

McDermott, G., S. M. Prince, A. A. Freer, A. M. HawthornthwaiteLawless, M. Z. Papiz, R. J. Cogdell, and N. W. Isaacs. 1995. Crystal-Structure of An Integral Membrane Light-Harvesting Complex from Photosynthetic Bacteria. *Nature* 374:517-521.

Miller, K. R. 1982. 3-Dimensional Structure of A Photosynthetic Membrane. *Nature* 300:53-55.

Monger, T. G., R. J. Cogdell, and W. W. Parson. 1976. Triplet-States of Bacteriochlorophyll and Carotenoids in Chromatophores of Photosynthetic Bacteria. *Biochimica et Biophysica Acta* 449:136-153.

Monger, T. G. and W. W. Parson. 1977. Singlet-Triplet Fusion in Rhodopseudomonas-Sphaeroides Chromatophores - Probe of Organization of Photosynthetic Apparatus. *Biochimica et Biophysica Acta* 460:393-407.

Monshouwer, R., M. Abrahamsson, F. Vanmourik, and R. Vangrondelle. 1997. Superradiance and exciton delocalization in bacterial photosynthetic light-harvesting systems. *Journal of Physical Chemistry B* 101:7241-7248.

Monshouwer, R., I. O. Dezarate, F. Vanmourik, and R. Vangrondelle. 1995. Low-Intensity Pump-Probe Spectroscopy on the B800 to B850 Transfer in the Light-Harvesting 2 Complex of Rhodobacter-Sphaeroides. *Chemical Physics Letters* 246:341-346.

Muller, D. J. and A. Engel. 1997. The height of biomolecules measured with the atomic force microscope depends on electrostatic interactions. *Biophysical Journal* 73:1633-1644.

Nagarajan, V. and W. W. Parson. 1997. Excitation energy transfer between the B850 and B875 antenna complexes of Rhodobacter sphaeroides. *Biochemistry* 36:2300-2306.

Papiz, M. Z., S. M. Prince, A. M. HawthornthwaiteLawless, G. McDermott, A. A. Freer, N. W. Isaacs, and R. J. Cogdell. 1996. A model for the photosynthetic apparatus of purple bacteria. *Trends in Plant Science* 1:198-206.

Prince, S. M., M. Z. Papiz, A. A. Freer, G. McDermott, A. M. HawthornthwaiteLawless, R. J. Cogdell, and N. W. Isaacs. 1997. Apoprotein structure in the LH2 complex from Rhodopseudomonas acidophila strain 10050: Modular assembly and protein pigment interactions. *Journal of Molecular Biology* 268:412-423.

Pullerits, T., M. Chachisvilis, and V. Sundstrom. 1996. Exciton delocalization length in the B850 antenna of Rhodobacter sphaeroides. *Journal of Physical Chemistry* 100:10787-10792.

Qian, P., H. A. Addlesee, A. V. Ruban, P. Y. Wang, P. A. Bullough, and C. N. Hunter. 2003. A reaction center-light-harvesting 1 complex (RC-LH1) from a Rhodospirillum rubrum mutant with altered esterifying pigments. *Journal of Biological Chemistry* 278:23678-23685.

Qian, P., P. A. Bullough, and C. N. Hunter. 2008. Three-dimensional reconstruction of a membrane-bending complex - The RC-LH1-PufX core dimer of Rhodobacter sphaeroides. *Journal of Biological Chemistry* 283:14002-14011.

Qian, P., C. N. Hunter, and P. A. Bullough. 2005. The 8.5 angstrom projection structure of the core RC-LH1-PufX dimer of Rhodobacter sphaeroides. *Journal of Molecular Biology* 349:948-960.

Reddy, N. R. S., G. J. Small, M. Seibert, and R. Picorel. 1991. Energy-Transfer Dynamics of the B800-B850 Antenna Complex of Rhodobacter-Sphaeroides - A Hole Burning Study. *Chemical Physics Letters* 181:391-399.

Roszak, A. W., T. D. Howard, J. Southall, A. T. Gardiner, C. J. Law, N. W. Isaacs, and R. J. Cogdell. 2003. Crystal structure of the RC-LH1 core complex from Rhodopseudomonas palustris. *Science* 302:1969-1972.

Shreve, A. P., J. K. Trautman, H. A. Frank, T. G. Owens, and A. C. Albrecht. 1991. Femtosecond Energy-Transfer Processes in the B800-850 Light-Harvesting Complex of Rhodobacter-Sphaeroides-2.4.1. *Biochimica et Biophysica Acta* 1058:280-288.

Siebert, C. A., P. Qian, D. Fotiadis, A. Engel, C. N. Hunter, and P. A. Bullough. 2004. Molecular architecture of photosynthetic membranes in Rhodobacter sphaeroides: the role of PufX. *Embo Journal* 23:690-700.

Straley, S. C., W. W. Parson, D. C. Mauzeral, and R. K. Clayton. 1973. Pigment Content and Molar Extinction Coefficients of Photochemical Reaction Centers from Rhodopseudomonas-Spheroides. *Biochimica et Biophysica Acta* 305:597-609.

Sundstrom, V., T. Pullerits, and R. van Grondelle. 1999. Photosynthetic light-harvesting: Reconciling dynamics and structure of purple bacterial LH2 reveals function of photosynthetic unit. *Journal of Physical Chemistry B* 103:2327-2346.

Sundstrom, V., R. Vangrondelle, H. Bergstrom, E. Akesson, and T. Gillbro. 1986. Excitation-Energy Transport in the Bacteriochlorophyll Antenna Systems of Rhodospirillum-Rubrum and Rhodobacter-Sphaeroides, Studied by Low-Intensity Picosecond Absorption-Spectroscopy. *Biochimica et Biophysica Acta* 851:431-446.

van Amerongen, H., L. Valkunas, and R. van Grondelle. 2000. Photosynthetic Excitions. World Scientific. Singapore.

van Grondelle, R. a. A. J. 1986. Excitation energy transfer in photosynthetic systems. Orlando: Academic Press, 191-224.

van Grondelle, R., J. P. Dekker, T. Gillbro, and V. Sundstrom. 1994. Energy-Transfer and Trapping in Photosynthesis. *Biochimica et Biophysica Acta-Bioenergetics* 1187:1-65.

van Grondelle, R. and V. I. Novoderezhkin. 2006. Energy transfer in photosynthesis: experimental insights and quantitative models. *Physical Chemistry Chemical Physics* 8:793-807.

van Oijen, A. M., M. Ketelaars, J. Kohler, T. J. Aartsma, and J. Schmidt. 1999. Spectroscopy of individual LH2 complexes of Rhodopseudomonas acidophila: localized excitations in the B800 band. *Chemical Physics* 247:53-60.

Visscher, K. J., H. Bergstrom, V. Sundstrom, C. N. Hunter, and R. Vangrondelle. 1989. Temperature-Dependence of Energy-Transfer from the Long Wavelength Antenna Bchl-896 to the Reaction Center in Rhodospirillum-Rubrum, Rhodobacter-Sphaeroides (Wt and M21 Mutant) from 77 to 177K, Studied by Picosecond Absorption-Spectroscopy. *Photosynthesis Research* 22:211-217.

Walz, T., S. J. Jamieson, C. M. Bowers, P. A. Bullough, and C. N. Hunter. 1998. Projection structures of three photosynthetic complexes from Rhodobacter sphaeroides: LH2 at 6 angstrom LH1 and RC-LH1 at 25 angstrom. *Journal of Molecular Biology* 282:833-845.

Zhang, F. G., R. Vangrondelle, and V. Sundstrom. 1992. Pathways of Energy-Flow Through the Light-Harvesting Antenna of the Photosynthetic Purple Bacterium Rhodobacter-Sphaeroides. *Biophysical Journal* 61:911-920.

Chapter 2

Light harvesting, energy transfer and electron cycling of a native photosynthetic membrane adsorbed onto a gold surface.

Abstract

Photosynthetic membranes comprise a network of light harvesting and reaction center pigment-protein complexes responsible for the primary photo-conversion reactions: light-absorption, energy transfer and electron cycling. The structural organization of membranes of the purple bacterial species *Rb. sphaeroides* has been elucidated in most detail by means of polarized light spectroscopy and atomic force microscopy. Here we report a functional characterization of native and untreated membranes of the same species adsorbed onto a gold surface. Employing fluorescence confocal spectroscopy and light-induced electrochemistry we show that adsorbed membranes maintain their energy and electron transferring functionality. Gold-adsorbed membranes are shown to generate a steady high photocurrent of 10 $\mu A\ cm^{-2}$ for several minutes and to maintain activity for up to three days while continuously illuminated. The surface adsorbed membranes exhibit a remarkable functionality under aerobic conditions, even when exposed to light intensities well above that of direct solar irradiation. The component at the interface of light-harvesting and electron cycling, the LH1 complex, displays exceptional stability, likely contributing to the robustness of the membranes. Peripheral light-harvesting LH2 complexes show a light-intensity dependent decoupling from photoconversion. LH2 can act as a reversible switch at low-light, an increased emitter at medium light and photobleaches at high light.

The contents of this chapter has been published in:
Gerhard J. Magis, Mart-Jan den Hollander, Willem G. Onderwater, John D. Olsen, C. Neil Hunter, Thijs J. Aartsma, and Raoul N. Frese. 2010. Light harvesting, energy transfer and electron cycling of a native photosynthetic membrane adsorbed onto a gold surface. *Biochimica et Biophysica Acta* 1798:637-645.

2.1 Introduction

Photosynthetic membranes are compartmentalized cellular structures containing the solar-energy transducing machinery. The most abundant protein complexes constituting this machinery are light-harvesting (LH) complexes, which are responsible for the absorption of sunlight and subsequent excited state energy transfer, and reaction centers (RC), where the energy is utilized to initiate the primary charge-transfer reactions (Fleming and van Grondelle, 1994). Because of their relative simplicity, the photosynthetic membranes from purple bacteria have been characterized in detail by near infrared (NIR) spectroscopy and, more recently, by atomic force microscopy (AFM, (Bahatyrova et al., 2004a;Cogdell et al., 1996;Frese et al., 2004;Hunter et al., 1982;Sturgis et al., 2009)).

The purple bacterium *R. sphaeroides* synthesizes vesicle-shaped membranes, or chromatophores, that contain two types of LH complexes, the peripheral LH2 complex and the LH1 complex that surrounds the RC complex. The RC-LH1-PufX complexes of *R. sphaeroides* form a dimeric supercomplex that forms extended linear arrays in the native membranes. The polypeptide PufX has been shown to be the determinant factor for RCLH1 dimerization (Frese et al., 2000;Jungas et al., 1999;Qian et al., 2008;Siebert et al., 2004). In the wild-type (WT) photosynthetic membrane, these linear arrays are interspersed by LH2 complexes (Bahatyrova et al., 2004a).

In conjunction with structural models of the LH and RC complexes, and data from polarized light-spectroscopic measurements on intact membranes, a detailed description of the supramolecular organization of *R. sphaeroides* membranes has been developed (Frese et al., 2004;Sener et al., 2007). Similar investigations on *R. sphaeroides* mutant membranes with altered composition (monomeric RC-LH1 and LH2) showed that packing effects reminiscent of colloidal systems, rather than specific protein-protein interactions, are a driving force for the observed supramolecular organizations (Frese et al., 2008). In the case of *R. sphaeroides* and other species, AFM images revealed a close packing of the photosynthetic components which is a prerequisite for a highly efficient energy transferring network.

Nevertheless such images do raise the question whether these native membranes are still capable of performing their energy transducing function upon adsorption to a solid support, or if the isolation and adsorption has an adverse effect. Surface-adsorbed photosynthetic membranes have not been characterized functionally before. A functional assessment comprises the light absorbing and subsequent energy transferring mechanisms as well as the ability for electron cycling. These functions can be probed by means of confocal

spectroscopy and light-induced electrochemistry (Guidelli, 2001;Nie and Zare, 1997). The latter technique is facilitated by the attachment of a preparation onto a conducting surface that serves as an electrode to or from which electrons can be channeled; typically, this electrode consists of gold. This technique has been applied on several photosynthetic complexes, which were either engineered for specific attachment or adsorbed via functionalized groups on the surface (Kondo et al., 2007;Lebedev et al., 2006;Lu et al., 2007;Suemori and et al., 2006;Trammell et al., 2006).

In all these cases surface-immobilization of the complexes involved functionalized gold surfaces using self-assembled monolayers (SAM's) with specific terminal functionality. In contrast, we recently observed the possibility of directly adsorbing isolated RC complexes onto a bare-gold electrode without functionalisation of the surfaces or the proteins. Moreover, applying an external potential within the range of the open circuit potential of the RC and charge carriers, i.e. cytochrome-*c* (cyt-*c*) and extrinsic quinones (Q-0), light-induced currents could be observed under ambient conditions.

Here we present a study by light-induced electrochemistry and confocal spectroscopy on native membranes of *R. sphaeroides* adsorbed directly onto a solid gold support. In contrast to mica or glass, we find that intact chromatophores vesicles adhere as flattened structure onto gold, withstanding rinsing and drying steps. Wavelength dependent fluorescence excitation and current-action spectra indicate that these untreated, wild-type (WT) chromatophores adsorbed on gold retain their energy- and electron transferring capabilities. Surprisingly, membranes remain functional under aerobic conditions.

Fluorescence emission and excitation spectra were obtained under similar conditions. In all cases, we find that all three pigment-protein complexes responsible for the primary photoconversion reactions remain functional, although a decreased contribution of the peripheral LH2 complex is observed. This decrease as well as the possibility for reversibility showed to be variable with light illumination intensity. Results are compared with photosynthetic preparations in solution and purified LH1 adhered onto a surface. Our work shows the feasibility of coupling photo-active biological systems to non-biological surfaces, with retained functionality when exposed to relatively intense light and to air.

2.2 Materials and Methods

2.2.1 Biological membranes

Wild-type cells of *R. sphaeroides* NCIB 8253 were grown photosynthetically at intermediate light intensity (500 W m^{-2}) for 18-20 hours. Cells were disrupted through

ultra-sound sonication and subsequently loaded onto a sucrose gradient. The gradient was spinned for 20 hours and the red colored band was isolated.

2.2.2 RCLH1 membranes

Cultures were grown semi-aerobically in a shaker incubator at 34 ^{o}C and 180 rpm. The cells were pre-treated with 2 mL of 10 mg/mL lysozyme (Sigma Chemicals) for 30 minutes on ice and then lysed by two passages through a French Press at 18,000 psi. The resulting lysate was treated with DNAse to digest the genomic DNA prior to loading onto a 15/40% w/w sucrose (in 10mM HEPES pH 7.5, 1mM EDTA, 1mM DTT buffer) discontinuous gradient and centrifugation at 27 krpm for 10 hours. The pigmented membranes were harvested from the 15/40% interface and frozen at -20 ^{o}C until use.

2.2.3 Isolated photosynthetic complexes

LH2 membranes were solubilised by the addition of β-OG to a final concentration of 2.5% and stirring for 30 mins at 4 ^{o}C. The solubilised membranes were applied to a pre-equilibrated DEAE sepharose column (Sigma Chemicals) and washed extensively with increasing concentrations of NaCl for a minimum of 90 minutes. The purified protein was eluted from the column using a 150-400 mM NaCl gradient over 60 mins and 4 mL fractions were collected. The elution profile showed two peaks of which the second peak was demonstrated by EM analysis to consist of monodisperse LH2 complexes. These fractions were then used in all subsequent experiments. The preparation of the LH1-only purified complexes was identical except for the use of the detergent β-DDM. During solubilisation β-DDM was added to a final concentration of 1% and all the columns were run at a concentration of 0.03% β-DDM.

2.2.4 Gold surface preparation

A 1 nm adhesion layer of molybdenum germanium (MoGe) was first sputtered on mica using an ATC-1800 magnetron sputtering system with a deposition rate of 1.32 nm per minute (10 mTorr Argon environment). On top of this 20 nm thick gold films were sputtered with a deposition rate of 9.2 nm per minute (5 mTorr environment composed of a mixture of Argon with 1% oxygen). This resulted in gold films with a typical RMS roughness of 0.3 nm.

2.2.5 Protein immobilization for spectroscopy

Attachment of purified LH1 on gold

25 µL of bulk LH1 solution (OD_{870} 2-3 in a buffer containing 10 mM HEPES (pH 8), β-DDM (0.03%), 150 mM NaCl and 10 mM DTT) was diluted with 175 µL buffer (10 mM HEPES (pH 8) and β-DDM (0.03%)) and loaded on the surface. After 15 minutes incubation the sample was rinsed with 1 mL of buffer. This loading and rinsing was repeated 2 times after which the surface was gently blown dry under a mild stream of nitrogen gas.

Attachment of WT chromatophores on gold

A 50 µL sample was loaded on the gold surface and left to incubate for 30 minutes. After this the surface was rinsed with 1 mL of buffer (10 mM HEPES at pH 7.5 – 8) and gently blown dry under a mild stream of nitrogen-gas.

2.2.6 Atomic Force Microscopy

Atomic Force Microscopy (AFM) images of the samples were obtained using a commercial AFM (Nanoscope IIIa, Veeco, Santa Barbara, CA, USA). Tapping mode images in air were acquired with an E-scanner (14 µm range) and using Si probes with a resonance frequency of 75 kHz and a nominal spring constant of 2.8 N m^{-1}.

2.2.7 Spectroscopy

Experiments were performed at room temperature with a home-built confocal microscope setup with the objective mounted inside a cryostat. The latter enables measuring in an air free environment by vacuum pumping the cryostat. Homogeneity of the sample distribution on the surface was checked by confocally scanning the laser over a wide-range (hundreds of micrometers) at a fixed excitation wavelength (800 or 850 nm for LH2, 870 nm for LH1) and monitoring the fluorescence-signal using an avalanche photodiode (APD, Perkin-Elmer SPCM-AQR-16).

Fluorescence emission spectra were recorded by directing the emitted fluorescence via a series of long-pass filters with a transmission between 815 and 1015 nm (Hugo Anders, Germany), towards a blazed grating (Richardson Gratings) that disperses the collimated fluorescence. A lens is finally used to project the diffracted beam onto a liquid-nitrogen-cooled CCD camera (Roper Scientific, USA). The excitation intensity used to record an emission spectrum was 200 W cm^{-2} or indicated in the text. Integration times were typically 60 seconds. The recorded spectra were all corrected for the sensitivity of the CCD camera.

Fluorescence excitation spectra were recorded in vacuum at room temperature, unless otherwise stated. A series of 3 identical interference band pass filters were employed in the detection path to remove most of the stray light (residual excitation light passing through the detection-filters). Two sets of filters were used depending on the sample under investigation, one with a transmission between 875 and 910 nm (for purified LH2 measurements), and the other with a transmission between 905 and 940 nm (for purified LH1 and membrane measurements). Excitation-spectra were recorded by scanning the wavelength of the titanium sapphire (TiSa) laser from 790 nm (lower limit of the laser) to either 870 or 900 nm, depending on which filter-set is used.

2.2.8 Photostability measurements

On a surface

The scheme for fluorescence emission spectroscopy as mentioned above was employed with the exception that the long-pass filters for emission detection are replaced by a series of 3 identical interference band pass filters (transmission between 875 and 910 nm for LH2, transmission between 905 and 940 nm for LH1). This limits the detection of the emission to the red part of the fluorescence, but the main advantage of this scheme is that we can now excite LH1 at a longer wavelength where the complex has more absorption. The detected fluorescence signal was integrated for 60 seconds.

In solution

Samples were diluted in the appropriate buffer to an OD of 0.1 before loading into the cuvette. The cuvette has a volume of 60 µL and during the photostability measurements in solution approximately half this volume was illuminated. Measurements were conducted on a home-built setup integrating a spectrophotometer (Ocean Optics, QE6500) for absorbance measurements and fluorescence detection (cut-off filter transparent at 700-1000 nm, and a halogen-lamp for long-term illumination (400-1000 nm) and excitation (cut-off filter transparent at 400-700 nm). The power of the white-light was 135 mW cm^{-2} on the cuvet open to air. Long-term illumination (and excitation) light was passed through a 10 cm water-filter to prevent heating. The samples were continuously illuminated until no reduction in absorption or emission was observed.

2.2.9 Electrochemistry

The bare-gold working electrode was cleaned prior to use by sonicating and rinsing with purified water and subsequent grinding. A drop of 10 µL of solution containing membrane was deposited onto cleaned bare-gold electrodes and left to incubate for 1 hour in the dark at 277 K. Subsequently, the electrodes were rinsed 3 times with 3 mL 10 mM phosphate

buffer, inserted into a home-built cell, and immersed in the measuring buffer (volume approximately 7 mL). The buffer solution contained 20 µM horse heart cytochrome *c* (Sigma, 97% purity) and 100 µM Q-0 (or 2,3-dimethoxy-5-methyl-1,4-benzoquinone, Aldrich, 99% purity). The potential was set at a specific value and the whole system was left to equilibrate in the dark until the dark current reached a typical value of a few nano-amperes. We then switched on the light and measured the response in current, after which the light was switched off again. Electrodes and potential were controlled by a commercial potentiostat from CHI-instruments with the standard three-electrode configuration: a working electrode on which the membranes were deposited, a platinum counter electrode to measure the current and a reference electrode with fixed potential relative to which the potential was set. The reference electrode was a standard calomel electrode (SCE): KCl saturated (Hg/Hg_2Cl_2) electrode. Illumination was accomplished by light from light emitting diodes (LEDS), with a broadband excitation at 870 nm (approximately 50 nm FWHM) or by a home-built halogen lamp-monochromator design. Wavelength dependent action spectra were obtained from step-wise scanning the monochromator design with a computer-controlled shutter.

2.3 Results and Discussion

2.3.1 Adsorption of membranes onto a gold surface

Isolated *R. sphaeroides* membranes were directly deposited onto a gold surface or gold-electrode or mica-surface. The preparations were left to incubate in the dark for 30 minutes to one hour at 277 K and subsequently rinsed with buffer solution and blown dry with a gentle flow of nitrogen gas.

A comparison of the adsorption of untreated membranes on mica and gold obtained by low-resolution atomic force microscopy (AFM) is shown in figure 1. Panel A shows the isolated membranes adsorbed onto mica. A range of high semi- spherical shapes (height 20 to 70 nm, width between 100-700 nm) can be observed, reminiscent of collapsed spherical chromatophores as well as larger structures as observed before in electron microscopy images (Fraker and Kaplan, 1971). The larger structures are a consequence of the simple purification procedure, designed to isolate photosynthetic membranes with minimal disturbance. Panel B shows similarly prepared membranes on a mica surface covered with a 20 nm layer of gold. Great care was taken to produce a uniformly flat gold surface ($\approx$ 0.3 nm surface roughness) for easy identification of adsorbed structures by scanning probe techniques. The height profile of such an image shows uniformly flat, singular membranes of about 7 nm height and 100-200 nm in diameter, dimensions which are similar to fragments of detergent-treated membranes adsorbed onto mica for high-resolution AFM

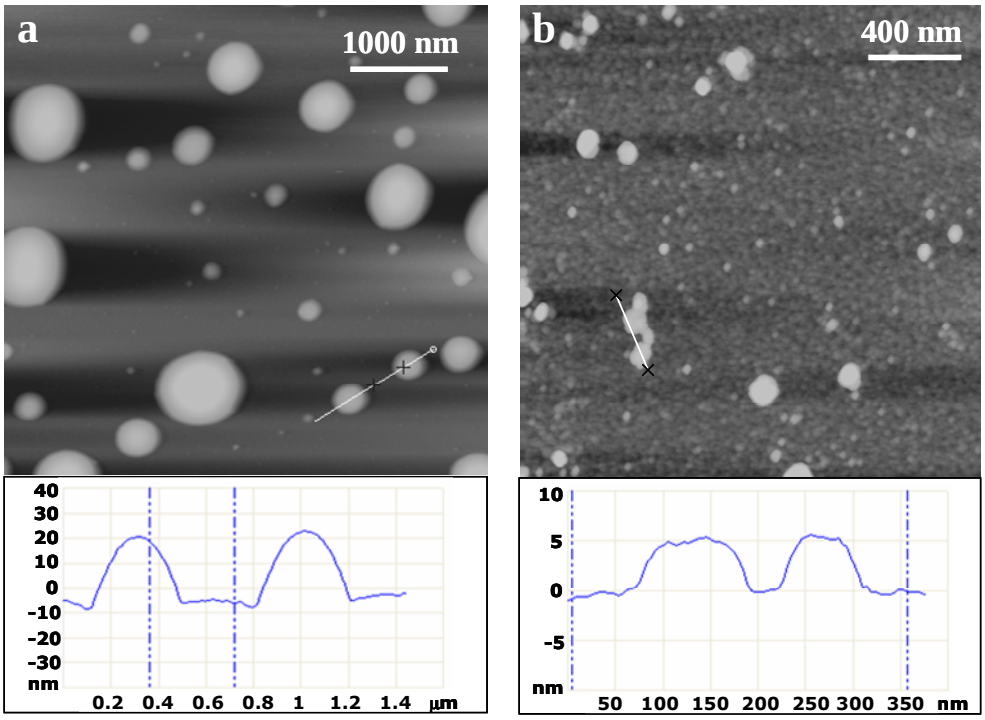


Figure 1. Tapping Mode AFM images in air of membranes adsorbed onto a mica and gold surface.
(A) AFM topography image of isolated WT chromatophores adsorbed on a mica surface (top panel) and height profile along the white line (bottom panel). Grey scale 70 nm.
(B) AFM topography image of WT chromatophores adsorbed on a gold substrate (top panel) and height profile along the white line (bottom panel). Grey scale 12 nm.
White lines in the topography images indicate the lines along which the height profiles are measured; the crosses in the topography images correspond to the dash-double dot lines in the height profiles.

imaging (Bahatyrova et al., 2004a). We investigated several methods of membrane adsorption to the mica and gold surfaces. We either consecutively replaced the liquid droplet containing membranes by buffer or rinsed the surfaces with buffer. In all cases the mica surface showed larger structures compared to the gold surface. It appears that chromatophores retain their intact vesicular structure more upon adsorption to mica, whereas they open up, or rupture to form single membrane bi-layers when they adsorb onto gold. This disruption might be caused by strong attractive forces between the gold and the vesicular membranes, sufficient to overcome the native forces that determine the shape of the vesicles.

2.3.2 Electron-transfers of photosynthetic membranes adsorbed onto a gold-electrode

A membrane-covered gold-electrode was immersed in buffer solution, which contained cytochrome *c* (cyt-*c*) and extrinsic quinones (Q-0) as electron carriers. The light-induced current action spectra and absorbance of the chromatophores in buffer solution (crosses) are shown in figure 2A. Current action spectra are obtained by measuring light-on light-off traces at 5 nm wavelength intervals, upon illumination by the output of a scanning monochromator with a tungsten light source. We found that maximum current is generated at a potential of −100 mV (referenced to a standard calomel electrode or SCE). At this potential the electrons flow from the gold to reduce the RC's, either directly or with cyt-*c* as mediator, while current cycling is enabled via Q-0 towards the counter electrode (Lu et al., 2007;Trammell et al., 2006). The wavelength dependent current action spectrum (black squares) closely follows the absorbance bands of the chromatophores. Both spectra are dominated by the most abundant light-harvesting complex LH2, which absorbs around 800 nm and 850 nm. The other light-harvesting complex LH1 appears as a pronounced shoulder at 870 nm. The electron transferring reaction center complex, which is responsible for the light-induced current, is not visible in both spectra since the absorbance is much smaller compared to the LH complexes. We conclude that the light absorbed by all components within the membranes contribute to the induced current. Clearly, these membranes remain functional while adsorbed onto a gold-electrode.

The induced photocurrent and the absorbance spectrum did not completely match, however, and therefore we inspected the light-intensity dependence of current generation. In figures 2A and 2B, measurements of light-induced currents from native membranes are shown as a function of illumination power (represented as percentage of maximum illumination). In order to show the contribution of the LH-systems relative to the RCs, the absolute currents (figure 2B) were normalized at 750 nm, where two intrinsic RC pigments, bacterio-pheophytins, dominate absorption (figure 2A). The effect of higher illumination power is striking: more light results in a higher photocurrent (figure 2B) but with a strong decrease in contribution from the LH2 complexes relative to the RCs (figure 2A). At the lowest power at which we can measure a photocurrent, LH2 does not contribute fully to the action spectrum (black squares). At highest illumination, also LH1 appears not to fully contribute to the photocurrent. At this illumination intensity the correspondence between the current action spectrum and the absorbance is lost. Here the spectral signature of the LH complexes is lost and mostly RCs appear to generate currents. We note that the change of the current action spectrum upon changing the illumination-intensity is fully reversible, which shows that this effect is not caused by photobleaching.

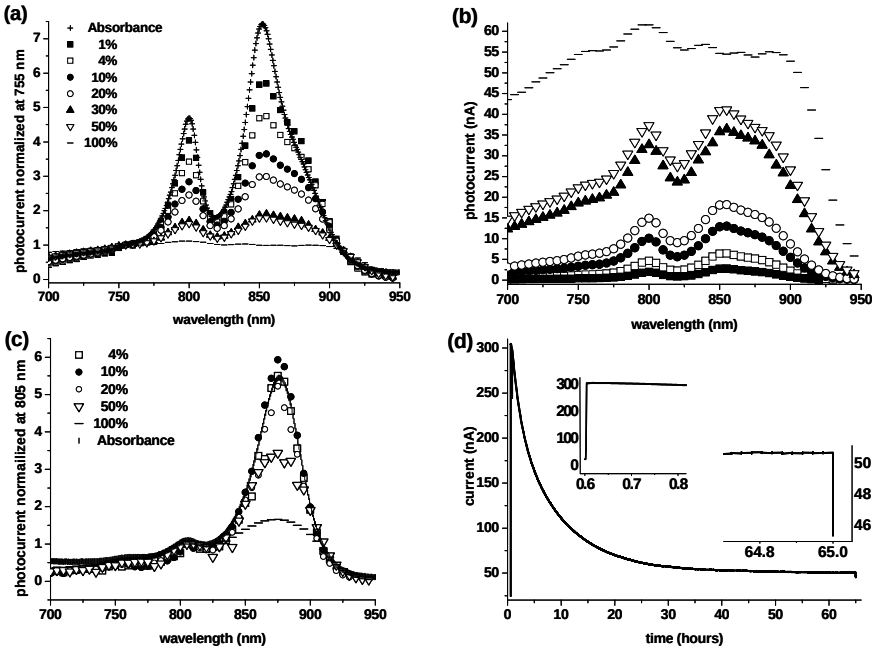


Figure 2. Absorbance and light-induced-current action spectra of membranes adsorbed onto a gold surface.
(A) Light-induced current action and solution absorbance spectra from WT chromatophores. Illumination powers indicated as percentage of maximum (100%) illumination that is 15 mW cm^{-2}; spectra normalized at 750 nm.
(B) Absolute light-induced currents from WT chromatophores with illumination powers as in panel A.
(C) Light-induced current action and solution absorbance spectra from RCLH1 mutant membranes. Illumination powers as in panel a; spectra normalized at 805 nm.
(D) Light induced current during continuous illumination with a LED centered at 850 nm, V = -100 mV vs. SCE.
Inset: magnifications of the first and last ten minutes of the light induced current. At 0.6 hours the light was turned on and after 65 hours the light was turned off.

We find no indication that saturation effects occur, because within the illumination regime where LH2 contribution can be observed, the induced current is proportional with light intensity; the slight deviations may be due to non-homogeneous illumination at different powers. Moreover, as discussed in more detail below, broadband illumination results in much higher currents, indicating the absence of limiting factors concerning electron transfers within the gold-membrane-buffer system.

We also investigated membranes of a mutant strain that contains only RC-LH1 complexes, without LH2 or PufX. The absorbance and action spectra (figure 2C) are dominated by the LH1 complex, with small RC bands visible at 800 nm and 750 nm. For this preparation the light dependent current closely matched the absorbance spectrum at 20% of the maximum

illumination intensity. Upon further increase of the intensity the contribution of LH1 to the photocurrent decreases similarly as for the LH2 component within WT membranes (figure 2A). Generally, the contribution of LH1 to the photocurrent is similar in RC-LH1-only and WT membranes.

Our photocurrent data suggest a light-dependent decoupling of the light-harvesting complexes to further energy transfer or photoconversion mechanisms. Light-induced decoupling starts off at a light intensity below our experimental limit (~ 150 µW cm^{-2} at 870 nm) in the case of LH2, and between 3 and 7 mW cm^{-2} at 870 nm for LH1. At maximum intensity (15 mW cm^{-2} at 870 nm) LH2 does not participate significantly in photocurrent generation, while approximately 20% of LH1 still contributes.

For both the RC-LH1 mutant and WT membranes, the addition of cyt-*c* proved to be essential in order to achieve high (> 5nA) photocurrents (data not shown). Cyt-*c* has been shown to act as a molecular relay between RC's and the electrode to enhance electron transfer (Lu et al., 2007). Since membranes are large and curved structures, an unequal distance between many RCs and the electrode is expected and thus the necessity for cyt-*c* as a mediator.

In figure 2D we show the result of testing the photostability of the native membranes towards current generation under continuous illumination, while exposed to air. Using a broadband LED (FWHM 50 nm) centred at 850 nm for illumination we achieve an initial photocurrent of 10 µA cm^{-2}. This current did not show a significant decrease for several minutes (in terms of the induced current, LED illumination was equivalent to 870 nm single-wavelength excitation at 20 mW cm^{-2} or 0.5 µmol photons / m^2s). This represents the highest photocurrent per illumination photon from photosynthetic material adsorbed onto an electrode to date. During three days of illumination under aerobic conditions, membranes sustain a significant photocurrent. At the end of this experiment the residual light-induced current was approximately 0.5% of the initial value (see inset). In total, during these three days 10 to 17 mC of charge was transferred by photoconversion in the membranes. Since there is also LH2 present in at least a 1:3 ratio, this would imply for a fully covered electrode a lower limit of on average 5×10^6 turnovers per RC, or one electron cycled through the gold-membrane-buffer system every 50 ms. Part of the electrode may well be uncovered and many RCs may well be unfavourably positioned for electron transfer, therefore the real average number of turnovers per RC is likely much higher.

We conclude here firstly that WT chromatophores and RCLH1-only mutant membranes remain functional while adsorbed onto a bare gold-electrode, under aerobic conditions. Currents can be generated continuously for up to three days. Last, higher illumination intensity reduces the light harvesting contribution to the photocurrent.

2.3.3 Energy-transfer and photostability of photosynthetic membranes adsorbed onto a gold surface

The previous measurements indicated that on a gold surface, native vesicular shaped membranes open up spontaneously upon adsorption, without specific chemical treatment. To determine the intrinsic photostability of the system, we performed a spectral analysis of the gold-adsorbed membranes by confocal fluorescence excitation and emission spectroscopy. Fluorescence excitation spectra report on energy transferring capabilities of the complexes in the membrane, i.e. B800→B850 and LH2→LH1 transfer. Fluorescence emission spectra serve to indicate the photoactivity under various experimental conditions (vacuum, aerobic, and high illumination power).

WT chromatophores were prepared and adsorbed onto a gold surface similarly as for the previous electrochemistry measurements. Excitation and emission spectra of such preparations are compared to spectra of the same preparations in buffer solution. Fluorescence excitation spectra were obtained by scanning the excitation laser from 780 to 900 nm. Emission was detected between 905 and 940 nm. The power of the laser could be attenuated from 200 nW to 7 mW, which corresponds to a light intensity focused on the sample by a microscope objective of 20 W cm^{-2} (lowest) to 637 kW cm^{-2} (highest); note that the typical power for single-molecule spectroscopy is about 1 kW cm^{-2}.

In figure 3A we compare the absorbance of isolated membranes in solution and fluorescence excitation spectra of gold-adsorbed membranes in vacuum. We observe all three light-absorbing components within the membranes; originating from LH2, with bands centred at 800 nm and 850 nm, and LH1, centred at 870 nm. Since excitation spectra are measured at the emission wavelength of LH1, the excitation spectrum shows that intra-LH2 and LH2→LH1 energy transfer is retained. The excitation spectrum does appear to have a slightly larger width compared to the absorption spectrum in solution, which may be either due to normalization at 850 nm which does not take any loss of absorbance or emission into account or an increased disorder upon adsorption. Also the gold surface may interact more strongly with the B850 BChl's but such effect is not expected since we probe far off-resonance with the plasmon bands of gold. The gold surface is likely a decay channel for excitations though, quenching through direct dipole couplings, which may be tuned by the

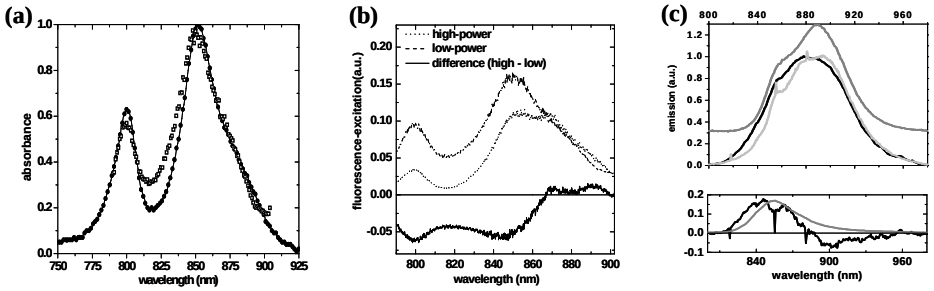


Figure 3. Fluorescence spectra of WT chromatophores on a gold substrate and solution.
(A) Isolated WT chromatophores: normalized absorbance in solution (open squares) and fluorescence excitation on a gold surface (black circles); excitation spectrum acquired in vacuum at 20 W cm^{-2},emission detected between 905-940 nm.
(B) Fluorescence excitation spectra in vacuum of WT chromatophores on gold with different excitation intensities: high-power 2750 W cm^{-2}, dotted curve) and low-power 20 W cm^{-2}, dashed curve). The spectra were normalized with respect to the excitation intensity. The solid line shows the difference spectrum (high-power minus low-power). Emission detected between 905-940 nm.
(C) Fluorescence emission spectra in vacuum of WT chromatophores on gold recorded with high- (light grey) and low-power (black) illumination and in solution (dark grey). The spectra were not normalized but both scaled to excitation power. Lower panel: difference spectrum of the emission spectra (high-power minus low-power; black line). Excitation on gold at 800 nm, in solution broad illumination range: 400-600 nm. The solid grey line shows the fluorescence emission of isolated LH2 complexes.

dielectric of the proteins. Because we do not observe a significant mismatch between the contribution of LH2 and LH1 to the excitation spectrum, quenching appears not to be different for LH2 and LH1.Together with the previous photocurrent data, this measurement shows the functional adsorption of unprepared membranes onto gold.

We continued by investigating the functioning of the membranes towards higher illumination intensities. In figure 3B, upper panel, we show the effect of changing illumination power from 20 to 2750 W cm^{-2}, (referred to as low- and high-power in this paragraph, respectively). We observe a decrease of the fluorescence excitation signal. The lower panel shows the difference between high and low power spectra. The lineshape of the difference signal indicates a decreased contribution of LH2 for the high power excitation spectrum. Figure 3C shows the fluorescence emission spectra for the same two illumination powers. Spectra were not normalized but scaled to the illumination power. Emission spectra closely resemble the emission from WT chromatophores in solution (figure 3C, upper trace). The low power emission band is smaller on the blue side compared to the high illumination emission. Panel 3D shows the difference between the two emission spectra and a comparison with emission of purified LH2 complexes. The two signals are spectrally similar, indicating an increase of LH2 emission for high power illumination. The increased LH2 emission is concomitant with the decreased contribution of LH2 to the high intensity excitation spectrum in figure 3B. Since we detect the

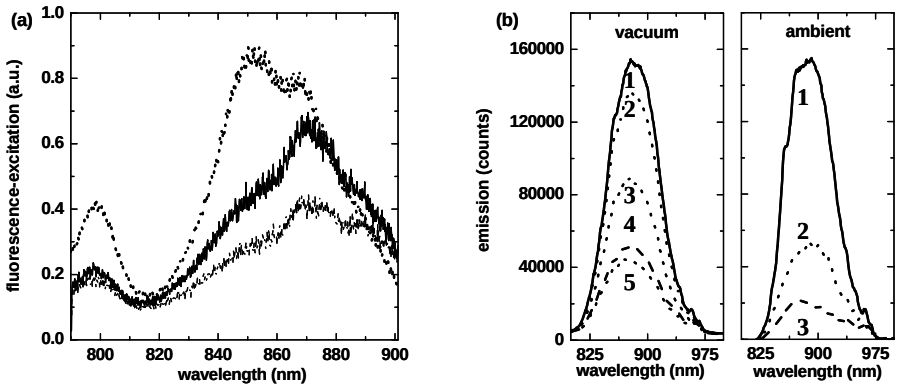


Figure 4. Fluorescence spectra of WT chromatophores on a gold substrate

(A) Fluorescence excitation spectra in vacuum of WT chromatophores before illumination (dotted curve), after illumination at 800 nm for 5 minutes with an intensity of 637 kW cm^{-2} (solid curve), and after illumination at 850 nm for 5 minutes with 443 kW cm^{-2} (dashed curve). All excitation-spectra were taken with an approximate excitation intensity of 150 W cm^{-2},emission detected between 905-940 nm.

(B) Fluorescence emission spectra of WT chromatophores in vacuum (left panel) and under aerobic conditions (right panel) by exciting at 800 nm with 50 kW cm^{-2}; integration time of 3 seconds.

Left panel: Between spectrum 1 and 2 the sample was illuminated for 5 minutes with 50 kW cm^{-2} at 800 nm. Between 2 and 3 the sample was illuminated with this same power for 30 minutes. Between 3 and 4 the sample was illuminated with 637 kW cm^{-2} for 30 minutes. Between spectrum 4 and 5 the shutter was closed for 30 minutes to measure the recovery of the sample.

Right panel: Between spectrum 1 and 2 the sample was illuminated with 50 kW cm^{-2} for 5 minutes at 800 nm. Between 2 and 3 a new spot of the sample was illuminated with 75 kW cm^{-2} for 30 minutes at 875 nm.

excitation signals as LH1 emission this implies that at high-power illumination energy transfer between LH2 and LH1 is reduced, consistent with an increased LH2 emission, and not for instance by LH2 photobleaching. We find similar effects for chromatophores in solution under prolonged white light illumination (not shown); in both cases these were not immediately reversible. Although an increased emission of LH2 may well explain the decoupling of LH2 to current generation as shown in the electrochemistry measurements, the differences in illumination powers applied does not allow a direct comparison between the two types of experiments.

Our photocurrent data showed the functionality of the gold-adsorbed membranes under aerobic conditions. We therefore compared the adsorbed native membrane assemblies under aerobic and vacuum conditions. We also investigated the effect of higher intensity illumination at 800 nm and 850 nm, probing mainly LH2 and both, LH2 and LH1, respectively. Figure 4 shows the results on the excitation and emission spectra for anaerobic and aerobic conditions and the effects of high power illumination. In figure 4A three fluorescence excitation spectra in vacuum are shown. The initial spectrum of the

native chromatophores (dotted curve, 150 W cm^{-2}), shows contributions from both LH2 (800 and 850 nm) and LH1 (875 nm). Also here we observed a decreased contribution of LH2 to the excitation spectrum relative to LH1, similar as in figure 3B. We observe significant bleaching (on a time scale of minutes) only when illuminating the sample at maximum laser output. After exposing the sample for 5 minutes to 800 nm light, at an intensity of 637 kW cm^{-2}, a decreased contribution of LH2 of 60% and LH1 of 15% of the initial peak value can be observed (solid line). A consecutive third spectrum was acquired after 5 minutes irradiation with 850 nm light, at 443 kW cm^{-2} (dashed curve). This results in a further reduction for both the B850 LH2 and LH1 signals and a minor effect on LH2 B800. A slight peak is observed at 890 nm of unknown origin, either it represents an effect of photobleaching or it may be emission leaking through the filters.

Light-irradiation dependent emission spectra of native membranes are shown in figure 4B. Emission spectra were obtained with excitation at 150 W cm^{-2}, in between spectral measurements the sample was exposed to high light intensities. In vacuum (left panel) we measure a 10% reduction in emission after irradiating the membranes for 5 minutes at 800 nm with 50 kW cm^{-2}. Only after prolonged irradiation (see legend for details) stronger photobleaching effects are observed. In air (right panel), we detect stable fluorescence emission at illumination power of 150 W cm^{-2} (solid line). In fact, also at higher light irradiation intensities we did not observe immediate photobleaching of LH1 or LH2 components. We illuminated membranes at 800 nm (5 minutes, 50 kW cm^{-2}, dotted line) and at 850 nm (30 minutes with 75 kW cm^{-2}, dashed line). Each measurement was performed on a fresh spot of the sample. We observed a gradually decreasing emission signal in time, down to 35% (800 nm excitation) and 15% (850 nm excitation) of the initial emission counts. A slight blue or red shift of emission maximum can be observed depending on the irradiation wavelength, indicating selective photobleaching of LH2 and LH1.

Our data show functional energy transfers and absence of photobleaching for gold-adsorbed membranes up to 2000 W cm^{-2} under anaerobic and 150 W cm^{-2} under aerobic conditions. It took several minutes of high power illumination before LH-systems started to become inactivated. But also at these high powers significant amounts of LH1 and LH2 remained photoactive, both in vacuum and under ambient conditions. LH2 complexes appear to be more easily photo-deactivated compared to LH1, first by decoupling energy transfer to LH1 under moderate intensities, then by photobleaching at higher intensities.

2.3.4 Photostability of isolated light-harvesting complexes

Results discussed in the previous section demonstrated the exceptional stability of the light-harvesting systems, even under aerobic conditions, when embedded within a membrane. These results are in stark contrast to many previously reported single-molecule experiments (Weiss, 1999). A large body of work exist on single-molecule fluorescence of the LH2 complex and all data confirm the rapid, irreversible photobleaching of this complex under aerobic conditions (Bopp et al., 1999). Membranes are assemblies of protein-complexes, forming an energy transfer network of hundreds of complexes, which in principle facilitates efficient energy dissipation even when some components are photobleached. From this viewpoint it is interesting to compare the photostability of the membrane-embedded pigment-protein complexes with that of isolated LH2 and LH1.

Fluorescence excitation and emission of isolated, detergent-solubilized LH1 and LH2 were measured under ambient conditions. Results on isolated LH1 and LH2 complexes bound onto a gold surface via engineered cysteine residues or mediated through self-assembled monolayers will be reported elsewhere. In all cases, the emission of isolated LH2 adsorbed on gold or other surfaces under aerobic conditions decreased within seconds to zero. LH1, most surprisingly, was much more stable under aerobic conditions. Figure 5A shows the excitation and emission spectra of WT LH1 complexes directly adsorbed onto a bare-gold surface and the emission counts at maximum obtained at various intervals of prolonged light irradiation. AFM images indicated the presence of approximately 100 well-separated, LH1 complexes within a focal spot (not shown). The excitation and emission spectra closely resemble LH1 solution spectra, showing no adverse effect on the structural and electronic configuration upon gold-adsorption. Irradiating LH1 for 6 consecutive hours with illumination powers of 73 to 647 W cm^{-2} only caused a few percent drop in LH1 emission. The superior photostability of LH1 is most clearly demonstrated by the fact that it required 10 to 15 hours of continuous irradiation with an intensity of 228 kW cm^{-2} to finally reduce the emission of LH1 down to 20% of the initial level.

Similar measurements were conducted on isolated LH1 complexes adsorbed onto a glass surface and again a steady emission signal was observed with high photostability (not shown). We also probed the stability of LH complexes dissolved in buffer solution under continuous white-light illumination. Also in this case the rate of photobleaching of LH2 was, as measured by emission intensity, 2 orders of magnitude faster than for LH1 (figure 5B). During this procedure, no significant change in the absorption spectra could be detected.

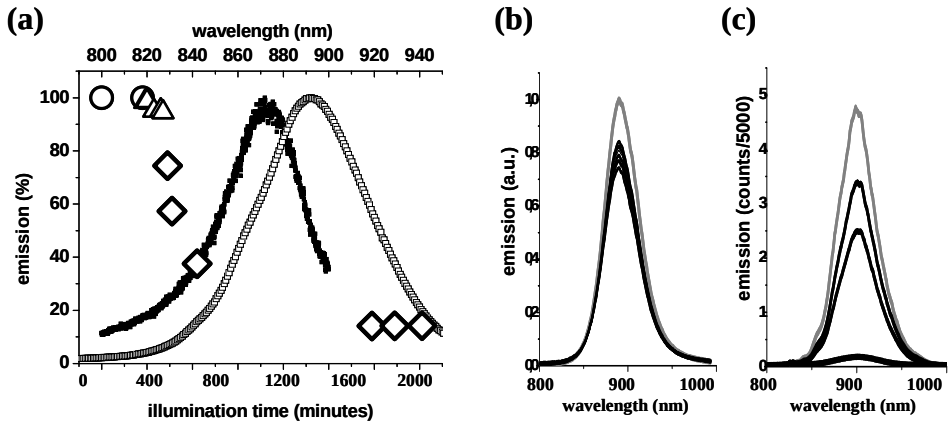


Figure 5. Photoactivity of LH1 in solution and adsorbed onto gold.

(A) Purified LH1 on gold: fluorescence excitation (black square) spectrum in vacuum and emission spectrum (open square spectrum in vacuum) and emission counts (circles, triangles and diamonds) at maximum in air. Power for excitation and emission spectra in vacuum 150 W cm^{-2}.

Emission counts obtained in air with illumination power of 73 W cm^{-2}, in between emission measurements light-irradiation powers were employed of 73 W cm^{-2} (circles), 647 W cm^{-2} (triangles), and 228 kW cm^{-2} (diamonds).

(B) LH1 in solution; emission spectra before (grey curve) and during (black curves) continuous white light illumination: Lowest curve obtained after 3 hours. Emission spectra obtained by broad excitation: 400-600 nm.

(C) LH1 in PVA spincoated on gold: consecutive confocal fluorescence emission spectra before (grey curve) and after removing the vacuum (black curves). Excitation at 825 nm, time between each spectrum is 60 seconds.

For comparison we also investigated purified WT-LH1 complexes in polyvinylalcohol, PVA, the preferred matrix for single-molecule experiments on photosynthetic complexes (Hofmann et al., 2003;Richter et al., 2007;van Oijen et al., 1999), spincoated onto a gold surface. Consecutive confocal fluorescence emission spectra of such preparation are shown in figure 5C, obtained at 60 seconds intervals. The initial emission spectrum displays an 8 nm red-shifted maximum compared to solution spectra or gold-adsorbed LH1 (figure 5A). Strikingly, upon release of the vacuum the emission vanishes rapidly. Apparently, the photostability of LH1 under aerobic conditions is lost in the PVA-matrix. PVA provides a dehydrated and rigid environment for LH1 that may induce structural distortions. AFM images of LH1 complexes showed large variations in shape attributed to the intrinsic flexibility of the circular LH1 proteins (Bahatyrova et al., 2004b). Our data here indicates that PVA acts upon this flexibility leading to structural deformations, resulting in a reduced photoactivity when exposed to air.

2.3.5 The function of LH2 and LH1 within membranes

Summarizing our results: we have shown that untreated, native chromatophores adsorb onto gold, and open up to form single membrane patches, while maintaining their primary

photoconversion function. Photocurrent generation and energy transfer are also retained under aerobic conditions. We found different contributions to the functioning of these membranes for the light-harvesting complexes LH2 and LH1. An important clue about these differences was obtained by comparing the photocurrent generation of RC-LH1-only mutant with that of native WT membranes. Where LH1 absorption can contribute fully to the photocurrent, LH2-born excitations were already partially inactive at the lowest light intensities applicable and more strongly upon increased light intensities. Concomitantly, applying confocal fluorescence spectroscopy we found an increased emission for the LH2 component within the membranes upon increasing the light intensity. This suggests a reduced energy transfer from LH2→LH1 accounting for a decreased fluorescence excitation signal.

Whereas isolated LH2 complexes photobleach immediately under ambient conditions, in native membranes LH2 only shuts down after high intensity irradiation. In contrast, isolated as well as membrane-embedded LH1 remained largely functional under the same conditions. From these observations we conclude firstly that within a network LH2 remains largely photostable. This is most likely due to the strongly reduced excited-state lifetime which reduces the probability of triplet state formation. Secondly, that at moderate light intensities the contribution of the LH2 complex to electron transfer is diminished. And thirdly, in comparison to LH2 the photostability of LH1 complexes proved to be extremely high. Likely it is this feature of LH1 that is responsible for the efficient functioning of the membranes under aerobic conditions.

It is tempting to relate these effects to physiological conditions. Within an aqueous environment bacteria will reside at optimum light intensity. But these may change over time, in dim light LH2 is synthesised to increase light absorption (Aagaard and Sistrom, 1972), but becomes superfluous when light intensity increases. Our data indicates three energy dissipating mechanisms: firstly, at low-light, LH2 becomes reversibly decoupled from photocurrent generation. Secondly, at intermediate-light we observed an increase in emission radiation, leading to less excitation transfer towards LH1 and ultimately the RC's. Unlike the former, this process is not immediately reversible. Last, at high-light LH2 shuts down completely. Obviously, some mechanism must exist to largely prevent the same effects to occur in LH1 because this would deplete the bacterium completely from energy. Indeed our data indicate that LH1 is designed to remain largely functional, also when exposed to air, even under harshest illumination conditions. We can only speculate about the possible causes for LH1 stability. Despite the similarity in the protein models of LH2 and LH1 significant differences must exist. There may be differences in carotenoid content

(Hunter et al., 1988). Carotenoids are also known to stabilise protein complexes, thus more carotenoids in LH1 would also make this complex more robust. But the main role of carotenoids is to prevent the BChl pigments from photo-oxidation via triplet exchange or singlet oxygen quenching (Cogdell et al., 2006). Both processes depend on the electronic structures of the BChl and carotenoids, the distances between them and the amount of carotenoids present, all yet unknown for LH1. The only other photosynthetic protein complex that has been shown to withstand photobleaching (up to 10 µW) when exposed to air is the peridinin-chlorophyll complex, or PCP that primarily consists of carotenoids (Wormke and et al., 2008). We showed that dissolving LH1 within a rigid PVA matrix removes this complex ability to function under aerobic conditions, likely by inducing structural deformations. Since these distortions cannot be short-range or specific, we speculate that the strong photoprotection of LH1 described here lies within a specific arrangement of each BChl-car unit within the ring of proteins.

2.4 Conclusion

Our work has demonstrated for the first time the possibility of interfacing native photosynthetic assemblies onto a gold-surface whilst retaining their optical activity and energy transforming capabilities. The native membranes are shown to be functional under aerobic conditions and withstanding illumination powers as high as direct solar irradiation.

Illuminating native membranes adsorbed onto a gold-electrode show the highest photocurrents generated to date and demonstrated a remarkable durability. The light-harvesting complexes have been shown to dissipate excess energy through decoupling, increasing emission radiation and photobleaching.

In contrast to isolated LH2 complexes, isolated LH1 complexes do not photobleach instantaneously under aerobic light conditions. We propose it is this robustness of the component linking energy- and electron transfers that allows photosynthesis to be largely retained in air, on a conducting surface and irradiated with high light. Our methodology presents a new way for detailed characterization of primary reactions of supramolecular light energy transducing assemblies.

Acknowledgement

Authors wish to thank Dre de Wit for growing the WT *Rb. sphaeroides* cells and isolating the chromatophores.

References

Aagaard, J. and W. R. Sistrom. 1972. Control of synthesis of reaction center bacteriochlorophyll in photosynthetic bacteria. *Photochem. Photobiol.* 15:209-225.

Bahatyrova, S., R. N. Frese, C. A. Siebert, J. D. Olsen, K. O. van der Werf, R. van Grondelle, R. A. Niederman, P. A. Bullough, C. Otto, and C. N. Hunter. 2004a. The native architecture of a photosynthetic membrane. *Nature* 430:1058-1062.

Bahatyrova, S., R. N. Frese, K. O. van der Werf, C. Otto, C. N. Hunter, and J. D. Olsen. 2004b. Flexibility and size heterogeneity of the LH1 light harvesting complex revealed by atomic force microscopy - Functional significance for bacterial photosynthesis. *Journal of Biological Chemistry* 279:21327-21333.

Bopp, M. A., A. Sytnik, T. D. Howard, R. J. Cogdell, and R. M. Hochstrasser. 1999. The dynamics of structural deformations of immobilized single light-harvesting complexes. *Proceedings of the National Academy of Sciences of the United States of America* 96:11271-11276.

Cogdell, R. J., P. K. Fyfe, S. J. Barrett, S. M. Prince, A. A. Freer, N. W. Isaacs, P. McGlynn, and C. N. Hunter. 1996. The purple bacterial photosynthetic unit. *Photosynthesis Research* 48:55-63.

Cogdell, R. J., A. Gall, and J. Kohler. 2006. The architecture and function of the light-harvesting apparatus of purple bacteria: from single molecules to in vivo membranes. *Quarterly Reviews of Biophysics* 39:227-324.

Fleming, G. R. and R. van Grondelle. 1994. The primary steps of photosynthesis. *Physics Today* 47:48-55.

Fraker, P. M. and S. Kaplan. 1971. Isolation and fractionation of the photosynthetic membranous organelles from Rhodopseudomonas spheroides. *J. Bacteriol.* 108:465-473.

Frese, R. N., J. D. Olsen, R. Branvall, W. H. J. Westerhuis, C. N. Hunter, and R. van Grondelle. 2000. The long-range supraorganization of the bacterial photosynthetic unit: A key role for PufX. *Proceedings of the National Academy of Sciences of the United States of America* 97:5197-5202.

Frese, R. N., J. C. Pamies, J. D. Olsen, S. Bahatyrova, C. D. van der Weij-deWit, T. J. Aartsma, C. Otto, C. N. Hunter, D. Frenkel, and R. van Grondelle. 2008. Protein shape and crowding drive domain formation and curvature in biological membranes. *Biophysical Journal* 94:640-647.

Frese, R. N., C. A. Siebert, R. A. Niederman, C. N. Hunter, C. Otto, and R. van Grondelle. 2004. The long-range organization of a native photosynthetic membrane. *Proceedings of the National Academy of Sciences of the United States of America* 101:17994-17999.

Guidelli, R. 2001. New directions and challenges in electrochemistry: bioelectrochemistry at metal-water interfaces. *Journal of Electroanalytical Chemistry* 504:1-28.

Hofmann, C., T. J. Aartsma, H. Michel, and J. Kohler. 2003. Direct observation of tiers in the energy landscape of a chromoprotein: a single-molecule study. *Proceedings of the National Academy of Sciences of the United States of America* 26:15534-15538.

Hunter, C. N., J. D. Pennoyer, and R. A. Niederman. 1982. Assembly and structural organization of pigment-protein complexes in membranes of Rhodopseudomonas sphaeroides. *Progress in Clinical and Biological Research* 102 Pt B:257-265.

Hunter, C. N., J. D. Pennoyer, J. N. Sturgis, D. Farrelly, and R. A. Niederman. 1988. Oligomerization states and associations of light-harvesting pigment-protein complexes of Rhodobacter sphaeroides as analyzed by lithium dodecyl sulfate-polyacrylamide gel electrophoresis. *Biochemistry* 27:3459-3467.

Jungas, C., J. L. Ranck, J. L. Rigaud, P. Joliot, and A. Vermeglio. 1999. Supramolecular organization of the photosynthetic apparatus of Rhodobacter sphaeroides. *Embo Journal* 18:534-542.

Kondo, M., Y. Nakamura, K. Fuji, M. Nagata, Y. Suemori, T. Dewa, K. Lida, A. T. Gardiner, R. J. Cogdell, and M. Nango. 2007. Self-assembled monolayer of light-harvesting core complexes from photosynthetic bacteria on a gold electrode modified with alkanethiols. *Biomacromolecules* 8:2457-2463.

Lebedev, N., S. A. Trammell, A. Spano, E. Lukashev, I. Griva, and J. Schnur. 2006. Conductive wiring of immobilized photosynthetic reaction center to electrode by cytochrome c. *Journal of the American Chemical Society* 128:12044-12045.

Lu, Y., J. Xu, B. Liu, and J. Kong. 2007. Photosynthetic reaction center functionalized nano-composite films: effective strategies for probing and exploiting the photo-induced electron transfer of photosensitive membrane protein. *Biosensors & Bioelectronics* 22:1173-1185.

Nie, S. M. and R. N. Zare. 1997. Optical detection of single molecules. *Ann. Rev. of Biophys. and Biomol. Struc.* 26:567-596.

Qian, P., P. A. Bullough, and C. N. Hunter. 2008. Three-dimensional reconstruction of a membrane-bending complex - The RC-LH1-PufX core dimer of Rhodobacter sphaeroides. *Journal of Biological Chemistry* 283:14002-14011.

Richter, M. F., J. Baier, J. Southall, R. J. Cogdell, S. Oellerich, and J. Kohler. 2007. Refinement of the x-ray structure of the RC-LH1 core complex from Rhodopseudomonas palustris by single-molecule spectroscopy. *Proceedings of the National Academy of Sciences of the United States of America* 104:20280-20284.

Sener, M. K., J. D. Olsen, C. N. Hunter, and K. Schulten. 2007. Atomic-level structural and functional model of a bacterial photosynthetic membrane vesicle. *Proceedings of the National Academy of Sciences of the United States of America* 104:15723-15728.

Siebert, C. A., P. Qian, D. Fotiadis, A. Engel, C. N. Hunter, and P. A. Bullough. 2004. Molecular architecture of photosynthetic membranes in Rhodobacter sphaeroides: the role of PufX. *Embo Journal* 23:690-700.

Sturgis, J. N., J. D. Tucker, J. D. Olsen, C. N. Hunter, and R. A. Niederman. 2009. Atomic force microscopic studies of native photosynthetic membranes. *Biochemistry* 48:3679-3698.

Suemori, Y. and et al. 2006. Self-assembled monolayer of light-harvesting core complexes of photosynthetic bacteria on an amino-terminated ITO electrode. *Photosynthesis Research* 90:17-21.

Trammell, S. A., A. Spano, R. Price, and N. Lebedev. 2006. Effect of protein orientation on electron transfer between photosynthetic reaction centers and carbon electrodes. *Biosensors & Bioelectronics* 21:1023-1028.

van Oijen, A. M., M. Ketelaars, J. Kohler, T. J. Aartsma, and J. Schmidt. 1999. Unraveling the electronic structure of individual pigment-protein complexes. *Science* 285:400-402.

Weiss, S. 1999. Fluorescence spectroscopy of single biomolecules. *Science* 283:1676-1683.

Wormke, S. and et al. 2008. Single molecule fluorescence of native and refolded peridinin-chlorophyll-protein complexes. *Journal of Fluorescence* 18:611-617.

Chapter 3

Enhanced photocurrent generation by photosynthetic bacterial reaction centers through molecular relays, light-harvesting complexes, and direct protein-gold interactions.

Abstract

The utilization of proteins as nano-devices for solar cells, bioelectronics and sensors generally necessitates the transfer of electrons to or from a conducting material. Here we report on efforts to maximize photocurrent generation by bacterial photosynthetic reaction center pigment-protein complexes (RCs) interfaced with a metal electrode. The possibility of adhering RCs to a bare gold electrode was investigated with a view to minimizing the distance for electron tunneling between the protein-embedded electron transfer cofactors and the metal surface. Substantial photocurrents were achieved despite the absence of coating layers on the electrode, or engineered linkers to achieve oriented deposition of RCs on the surface. Comparison with SAM-covered gold electrodes indicated enhanced photocurrent densities were achieved due to the absence of an insulating layer between the photoactive pigments and the metal. Utilizing RCs surrounded by the Light-Harvesting 1 complex resulted in higher photocurrents, surprisingly not due to enhanced photo-absorption but likely due to better surface coverage of uniformly oriented RC-LH1 complexes and the presence of a tetraheme cytochrome that could act as a connecting wire. Introduction of cytochrome-*c* (cyt-*c*) as a molecular relay also produced increases in current, probably by intercalating between the adhered RCs or RC-LH1 complexes and the electrode to mediate electron transfer. Varying the order in which components were introduced to the electrode indicated that dynamic rearrangements of RCs and cyt-*c* occurred at the bare metal surface. An upper limit for current generation could not be detected within the range of illumination power available, the maximum current density achieved by RC-LH1 complexes being of the order of 25 μA cm^{-2}. High currents could be generated consecutively for several hours or days under ambient conditions.

The contents of this chapter has been published in:

Mart-Jan den Hollander, J. Gerhard Magis, Philipp Fuchsenberger, Thijs J. Aartsma, Michael R. Jones, and Raoul N. Frese. 2011. Enhanced photocurrent generation by photosynthetic bacterial reaction centers through molecular relays, light-harvesting complexes, and direct protein-gold interactions. *Langmuir* 27:10282-10294.

3.1 Introduction

Photosynthetic reaction centers (RCs) transduce the energy of sunlight into a biologically useful form by separating electric charge across the photosynthetic membrane (Heathcote et al., 2002). The quantum yield (charges separated per photon absorbed) with which this is achieved is close to unity, due to highly efficient transfer of excited-state energy through the antenna pigments of the photosystem to the RC and highly efficient charge separation inside the RC (figure 1A-C,E).

As a result there has been considerable interest in whether the high-yield photovoltaic properties of natural RCs can be exploited in a device setting, and a number of laboratories have investigated photocurrent generation by RCs encapsulated in a solar cell or adhered to a functionalized metal electrode. Photocurrents have been reported for Photosystem I and Photosystem II RCs from plants or cyanobacteria (Badura et al., 2006;Ciesielski et al., 2008;Ciobanu et al., 2007;Das et al., 2004;Faulkner et al., 2008;Krassen et al., 2009;Maly et al., 2005;Terasaki et al., 2007;Terasaki et al., 2009;Yehezkeh et al., 2010) and from purple bacterial RCs isolated mainly from *Rhodobacter (Rba.) sphaeroides* (Das et al., 2004;Guidelli, 2001;Ham et al., 2010;Janzen and Seibert, 1980;Katz, 1994;Lu et al., 2007;Lu et al., 2005;Lukashev et al., 2007;Trammell et al., 2006;Trammell et al., 2007;Xu et al., 2007;Zhao et al., 2002b;Zhao et al., 2002a).
Studies have also been conducted on photocurrents generated by purple bacterial RC-LH1 complexes (Kondo et al., 2007;Suemori and et al., 2006); these constitute the native state of the RC in all characterized species of purple photosynthetic bacteria (figure 1D,E), and comprise the RC encircled by a LH1 light-harvesting pigment-protein (Cogdell et al., 1996;Cogdell et al., 2004;Hu et al., 2002;Roszak et al., 2003). Other applications of RCs have also been explored, including photosensors (Govorov and Carmeli, 2007;Terasaki et al., 2007), optoelectronic components (Kaniber et al., 2009;Sepunaru et al., 2009), gating elements for phototransistors (Frolov et al., 2008;Terasaki et al., 2007) and biosensors for the detection of herbicides (Giardi et al., 2009;Nakamura and Karube, 2003;Rea et al., 2009;Ventrella et al., 2010) and other environmental pollutants (Sanders et al., 2001).

Although they differ in terms of precise composition and mechanism, the various types of RCs found in nature display common structural and mechanistic themes (Heathcote et al., 2002). All are integral membrane proteins that contain either one or two membrane-spanning chains of redox-active cofactors that transfer an electron across the membrane in response to the photoexcitation of a chlorophyll species. In the case of the *Rba. sphaeroides* RC, the subject of this report, (see figure 1A-C), absorbed light energy drives transfer of an electron from a pair of bacteriochlorophylls (BChls) located close to the

periplasmic side of the photosynthetic membrane (termed the primary electron donor or P) to a ubiquinone termed Q_A on the cytoplasmic side, forming the so-called $P^+Q_A^-$ radical pair (see (Jones, 2009;Zinth and Wachtveitl, 2005) for reviews). For convenience, in the following the periplasmic (primary donor) and cytoplasmic (quinone) "ends" of the RC are referred to as P-side and Q-side, respectively (see figure 1A,B). The high quantum yield is assured by a number of factors, one of which is reduction of the photo-oxidized primary donor BChls (P^+) by a water-soluble cytochrome (cyt) c_2 on a time scale that is orders of magnitude faster than recombination of $P^+Q_A^-$ (Axelrod and Okamura, 2005;Pogorelov et al., 2007).

If a high quantum yield, and hence optimal current, is to be achieved from RCs in a photovoltaic device then it is similarly required that stabilization of charge separation occurs before radical pair recombination, this stabilization being achieved by transfer of the separated electron and hole to mediators or opposing electrodes.

Most studies of photocurrent generation by RCs have reported current densities of up to a few hundred nA cm^{-2} in response to red light illumination of a few tens of W cm^{-2} (Janzen and Seibert, 1980;Katz, 1994;Lebedev et al., 2006;Solovev et al., 1991;Trammell et al., 2004;Trammell et al., 2007;Xu et al., 2007;Zhao et al., 2002b;Zhao et al., 2002a). A smaller number have reported higher current densities of up to 120 µA cm^{-2} in response to light intensity of up to 10 W cm^{-2} (Das et al., 2004) with some studies generating microamp currents involving incorporation of RCs into mesoporous metal oxide films (Lebedev et al., 2006;Lu et al., 2005;Lukashev et al., 2007).

A feature common to almost all studies of photocurrent generation by RCs has been the use of a self-assembling monolayer (SAM) of organic molecules to coat the metal working electrode and provide a surface to which the protein will adhere (see (Lu et al., 2007) for a review). The SAM provides an insulating layer that prevents protein degradation or modification of the redox properties of cofactor. An appropriately functionalized SAM can also serve to orient the RC at the electrode surface to promote optimal photocurrent amplitude, and some studies have utilized proteins modified with a poly-histidine tag to facilitate this (Badura et al., 2006;Das et al., 2004;Lebedev et al., 2006;Maly et al., 2005;Nakamura et al., 2000;Reiss et al., 2007;Terasaki et al., 2008;Trammell et al., 2004;Trammell et al., 2006;Trammell et al., 2007). However, a potential drawback with this approach is that the SAM increases the distance between the electrode surface and the redox centers of the RC, which can greatly slow electron tunneling rates and potentially lead to a drop in quantum yield through unproductive charge recombination (see below).

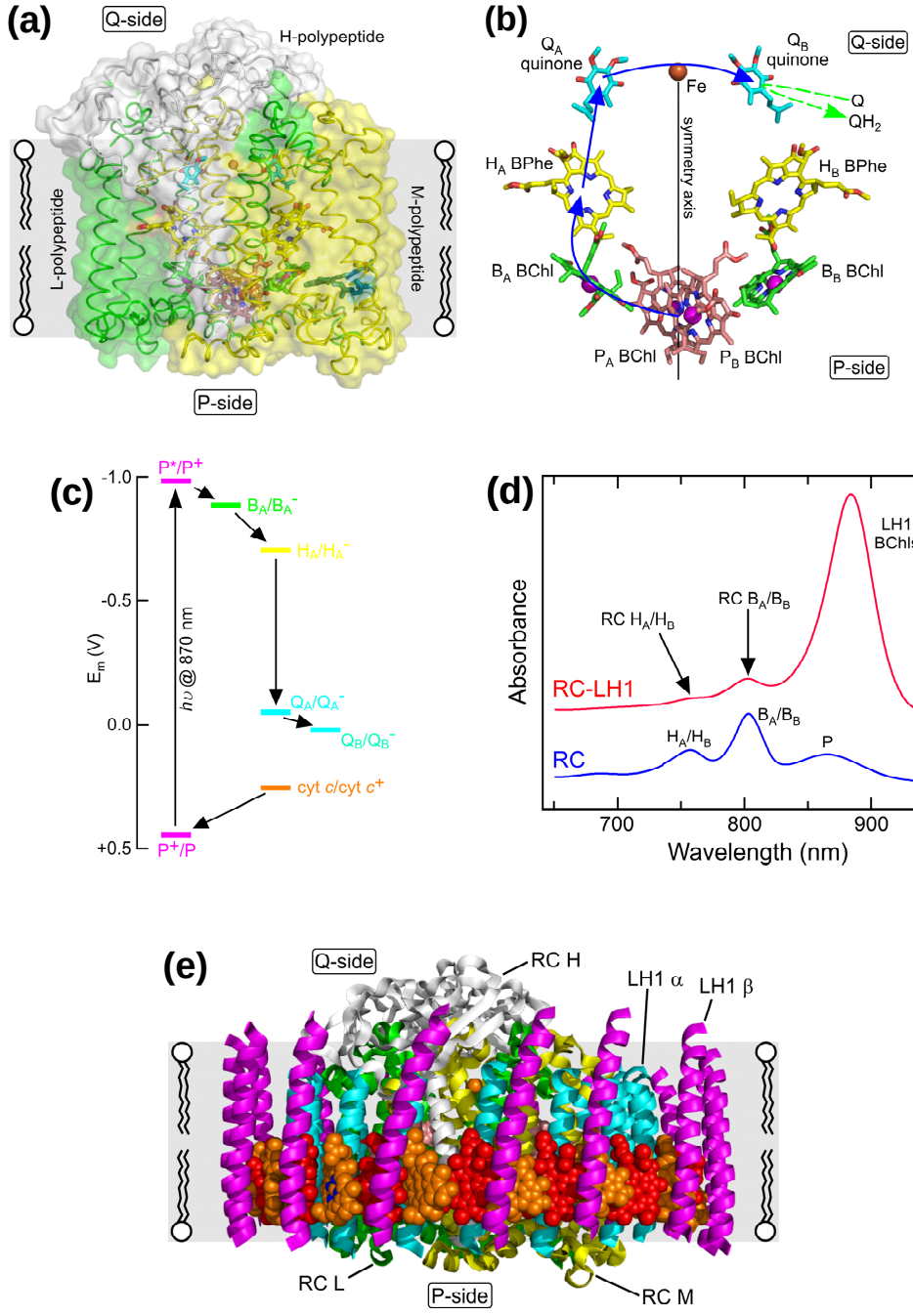

(a)
Q-side
H-polypeptide
L-polypeptide
M-polypeptide
P-side
(b)
Q_A quinone
Q_B quinone
Q-side
Fe
Q
QH_2
symmetry axis
H_A BPhe
H_B BPhe
B_A BChl
B_B BChl
P_A BChl
P_B BChl
P-side
(c)
E_m (V)
-1.0
-0.5
0.0
+0.5
P*/P+
B_A/B_A^-
H_A/H_A^-
Q_A/Q_A^-
Q_B/Q_B^-
cyt *c*/cyt c^+
P+/P
hυ @ 870 nm
(d)
Absorbance
LH1 BChls
RC H_A/H_B
RC B_A/B_B
RC-LH1
B_A/B_B
H_A/H_B
P
RC
700
800
900
Wavelength (nm)
(e)
Q-side
RC H
LH1 α
LH1 β
RC L
P-side
RC M

Figure 1.

Figure 1. Structure and pigment organisation in the photosynthetic reaction center of purple bacteria (Roszak et al., 2003).
(A) Overall structure. The protein surface shown as a semi-transparent object with the backbone fold of the H-, L- and M-polypeptides shown as white, green and yellow tubes, respectively. The approximate position of the membrane is shown as a grey box, with the primary donor side (P-side) and quinone side (Q-side) of the reaction center labelled. The embedded cofactors are shown as sticks, with the carotenoid (bottom left) shown with teal carbons.
(B) Enlarged view of the BChl, BPhe and quinone cofactors, color coded as in (A) with oxygens in red, nitrogens in blue and Fe and Mg atoms shown as brown or magenta spheres, respectively. Membrane-spanning electron transfer starts from the primary donor pair of BChls (P_A/P_B – pink carbons) and proceeds via the B_A BChl (green carbons), H_A BPhe (yellow carbons) and Q_A ubiquinone (cyan carbons). Electrons are passed on to the dissociable Q_B ubiquinone (cyan carbons), which can exchange with exogenous ubiquinone. The B_B BChl and H_B BPhe do not participate in electron transfer. For clarity the large hydrocarbon side-chains of the BChl, BPhe and quinone cofactors are not shown.
(C) Diagram of the redox potentials of the components relevant to the present study. Components are labelled with the convention reactant-redox-state/product-redox-state. Light absorption converts P into P*, triggering subsequent electron transfer to Q_B through a large change in redox potential. P^+ is reduced by cyt-*c*.
(D) Absorbance spectra of the *Rba. sphaeroides* RC and the *Rps. acidophila* RC-LH1, showing band attributions.
(E) Structure of the RC-LH1 complex from *Rps. palustris* (Roszak et al., 2003; PDB entry 1PYH – resolution 4.8 Å) The central RC, colored as for (A) and viewed from the same direction, is surrounded by concentric cylinders of multiple copies of alpha (cyan ribbons) and beta (magenta ribbons) polypeptides, sandwiching a ring of BChls (colored alternately red and orange).

Despite concerns about protein denaturation, a number of studies have been reported in which redox proteins were deposited directly on a bare metal or graphite electrode and found to retain full functionality. For example, yeast cyt-*c* was shown to remain functional on a bare-gold electrode surface despite the absence of an insulating layer (Heering et al., 2004). Interestingly, cyclic voltammetry yielded a rate of 1800 s^{-1} for reversible interfacial electron transfer between the electrode and the directly adsorbed cyt-*c* (Heering et al., 2004), in contrast to an earlier study in which a rate of 20 s^{-1} was obtained for yeast cyt-*c* adsorbed onto a gold electrode coated with a 3-mercapto-1-propanol SAM (Haas et al., 2001). This difference was attributed to the presence of an insulating SAM in the latter study, leading to slower electron tunneling between the cyt heme and the gold, although orientation effects also have to be considered (Heering et al., 2004).

To our knowledge, there have been only limited studies of photocurrent generation by RCs adsorbed to an unfunctionalized metal electrode. Site-directed mutants of the *Synechocystis* Photosystem I with an engineered surface-exposed cysteine have been adhered to a bare-gold electrode by incubation of the protein with the electrode for two hours at room temperature and have been found to be functionally active (Frolov et al., 2005). The adhered proteins were not removed by washing with deionized water, and it was also found that native Photosystem I complexes (which do not have any surface-exposed cysteines) could not be adhered by the same protocol, suggesting that the mutant Photosystem I complexes were attached to the electrode through the formation of a gold-sulphur covalent bond (Frolov et al., 2005). In the work of Heering and co-workers the yeast cyt-*c* was also believed to be attached to the bare-gold surface by a covalent bond with a surface-exposed cysteine side chain (Heering et al., 2004). Solovev and Erokhin (Solovev et al., 1991)

obtained a very small photocurrent from *Rb. sphaeroides* RCs adhered to a bare Pt electrode in the presence of cyt-*c*, but this was greatly enhanced if the Pt electrode was pre-coated with a SAM. In addition, Kondo et al. (Kondo et al., 2007) observed virtually no adherence of *Rps. palustris* RC-LH1 complexes to a bare-gold electrode, but did achieve adherence when the electrode was coated with a SAM.

Recently, we showed that it is possible to functionally connect patches of photosynthetic membrane from *Rba. sphaeroides* to a bare-gold surface, despite the fact that the pigment-proteins that are the major components of the membrane do not have surface-exposed cysteine residues (Magis et al., 2010). Remarkably, the adhered membranes remained functional for up to three days during continuous illumination under ambient conditions. These findings raise the question of whether photocurrents can be obtained from detergent-isolated pigment-proteins from such membranes simply by depositing them directly onto a bare-gold surface, and whether an intervening SAM or specialized linkers on the protein can be dispensed with.

In the present report we have attempted to adhere *Rba. sphaeroides* RCs and RC-LH1 complexes from *Rhodopseudomonas (Rps.) acidophila* to bare-gold electrodes. The proteins were found to attach to the electrode in a stable fashion and support large photocurrents. The findings demonstrate that there is much better compatibility between metal surfaces and proteins than is generally assumed, at least for this type of protein. Dynamic interactions at the membrane surface, including wiring by cyt-*c* first reported by Lebedev and co-workers for RCs adhered to a SAM-coated electrode (Lebedev et al., 2006), were also seen at the bare-gold electrode. The photocurrents obtained in the present study are among the highest reported to date, with the presence of intrinsic and extrinsic cytochromes as well as LH1 enhancing the photocurrent substantially. Possible reasons for this are explored.

3.2 Materials and Methods

3.2.1 Photosynthetic complexes

Rba. sphaeroides RCs were isolated according to procedures described previously (McAuley-Hecht et al., 1998) and suspended in 20 mM Tris-buffer (pH 8.0) and 0.1% lauryldimethylamine N-oxide (LDAO). *Rps. acidophila* RC-LH1 complexes were isolated according to Law (Law, C.J. Ph.D. thesis. 1999, University of Glasgow, Glasgow, United Kingdom), and suspended in 10 mM Tris-buffer (pH 8.0) containing 0.1% LDAO and 1 mM EDTA. Charge carriers in the medium were horse heart cyt-*c* (Sigma, 97% purity), and the water-soluble ubiquinone-0 (Q-0) (Aldrich, 99% purity).

3.2.2 Adhesion protocol

A bare-gold working electrode of 1 mm radius from BAS (United Kingdom) was cleaned prior to use by sonicating and rinsing with deionized water, then polishing in four stages using soft pads with aluminium oxide nanoparticles with decreasing sizes of 1000, 300, 50 and 15 nm diameter, the electrode being rinsed thoroughly after each stage. A 10 µL aliquot of RCs or RC-LH1 complexes (both at a concentration equivalent to an absorbance of 10 units at 870 nm) was deposited onto the cleaned electrode and left to incubate for 1 hour in the dark at 4 °C. The electrode was then rinsed three times with 3 mL of 10 mM potassium phosphate (pH 8) (measuring buffer) before insertion into the measuring cell.

3.2.3 Self-assembled monolayers

SAMs were prepared by immersing a gold electrode in a 1 mM solution of the desired alkanethiol molecule in a solution of degassed HPLC grade ethanol for 18 hours. The electrode was then placed in an ultrasonic bath for 5 minutes to remove any alkanethiol aggregates, rinsed in ethanol, dried under a stream of nitrogen and stored in pure ethanol. The alkanethiols used were 11-mercaptoundecanoic acid (C10 plus one carbon atom in the carboxyl group) and mercaptopropanoic acid (C2 plus one carbon atom in the carboxyl group) (Sigma Aldrich).

3.2.4 Experimental apparatus

The experimental apparatus had a standard three-electrode configuration, as described recently (Magis et al., 2010). The working, counter and reference electrodes were inserted into a home-built cell of 7 mL volume with an illumination window and ports for gassing. Most photocurrents were measured at applied potentials of between −0.1 and +0.1 V versus the standard calomel electrode (SCE) under ambient conditions, i.e. the sample was exposed to air. In experiments involving more negative or positive potentials the cell and buffer were bubbled with argon, and measurements were performed under an argon atmosphere.

Illumination was provided either from a home-built set of light emitting diodes (LEDs) with broad-band excitation (approximately 50 nm FWHM centered at 850 nm) from a white light source passed through a monochromator or from an argon-pumped Titanium-Sapphire (Ti-Sa) laser system (Coherent). The Ti-Sa laser also served as a calibration source for the illumination power of the other light sources. In particular, 850 nm LED illumination resulted in the same current as 20 mW cm^{-2} Ti-Sa excitation at 870 nm, and for the monochromator-based excitation the highest output at 870 nm corresponded to 15 mW cm^{-2}. A computer-controlled shutter was used to switch illumination on or off.

3.3 Results

3.3.1 Characteristics of RCs adhered to a bare-gold electrode

Rba. sphaeroides RCs were adhered to a clean bare-gold electrode of 1 mm radius by simply depositing 10 µL of a concentrated solution of RCs onto the electrode surface and incubating for one hour at 4 °C (see Materials and Methods). After rinsing to remove unadhered proteins, the electrode was immersed in a measuring cell (see Materials and methods) filled with 7 mL of 10 mM potassium phosphate (pH 8) supplemented with 100 µM Q-0 and 20 µM cyt-*c* to act as redox mediators (termed cyt-*c*/Q-0 buffer). The adherence of RCs to the electrode was tested by measuring their capacity to generate a photocurrent. The open circuit potential was set at −0.1 V (vs SCE), and the cell was illuminated with a white light source passed through a monochromator (intensity 1 mW cm^{-2} at 870 nm). Despite the use of an unfunctionalized electrode, illumination gave rise to a strong photocurrent that dropped to zero when illumination was terminated (see inset to figure 2A). The action spectrum of the photocurrent amplitude (figure 2A, black trace, with the amplitudes achieved when the light was turned on, shown as black squares) showed an excellent match to the absorbance spectrum of the RC in solution (figure 2A, red line). This action spectrum was obtained by repetitively switching of the light on and off for 10 second periods and stepping the excitation wavelength at 5 nm intervals during the dark periods while monitoring the current produced by a RC-adhered electrode in cyt-*c*/Q-0 buffer. This close approximation showed that the light-induced current arose from the RCs adhered to the bare-gold electrode. The maximum current at 800 nm excitation was approximately 2 nA, which equated to a current density of ~64 nA cm^{-2} (given that the surface area of the electrode was 3.14 mm^2). No currents were obtained if bare-gold electrodes with adhered RCs were suspended in measuring buffer lacking both Q-0 and cyt-*c* (data not shown).

These findings demonstrated that it was possible to adhere RCs to an unfunctionalized gold electrode using a very simple protocol, with the direction of the photocurrent indicating the flow of electrons from the gold electrode to the adhered RCs. Given what is known about charge separation in the RC, this implied reduction of the photo-oxidized primary electron donor (P^+) by the electrode, with the cycling of electrons from the quinone terminal of the RC to the counter electrode via a mobile redox carrier, is logically the Q-0 in the buffer. This further implied that the currents generated were from adhered RCs that were oriented P-side down on the bare-gold electrode.

Figure 2B compares the RC absorbance spectrum (red triangles) with an action spectrum for adhered RCs in cyt-*c*/Q-0 buffer recorded at the same potential of -0.1 V (black squares) and a higher illumination intensity of 10 mW cm^{-2}. Interestingly, this action

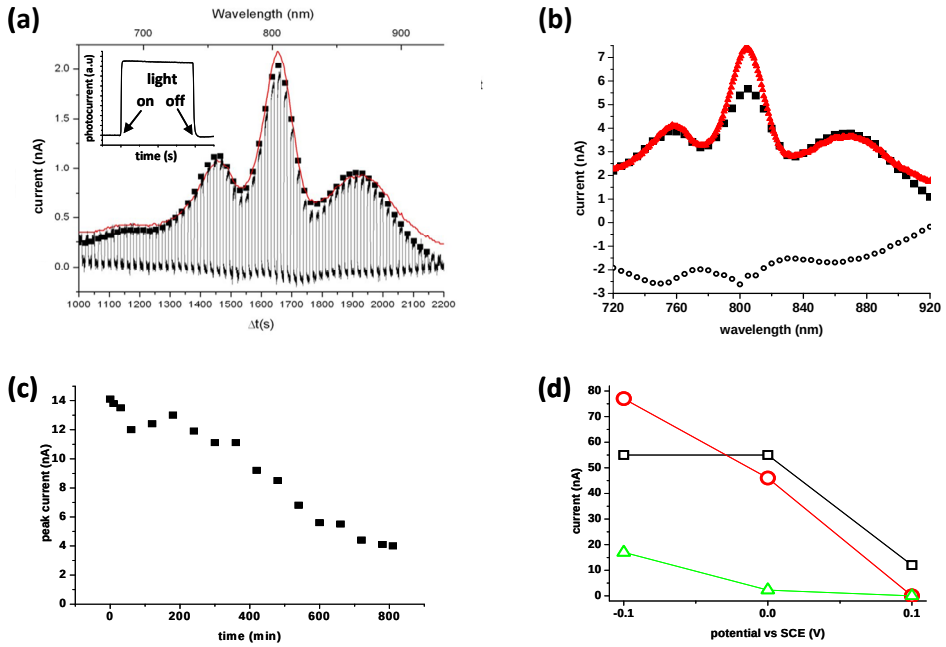


Figure 2. Photocurrents and action spectra obtained from RC complexes adhered to a bare-gold electrode.
(A) Action spectrum of photocurrent amplitude compared with the solution absorbance spectrum (solid red line). The raw data recorded over a period of 1200 seconds is shown as a continuous black trace, with the maximum amplitude of the current after each light-on event shown as a black square. The inset shows an individual light-on/light-off trace.
(B) Action spectra at a potential of -0.1 V (black squares) or -0.5 V (black open circles) compared with the solution absorbance spectrum (red triangles).
(C) Time dependence of the maximum photocurrent obtained during prolonged illumination with an 850 nm LED at +0.1 V.
(D) Maximum photocurrents obtained from RCs adsorbed onto a bare gold electrode (black squares), a C3-SAM (red circles) or a C10-SAM (green triangles) at three different applied potentials and illuminated with an 850 nm LED. The Power LED is equivalent to 20 mW cm^{-2} excitation at 870 nm. See the Materials and Methods section.

spectrum showed a decreased contribution of the accessory BChls at 802 nm relative to that of P at 867 nm and bacteriopheophytin (BPhe) at 760 nm (see figure 1E for attributions), in comparison with the action spectrum at the same potential obtained with a lower illumination power (figure 2A). The likely explanation for this is that the absorption coefficient of the accessory BChls is too high to utilize every absorbed photon for current generation.

An action spectrum was also measured at an applied voltage of -0.5 V (figure 2B - open circles). At this potential, the amplitude was strongly diminished and the current changed sign, indicating that the direction of electron transfer was reversed. At this potential, both the cyt-*c* and quinone are reduced, and it is also possible that the BPhe and perhaps

accessory BChl cofactors in the RC could be in the anion state (but not the special pair P). This reversed current was probably attributable to electron injection from P* into the gold electrode, with inefficient re-reduction of P^+ by the counter electrode mediated by the mobile redox carriers. This is consistent with the assignment that the RCs supporting the photocurrent were oriented P-side down on the bare-gold working electrode.

The adherence of the RCs to the bare-gold electrode was reasonably stable. Measurements on adhered RCs in cyt-*c*/Q-0 buffer at potentials between -0.1 V and +0.1 V using an 850 nm-emitting LED yielded near constant peak photocurrent amplitudes for the first 200 minutes (figure 2C). This was followed by a slow decrease such that after 10 hours of illumination the peak current was approximately 40% of the initial value. The prepared electrode could also be stored in the dark at 4 °C for several days without a loss of activity.

3.3.2 Comparisons with photocurrent generation by RCs adhered to an electrode coated with a SAM.

The observation of photocurrents derived from RCs adhered to a bare-gold electrode was somewhat surprising given the prevailing dogma that functionalization of a gold surface is required for stable binding of this type of protein. For comparison, photocurrents in cyt-*c*/Q-0 buffer were recorded for RCs adhered to gold electrodes functionalized with a 2-carbon (C2) or a 10-carbon (C10) SAM (see Materials and Methods). Measurements were made at applied potentials of +0.1, 0 and -0.1 V, and the peak currents obtained are plotted in figure 2D. At 0 V and -0.1 V, the currents obtained for the C2-SAM electrode (figure 2D, red circles) and the bare-gold electrode (figure 2D, black squares) were similar, whereas at +0.1 V a markedly lower current was obtained for the bare-gold electrode, and no current was obtained for the C2-SAM electrode. The simplest interpretation of this result was that the coverage of the electrode by RCs oriented in a manner favorable to the generation of a photocurrent was similar in the two cases.

At applied potentials of -0.1 and 0 V, a strong reduction in current was observed for the C10-SAM electrode (figure 2D - green triangles) relative to those obtained for the C2-SAM (figure 2D, red circles) and bare-gold electrode (figure 2D, black squares), whereas at + 0.1 V a current was not obtained with the C10-SAM electrode, matching the result with the C2-SAM electrode. In this case, the simplest interpretations of the data were either that the C10-SAM led to lower binding or a less favorable orientation of RCs at the electrode surface relative to that of the C2-SAM and bare-gold electrodes, or that photocurrent generation was lower because the thicker SAM resulted in a longer electron tunnelling distance between the adhered RCs and the electrode surface. This latter explanation would

be qualitatively consistent with the findings of Trammel et al (Trammell et al., 2007) that once the thickness of a SAM separating RCs from an electrode surface exceeds 10 Å the photocurrent declines by a factor of 0.8 per additional methylene group in the SAM. A well-ordered C2-SAM would be expected to form a coating layer of less than 10 Å thickness, whereas a well-ordered C10-SAM would be expected to be significantly thicker than 10 Å.

To summarize, within this range of open circuit potentials the presence of the C2-SAM had only modest effects on the peak photocurrent relative to that obtained with a bare-gold electrode, whereas a C10-SAM strongly reduced the peak current. Additional measurements will be required to determine whether these differences were due to variations in coverage of the electrode with RCs, differences in orientation of RCs at the surface, or differences in electron tunnelling distance between the adhered RCs and the gold electrode. However, it is possible to conclude that direct adhesion of RCs to the bare-gold electrode did not have an adverse effect on photocurrent generation relative to that observed for RCs adhered via an intervening C2 layer. This indicated that direct contact of the RC with the gold did not have an adverse effect on pigment-protein integrity or lead to decreased currents through the quenching of excitation by the adjacent metal surface.

3.3.3 The mechanism of photocurrent generation

The light-induced currents described above were obtained by simply immersing bare-gold electrodes with adhered RCs into a buffer containing 20 µM cyt-*c* and 100 µM Q-0. The action spectrum for current generation matched the RC absorbance spectrum and the direction of current indicated electron flow from the gold electrode to the adhered RCs and then on to the counter electrode via the redox mediators. No photocurrents were obtained when both Q-0 and cyt-*c* were omitted from the measuring buffer (data not shown). As explained above, the simplest way to interpret these data is that the RCs were adhered P-side down on the electrode with Q-0 acting as the redox mediator. If this is correct, then electron cycling could in principle be achieved with only Q-0 in the buffer solution if the gold electrode can directly reduce P^+. Accordingly, the requirement for cyt-*c* was investigated in a so-called QCQ measurement.

A bare-gold electrode with adhered RCs was inserted into a cell filled with measuring buffer containing only 100 µM Q-0 (referred to as Q-0 buffer). A small photocurrent with a peak value of ~0.2 nA was recorded in response to 22 s of illumination at an applied potential of -0.1 V (figure 3A - black squares, shown on a ten times expanded scale). This buffer was then replaced with measuring buffer containing only 20 µM cyt-*c* (cyt-*c* buffer),

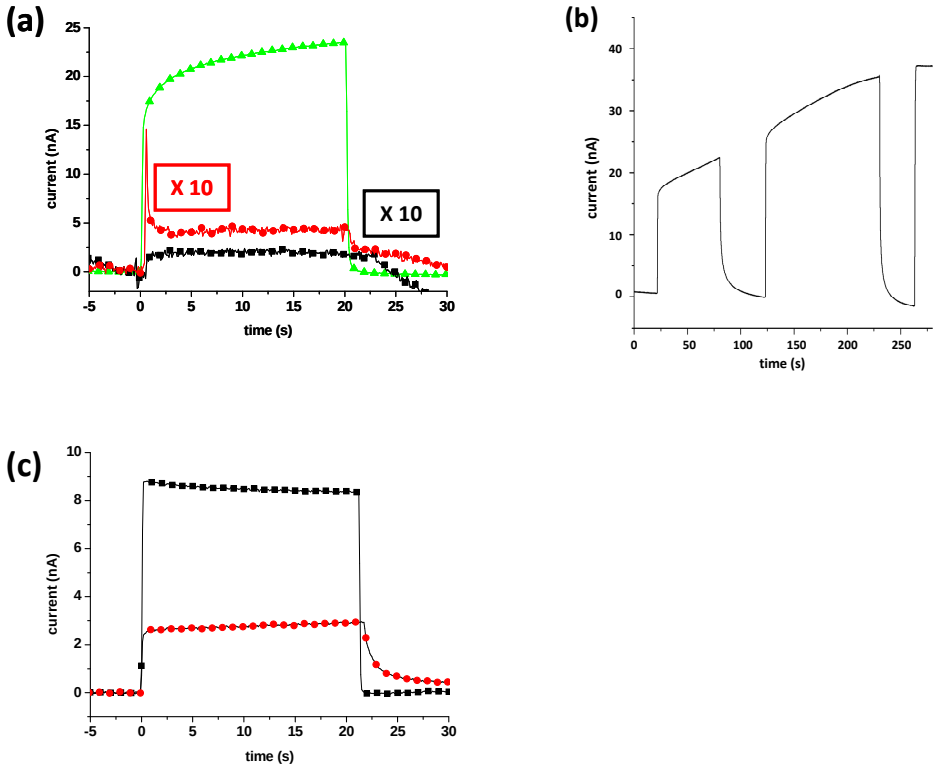


Figure 3. Effects of cyt-*c* on RC photocurrents.

(A) Photocurrents recorded during a QCQ measurement with Q-0 buffer (black squares, x10), cyt-*c* buffer (red circles x10), and a repeat of the Q-0 buffer (green triangles, not expanded).

(B) Increase in photocurrent amplitude after adding cyt-*c* to an RC-adhered electrode in Q-0 buffer. The light was switched off and then on twice during this measurement.

(C) Photocurrents recorded in UQ-0 buffer when cyt-*c* was added to a bare-gold electrode before (black squares) and simultaneously with (red circles) RCs. For all three panels, illumination was with an 850 nm LED and the applied potential was -0.1 V. The power LED is equivalent to 20 mW cm^{-2} excitation at 870 nm (see Materials and Methods).

and a similarly small photocurrent with a steady value of 0.5 nA was recorded in response to 20 s of illumination (figure 3A - red circles, shown on a ten times expanded scale). However, when this cyt-*c* buffer was replaced with a second volume of Q-0 buffer there was an ~ 50-fold increased amplitude in the measured photocurrent to a peak value of about 23 nA after 20 s (figure 3A - green triangles, not expanded).

This experiment demonstrated that sizeable photocurrents were obtained with only Q-0 in the buffer after exposure of the electrode to cyt-*c*. As outlined above, the probable role of Q-0 is to act as a redox mediator between the Q-side of the RC and the counter electrode.

The observed enhancement of the photocurrent amplitude by cyt-*c* was consistent with observations reported previously by Lebedev and co-workers for RCs oriented by a His_7 tag on a gold electrode coated with a Ni^{2+}-chelated nitrilotriacetic acid-terminated SAM (Lebedev et al., 2006). In that work, a ~20-40 fold increase in photocurrent was obtained from this electrode when a buffer containing 40 µM Q-2 was supplemented with 1 µM cyt-*c*. Under continuous illumination, the enhancement of current was seen to develop over an ~70 second period after the introduction of the cyt-*c* into the buffer, and it was retained when the electrode was rinsed and immersed in buffer lacking cyt-*c* (Lebedev et al., 2006). To account for these observations, it was proposed that molecules of cyt-*c* become sequestered between the adhered RCs and the gold surface, achieving "conductive wiring" of the RC cofactors to the substrate (Lebedev et al., 2006).

As indicated in figure 3A, a time-dependent increase in photocurrent amplitude was also seen for RCs adhered to a bare-gold electrode. This was examined more explicitly by adding cyt-*c* to a final concentration of 10 µM to an RC electrode immersed in Q-0 buffer and monitoring the resulting photocurrent. As shown in figure 3B, an increase in photocurrent to ~37 nA was observed over a period of ~250 seconds. Again, replacing the buffer in which this electrode was immersed with fresh Q-0 buffer did not produce a significant decrease in current amplitude (not shown), indicating that the cyt-*c* that had enhanced the current was strongly associated with the RC/gold electrode.

Figure 3C shows the consequences of two alternative fabrication sequences. In the first, a clean bare-gold electrode was pre-incubated with cyt-*c* buffer for one hour, rinsed, incubated with RCs for one hour, and rinsed again, and the photocurrent was measured in Q-0 buffer (figure 3C, red circles). This electrode generated a steady photocurrent of ~3 nA, which although small was 15-fold higher than that obtained with RCs adhered onto a bare-gold electrode without pre-incubation with cyt-*c* (figure 3A - black squares). In the second fabrication sequence, a clean bare-gold electrode was incubated with a mixture of RCs and cyt-*c* for one hour and rinsed, and the photocurrent was measured in Q-0 buffer (figure 3C, black squares). This electrode produced a higher peak-current of about 9 nA.

The finding from the first of these procedures demonstrated that cyt-*c* was adhered to the bare-gold electrode sufficiently tightly to resist washing and then formed additional interactions with the deposited RCs that enhanced the photocurrent relative to that seen with adhered RCs but not cyt-*c*. The higher current obtained when an electrode was incubated with a mixture of RCs and cyt-*c* could indicate that cyt-*c* first binds to RCs in solution before adherence to the gold such that the wiring phenomenon is more extensive

or efficient. However, the data in figure 3A indicated that the deposition procedure that produced the highest currents comprised the adherence of RCs to the electrode first and then adding cyt-*c* to enhance the electron flow. This suggests that adherence of the RC to the electrode is less efficient in the presence of cyt-*c* or it is more easily removed by rising.

3.3.4 Comparison of photocurrent generation by pre-adhered RCs and RCs in solution.

In principle, substantial electron transfer between the RCs and the gold surface, in either direction depending on applied potential, might also be obtained with RCs, cyt-*c* and Q-0 free in solution if: (1) cyt-*c* shuttles electrons from the anode to P^+, (2) Q-0 shuttles electrons from the photoreduced RC quinones to the cathode, and (3) there is sufficiently slow direct redox equilibration between the pools of reduced Q-0 and oxidized cyt-*c* (i.e., there is the absence of an internal short circuit). To investigate whether photocurrents could be obtained under such conditions, the response of an electrode immersed in a buffer containing RCs, Q-0 and cyt *c* was compared with those of electrodes fabricated using the sequential procedures described above.

Figure 4A compares data obtained from electrodes illuminated for between 20 and 33 seconds at an applied potential of -0.1V. A bare-gold electrode immersed in a measuring buffer solution supplemented with 100 µM Q-0, 20 µM cyt-*c* and 20 µM RCs gave rise to a steady photocurrent with a peak value of around 125 nA (figure 4A - black triangles). This was approximately twice the amplitude of the current obtained from an electrode with adhered RCs immersed in a mixture of 20 µM cyt-*c* and 100 µM Q-0 (figure 4A - red circles), and ~ 6-fold greater than the current obtained in the final stage of a QCQ measurement in which an electrode with adhered RCs was exposed to Q-0, then cyt-*c*, and then Q-0 again, with washing between steps (figure 4A - green squares). To examine whether this high 125 nA current was attributable to RCs that had adhered to the electrode, the buffer containing RCs, cyt-*c* and Q-0 was removed and replaced by buffer containing only cyt-*c* and Q-0. The maximum amplitude of the photocurrent obtained following buffer replacement was approximately 20% of that before replacement, suggesting that at least part of the original photocurrent was supported by RCs that had adhered to the electrode (data not shown).

Figure 4B shows equivalent data recorded at +0.1 V; a substantial current was obtained only for the experiment where all components were in solution (figure 4B, black triangles). The negative sign of the observed photocurrent indicated the flow of electrons into the gold electrode, probably with the Q-0 shuttling electrons between the quinone sites of the RCs

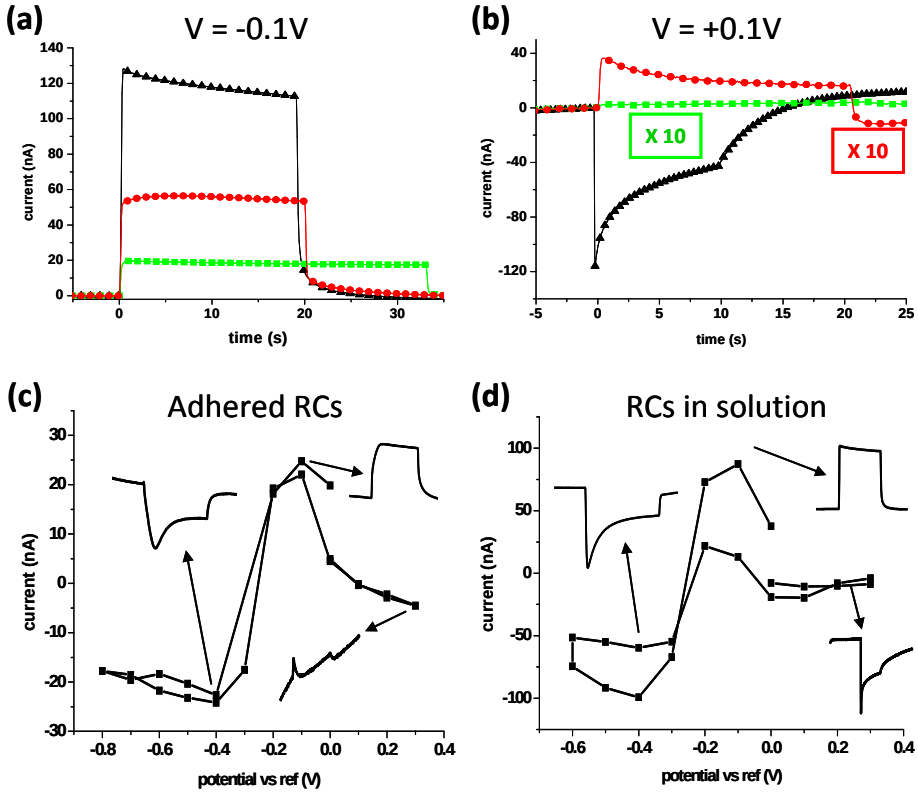


Figure 4. Photocurrents obtained with RCs adhered to the electrode and in solution.
(A,B) Photocurrents obtained at reducing (A) and oxidizing (B) potentials with RCs in a solution comprising measuring buffer with 100 µM Q-0, 20 µM cyt-*c* and 20 µM RCs (triangles), adhered onto an electrode immersed in cyt-*c*/Q-0 buffer (circles), and in a QCQ measurement as in figure 3. In (B), the traces with squares and circles are shown on a 10-fold expanded scale.
(C,D) Effects of cycling the applied potential on the maximum photocurrent obtained from RCs adhered to an electrode (C) and in solution (D). The insets show the light-on/light-off block currents at the potentials indicated by the arrows. In (C,D), measurements were performed under an argon atmosphere in cyt-*c*/Q-0 buffer. For all panels illumination was with an 850 nm LED. The Power LED is equivalent to 20 mW cm^{-2} excitation at 870 nm (see Materials and Methods).

in solution and the gold surface. The peak current, -120 nA, was comparable to that of the positive current at -0.1V. This demonstrates first that, in contrast to electrodes with adhered RCs, it was possible to reverse the direction of electron transfer at this potential when all three components were in solution and second that electron transfers at both potentials occur with the same likelihood.

Figures 4C and 4D show the variation in the peak photocurrent during cycling of the applied potential for adhered RCs in cyt-*c*/Q-0 buffer and for RCs in solution. These

measurements were conducted under an argon gas atmosphere with buffers that had been flushed with argon-gas. Currents were initially measured at 0 V and then adjusted to negative potentials and then to positive potentials. Individual light-on/light-off current traces at selected potentials are shown as insets. For both types of samples, substantial negative photocurrents (electrons injected into the gold-electrode) were recorded at applied potentials of -0.8 to -0.3 V, substantial positive currents were recorded at potentials of -0.2 to -0.1 V, and small negative currents were obtained at potentials of +0.1 to +0.3 V. Perhaps surprisingly, RCs in solution exhibited a stronger decrease in current amplitude upon potential cycling than adhered RCs. Nevertheless, we again found a substantial current for RCs in solution at +0.1V in contrast to that for adhered RCs. The reduction in current upon potential cycling for RCs in solution may be indicative of a history effect on the redox state of the charge carriers in the medium upon changing the potential. Currents from adhered RCs remained more constant, giving rise to similar peak-currents during two consecutive cycles of applied potential.

3.3.5 Photocurrent generation by RC-LH1 complexes

Having established that RCs could be adhered to an unfunctionalized gold electrode in a manner that supported sizeable photocurrents, it was also of interest to determine whether an RC-LH1 complex could be adhered in a similar fashion. A potential complication with using the *Rba. sphaeroides* RC-LH1 complex for such measurements is that it displays a dimeric architecture, with two RCs interconnected by an S-shaped LH1 antenna and a pronounced tilt of the two halves of the dimer relative to one another (Qian et al., 2008). This architecture contributes to the pronounced curvature of the photosynthetic membrane in *Rba. sphaeroides* and in principle it is not well suited to bringing the primary electron donor BChls of the RC into close proximity to an underlying planar electrode surface (see figure 3B of Qian et al. (Qian et al., 2008), for an illustration of this point). Previous studies of photocurrent generation by RC-LH1 complexes have utilized proteins from *Rhodospirillum (Rsp.) rubrum* (Ogawa et al., 2004;Suemori et al., 2007;Suemori and et al., 2006) and *Rps. palustris* (Kondo et al., 2007;Suemori and et al., 2006), but have generated rather small photocurrents with a density of 1-10 nA cm^{-2}.

As an alternative, we studied photocurrent generation by RC-LH1 complexes isolated from *Rps. acidophila*, a species that assembles monomeric RC-LH1 complexes housed in planar photosynthetic membranes (Tauschel and Hoeniger, 1974). Unlike the RCs from *Rba. sphaeroides*, *Rps. palustris* or *Rsp. rubrum*, the *Rps. acidophila* RC is associated with a tetra-heme cytochrome on the periplasmic side of the membrane that acts as the immediate reductant for the photo-oxidized primary electron donor (Matsuura and Shimada, 1986).

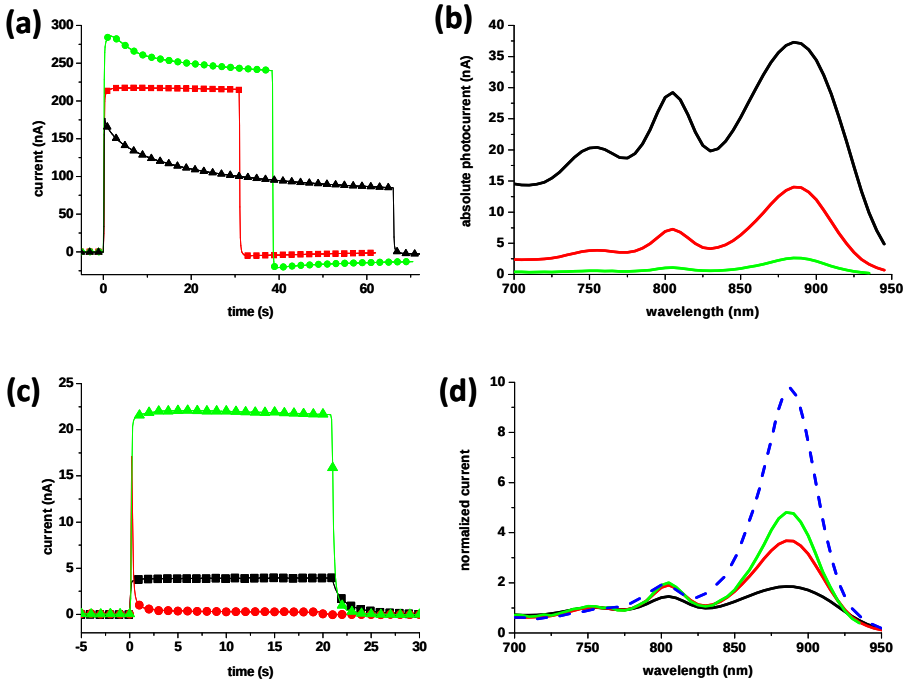


Figure 5. Photocurrents and action spectra obtained from RC-LH1 complexes adhered to a bare-gold electrode.
(A) Light-on/light-off photocurrents obtained from RC-LH1 complexes in a buffer containing 100 µM Q-0 and 20 µM cyt-*c* (triangles), 700 µM Q-0 and 20 µM cyt-*c* (squares), and 1000 µM Q-0 and 100 µM cyt-*c* (circles). Illumination was with an 850 nm LED.
(B,D) Wavelength dependence of RC-LH1 photocurrents at excitation powers of 0.5 (green), 3 (red), and 15 mW cm^{-2} (black) either not-normalized (B) or normalized at 750 nm (D). In (D), the solution absorbance spectrum of the RC-LH1 complex is also shown (blue dash).
(C) Photocurrents recorded during a QCQ measurement with Q-0 buffer (squares), cyt-*c* buffer (circles), and a repeat of the Q-0 buffer (triangles). Illumination was with an 850 nm LED. The power LED was equivalent to 20 mW cm^{-2} excitation at 870 nm (see Materials and Methods).

Figure 5A shows light-on/light-off photocurrents obtained with *Rps. acidophila* RC-LH1 complexes adhered to bare-gold electrodes at an applied potential of -0.1 V, and with increasing concentrations of Q-0 and cyt-*c* present as a mixture in the measuring buffer. The period of illumination varied between 30 and 66 seconds. A photocurrent peaking initially at ~175 nA and then decreasing was obtained with 100 µM cyt-*c* and 200 µM Q-0 (figure 5A, black triangles). For comparison, under similar conditions a maximum photocurrent 55 nA was observed for RCs adhered to a bare-gold electrode. At higher concentrations of cyt-*c* and Q-0, the RC-LH1 electrode achieved higher peak currents of 210 and 270 nA (figure 5A, red squares and green circles) and showed a less-pronounced decay. These values appeared to be the maximum current achievable solely by increasing

the concentrations of the charge carriers, with the 270 nA current recorded at 1000 µM Q-0 and 100 µM cyt-*c* equating to a current density of 8.6 µA cm^{-2} of the electrode surface.

Figure 5B shows photocurrent action spectra under illumination intensities (at 870 nm) of 0.5 (green), 3 (red) and 15 mW cm^{-2} (black). The absorbance bands of the RC at 760 and 802 nm and of LH1 at 885 nm (see figure 5C, blue dashed line) were clearly visible in these action spectra, demonstrating the origin of the photocurrent, and higher illumination intensities resulted in higher photocurrents. The same photocurrent action spectra are shown in figure 5C, normalized to a fixed amplitude of the band with a maximum near 760 nm, which arises from the BPhe pigments of the RC. For comparison, the solution absorption spectrum of the RC-LH1 complex (blue dash) is shown. A comparison of figures 4b and 4c shows that at lower illumination intensities the relative contribution of the LH1 antenna BChls at 885 nm to the light-induced current was much greater than at higher intensities. At the highest illumination power, the contribution of the LH1 BChls to the current was only approximately 20% of their absorbance (figure 5C). In fact even at lowest excitation power possible, 0.5 mW cm^{-2}, the LH1 chromophores contributed only 50% relative to the absorbance spectrum. Similar effects have been observed with RC-LH1 and LH2 complexes in photosynthetic membranes (Magis et al., 2010) and may be partially explained by the quenching of excitations by the gold (Lakowicz, 2001). However, illuminating with much higher light intensities (see below) resulted in a steady increase of photocurrent showing the electron transfer not to be a bottleneck. Taken together with our previous data on membranes (Magis et al., 2010), this indicates that light harvesting complexes make the strongest contribution to photocurrents at very low light intensities.

The excitation power dependency of the action spectra showed very similar characteristics for an electrode precoated with a C2-SAM before adherence of RC-LH1 complexes (data not shown). This indicated that the reduction in the relative contribution of LH1 to the current did not depend on the distance between the complexes and the gold and was not due to a partially destructive effect of the bare-gold surface on the LH1 pigment-protein.

Figure 5D shows results of a QCQ measurement on adhered RC-LH1 complexes using 100µM Q-0 and 20 µM cyt-*c*. In contrast to the situation for RCs, a sizeable steady-state current of about 4 nA was obtained initially with only Q-0 in the medium (figure 5D - black squares). After removing Q-0 and adding cyt-*c*, a high initial current was observed that quickly decreased to zero (figure 5D - red circles), the expected result in the absence of the mediator that shuttles electrons between the Q-side of the RC and the counter electrode. After the cyt-c buffer was removed and Q-0 was added, again a steady current of 22 nA

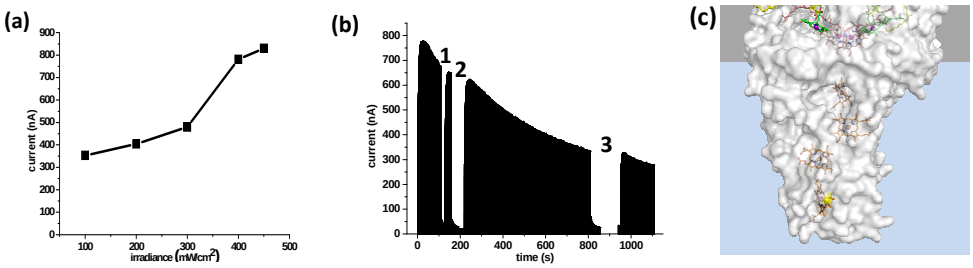


Figure 6. Light intensity and time dependence of maximum photocurrents obtained with RC-LH1 complexes adhered to a bare-gold electrode.

(A) Illumination with a Ti-Sa laser at 870 nm at different intensities.

(B) Photocurrent obtained during prolonged laser illumination at maximum intensity. Periods during which currents are generated indicated in black; the three dark periods are indicated by 1-3.

(C) View of the tetraheme cytochrome attached to the periplasmic face of the membrane-embedded subunits of the *Rps. viridis* RC (PDB entry 1R2C – Baxter et al. 2004). The protein is shown as a semi-transparent surface with the approximate positions of the membrane and aqueous phases shown as grey and light-blue boxes, respectively. The embedded heme and the BChl and BPhe cofactors are shown as sticks, with the cysteine sulphur mentioned in the text shown as a yellow sphere. For the cofactors, oxygen is shown in red, nitrogen is shown in blue, and iron and magnesium are shown as brown and magenta spheres, respectively. Only part of the membrane-embedded region is shown, with P_A/P_B BChls having pink carbons, B_A/B_B BChls having green carbons, and H_A/H_B BPhes having yellow carbons (see figure 1).

was obtained (figure 5D - green triangles). Thus, for RC-LH1 complexes a photocurrent could be obtained in the absence of cyt-*c*, but a ~6-fold increase in the current was seen on adding cyt-*c*. Cycling the potential did not result in a change in the sign, lineshape, or magnitude of these photocurrents (not shown).

Photocurrents induced by much higher light intensity laser illumination were also investigated using adhered RC-LH1 complexes with cyt-*c* and Q-0 in the buffer. Increasing light intensities from 100 to 450 mW cm^{-2} (at 870 nm), the maximum achievable with this excitation source, increased the peak current continuously up to approximately 800 nA (figure 6A), equating to a current density of ~25 µA cm^{-2}. This suggests that the current over this range of excitation intensities was not limited by the rate of electron tunnelling between the gold surface and the RCs or between the RCs and the counter electrode, but rather by the rate of photoexcitation. A continuous illumination of adhered RC-LH1 complexes at the highest power over a 20 minute period produced a steadily decreasing photocurrent (figure 6B). During this decrease, the light was blocked at three intervals, numbered in figure 6B. For the first 100 seconds of this experiment, there was a rapid decrease in the current, and the initial short, dark period at 100 seconds did not seem to prevent further reduction. A second, somewhat longer dark period starting at 160 seconds did seem to result in a less rapid reduction in current, as assessed from the initial current

amplitude obtained when illumination was restored. Interestingly, after the third dark period, between 800 and 950 seconds, the currents resumed at a similar value to that present when illumination was blocked at 800 seconds. Thus, after the initial fast decrease from the highest values a regime was reached where the current decreased only because of illumination.

It should be noted that decay of the current obtained with RC-LH1 complexes on switching off the light was not instantaneous (figure 5D, squares), so it was possible to gain information about the coverage of the electrode from the steady state amplitude of the light response current (4 nA) and the rate of exponential decay to the background level ($t_{1/2}$ ~ 1 s). The total amount of charge removed from the electrode after the light was turned off was Q = (amplitude * $t_{1/2}$) / ln 2 = 5.5 nC, and to take this amount of charge from the electrode, a minimum of $5.5 \times 10^{-9}/1.6 \times 10^{-19} = 3.4 \times 10^{10}$ RC special pairs would have to be oxidized at the point at which the light was switched off. This number coincides well with a fully covered electrode; the area of one RC-LH1 complex is approximately 144 nm^2 (Roszak et al., 2003), and thus the number of RC-LH1 complexes in a tightly-packed monolayer on an electrode with a surface area of 3.14 mm^2 is expected to be 3.5×10^{10}. This calculation is therefore consistent with a fully covered electrode with most RC-LH1 complexes oriented with the P-side facing the gold.

3.4 Discussion

3.4.1 Is it possible to dispense with a SAM for adherence of RCs to a gold electrode?

Although it is known that redox proteins can be adsorbed onto an unmodified gold electrode in a manner that retains functionality, documented cases of protein degradation on bare metal surfaces have led to a common approach in the construction of RC-coated electrodes in which the metal surface is first coated with a SAM of some description. This SAM not only insulates the RC from the bare-metal surface but also provides options for orienting the RC at the electrode through the use of a poly-His tag or by binding surface-exposed basic residues. However, as explored experimentally using Photosystem I RCs, a SAM of over a certain thickness can also reduce the rate of electron tunnelling between the metal electrode and the redox centers of the RC (Trammell et al., 2007), so benefits derived from improved protein stability/optimized protein orientation have to be balanced against drawbacks deriving from the insulating effect of the SAM.

The experiments described above demonstrate that unmodified RCs and RC-LH1 complexes can be stably adhered to a bare-gold electrode by simply incubating the metal

surface with a concentrated solution of protein for one hour at 4 °C. Complexes adhered to the electrode sufficiently strongly to resist rinsing and in the case of RCs produced a photocurrent with maximum amplitude of 0.2 nA when exposed to illumination in the presence of Q-0 as a redox mediator. Given the area of the electrode, this equated to a current density of ~6.4 nA cm^{-2}. The addition of 100 µM cyt-*c* to the measuring buffer containing Q-0 brought about a large time-dependent increase in this current density to ~1178 nA cm^{-2}. Cyt-*c* was also found to be bound to the surface of a bare-gold electrode in a fashion that resisted rinsing, and when it was adhered prior to RC binding, a current density of 96 nA cm^{-2} was obtained. Sizeable photocurrents were also obtained by incubating electrodes with a mixture of RCs and cyt-*c* (287 nA cm^{-2}).

This enhancement of photocurrent density by cyt-*c* was presumably through the "conductive wiring" effect first reported by Lebedev et al. (Lebedev et al., 2006). Our observations extend those of Lebedev and co-workers by showing that this enhancement was also seen when cyt-*c* was bound to the electrode prior to the addition of RCs or when electrodes were incubated with a mixture of cyt-*c* and RCs and that the protein-protein interactions involved can form when the RCs and cyt-*c* are adhered to a metal electrode that has not been coated with a SAM. The highest current density was obtained when RCs were adhered to the electrode first and then cyt-*c* was added to the measuring buffer.

3.4.2 How do RCs and RC-LH1 complexes adhere to a bare-gold electrode?

As far as we are aware, there have been only three published reports of attempts to adhere RC or RC-LH1 complexes to an unfunctionalized metal electrode. As summarized in the Introduction, the adherence obtained and photocurrents generated were either zero or extremely low (Frolov et al., 2005;Kondo et al., 2007;Solovev et al., 1991).

In the experiments described above. both *Rba. sphaeroides* RCs and *Rps. acidophila* RC-LH1 complexes were found to adhere to a bare-gold electrode sufficiently strongly to resist several steps of rinsing and buffer exchange and in a sufficient quantity to support relatively high photocurrents. The mechanism of binding of these complexes to the metal surface is not clear. In the case of the *Rba. sphaeroides* RCs, it is known that the protein sequence includes five cysteine residues, but none is in a position that would be conducive to anchoring the P-side of the RC to an underlying metal surface. The X-ray crystal structure shows that three of these cysteines are buried and the fourth is exposed at the intramembrane surface of the protein and therefore presumably screened by the detergent micelle (Allen et al., 1987). The fifth is located close to the cytoplasmic surface of the H-polypeptide (Cys H156) and has been used by at least two laboratories to anchor the RC Q-

side down onto a functionalized surface via a linker molecule coated onto the electrode as a SAM (Katz, 1994;Reiss et al., 2007). This cysteine is partially buried, and it is not clear that it could bind directly to a gold surface without significant distortion of the protein structure.

In the case of the *Rps. acidophila* RC-LH1 complex, it is known that the LH1 polypeptides do not contain cysteines (Brunishoz and Zuber, 1992), but to our knowledge, the sequences of the four RC polypeptides have not been reported. However, it is worth noting that the tetraheme cytochrome subunit of this type of RC has four pairs of conserved cysteines that bind the four c-type hemes, and according to the X-ray crystal structures of the *Blastochloris viridis* and *Thermochromatium tepidum* RCs (Deisenhofer et al., 1995;Nogi et al., 2000), one of these is surface-exposed near the tip of the cytochrome subunit at a point furthest away from the membrane (figure 6C). It is possible that this cysteine could form an interaction with the gold surface, although this would require a disruption of the binding of the heme furthest from the bacteriochlorin cofactors of the intramembrane part of the RC. This could explain the fact that the binding of RC-LH1 complexes was seen in the present case but not in the studies of Kondo and co-workers on *Rps. palustris* RC-LH1 complexes (Kondo et al., 2007).

3.4.3 Is it necessary to adhere RCs to the working electrode to achieve high photocurrents?

To our surprise, the highest RC photocurrents were obtained by simply immersing a bare-gold electrode in a buffer solution containing RCs, cyt-*c* and Q-0. A maximum current density in the region of 3980 nA cm^{-2} was obtained, some 3 to 4 times greater than when RCs were pre-adhered to the bare-gold electrode and cyt-*c* was added. This is in marked contrast to the general idea that it is necessary to attach oriented RCs to the electrode prior to immersion in a buffer containing mediators. This requirement is based on sound principles addressing the need to avoid short-circuits by ensuring that the process that delivers electrons to the photo-oxidized “terminal” of the RC is separate from the process that removes electrons from the photoreduced terminal. In the present case, for example, a high rate of oxidation of the reduced form of Q-0 by oxidized cyt-c_2 would result in unproductive cyclic electron transfer from the Q-side of the RC to the P-side and a diminished (or zero) current through the external circuit. A way to minimize such unproductive redox reactions in the measuring buffer is to couple the P-side of the RC to the working electrode in such a way that there is direct reduction of the photo-oxidized primary electron donor by the metal electrode (or indirect transfer via sequestered molecules of cyt-*c*). The finding in the present work that the highest currents were obtained

by simply immersing a bare-gold electrode into a buffer containing RCs, cyt-*c* and Q-0 could mean that these conditions are optimal for adhering RC/cyt-*c* complexes to the working electrode. Alternately, it could be that the particular choice of redox mediators in this experimental setup, horse heart cyt-*c* and ubiquinone-0, leads to a sufficiently small amount of futile cycling of electrons by which a large photocurrent can be supported. It seems likely that the observed high current in this experiment was supported partially by adhered RCs and partially by RCs free in solution, where replacing the measuring buffer with one containing only cyt-*c* and Q-0 led to the production of a photocurrent that had 20% of the original amplitude, indicating that some of the RCs were adhered to the bare-gold electrode.

3.4.4 Microamp photocurrents obtained from RC-LH1 complexes adhered to a working electrode.

Previous studies of photocurrent generation by RC-LH1 complexes have focussed on the proteins from *Rsp. Rubrum* (Ogawa et al., 2004;Suemori et al., 2007;Suemori and et al., 2006) and *Rps. Palustris* (Kondo et al., 2007;Suemori and et al., 2006) adhered to SAM-coated gold or indium tin oxide electrodes, with sodium perchlorate and methyl viologen as redox mediators. These have reported small photocurrents with a density of 1-10 nA cm^{-2}, which is 3 to 4 orders of magnitude lower than the highest photocurrent for the *Rps. acidophila* RC-LH1 complex obtained in this work (~25 µA cm^{-2}). This difference could be due to a number of factors, such as illumination intensities (previous studies employed monochromatic excitation as in the present work but incident intensities were not reported) and differences in redox mediators, cyt-*c*/Q-0 in the present work, and sodium perchlorate/methyl viologen in previous studies (Kondo et al., 2007;Ogawa et al., 2004;Suemori et al., 2007;Suemori and et al., 2006). Another possibility is that the presence of the RC tetraheme cytochrome in the *Rps. acidophila* RC-LH1 complexes used in the present report produced the very high currents by acting as a "wire" for conducting electrons from the gold electrode to the RC BChl cofactors (figure 6C) with further enhancement by sequestered molecules of cyt-*c*. Finally, the lack of an intervening SAM in the present study may also have contributed to the observed high currents. Kondo et al (Kondo et al., 2007) have reported that photocurrent densities for RC-LH1 complexes are sensitive to the type of underlying SAM.

3.5 Conclusions

This work demonstrates for the first time photocurrent generation by photosynthetic RC and RC-LH1 complexes interacting with a bare-gold electrode. These proteins and cyt-*c* remained intact and functional when associated with the bare-gold surface and under

ambient conditions. Electron transfer occurred both from the gold towards the RCs and vice versa, with the direction of current being determined by the applied potential. This work also shows for the first time substantial light-induced currents from RCs in solution rather than pre-adhered to the electrode, with a notably different potential dependency than for pre-adsorbed complexes. Very high photocurrents were also obtained from *Rps. acidophila* RC-LH1 complexes adhered to a bare-gold electrode but were not due to enhanced light absorption but possibly to the wiring of the RC bacteriochlorin cofactors to the electrode by the tetraheme cytochrome subunit associated with this type of RC. The findings demonstrate that the modification of the protein component with specific linkers or the functionalization of the metal electrode is not necessarily required to obtain high photocurrents from purple bacterial photovoltaic proteins, and greatly simplified fabrication procedures can be used.

Acknowledgement

We thank Nick Reynolds for help with the SAM protocol, Dre de Wit for growing the Rps. acidophila strain and purifying the RC-LH1 complexes, and Tatyana Kropacheva and Dirk Heering for help setting up the initial cyclic voltammetry experiments.

References

Allen, J. P., G. Feher, T. O. Yeates, H. Komiya, and D. C. Rees. 1987. Structure of the Reaction Center from Rhodobacter-Sphaeroides R-26 - the Cofactors .1. *Proceedings of the National Academy of Sciences of the United States of America* 84:5730-5734.

Axelrod, H. L. and M. Y. Okamura. 2005. The structure and function of the cytochrome c(2): reaction center electron transfer complex from Rhodobacter sphaeroides. *Photosynthesis Research* 85:101-114.

Badura, A., B. Esper, K. Ataka, C. Grunwald, C. Woll, J. Kuhlmann, J. Heberle, and M. Rogner. 2006. Light-driven water splitting for (bio-)hydrogen production: photosystern 2 as the central part of a bioelectrochemical device. *Photochemistry and Photobiology* 82:1385-1390.

Brunishoz, R. A. and H. Zuber. 1992. STRUCTURE, FUNCTION AND ORGANIZATION OF ANTENNA POLYPEPTIDES AND ANTENNA COMPLEXES FROM THE 3 FAMILIES OF RHODOSPIRILLANEAE. *Journal of Photochemistry and Photobiology B-Biology* 15:113-140.

Ciesielski, P. N., A. M. Scott, C. J. Faulkner, B. J. Berron, D. E. Cliffel, and G. K. Jennings. 2008. Functionalized Nanoporous Gold Leaf Electrode Films for the Immobilization of Photosystem I. *Acs Nano* 2:2465-2472.

Ciobanu, M., H. A. Kincaid, V. Lo, A. D. Dukes, G. K. Jennings, and D. E. Cliffel. 2007. Electrochemistry and photoelectrochemistry of photosystem I adsorbed on hydroxyl-terminated monolayers. *Journal of Electroanalytical Chemistry* 599:72-78.

Cogdell, R. J., P. K. Fyfe, S. J. Barrett, S. M. Prince, A. A. Freer, N. W. Isaacs, P. McGlynn, and C. N. Hunter. 1996. The purple bacterial photosynthetic unit. *Photosynthesis Research* 48:55-63.

Cogdell, R. J., A. T. Gardiner, A. W. Roszak, C. J. Law, J. Southall, and N. W. Isaacs. 2004. Rings, ellipses and horseshoes: how purple bacteria harvest solar energy. *Photosynthesis Research* 81:207-214.

Das, R., P. J. Kiley, M. Segal, J. Norville, A. A. Yu, L. Y. Wang, S. A. Trammell, L. E. Reddick, R. Kumar, F. Stellacci, N. Lebedev, J. Schnur, B. D. Bruce, S. G. Zhang, and M. Baldo. 2004. Integration of photosynthetic protein molecular complexes in solid-state electronic devices. *Nano Letters* 4:1079-1083.

Deisenhofer, J., O. Epp, I. Sinning, and H. Michel. 1995. CRYSTALLOGRAPHIC REFINEMENT AT 2.3-ANGSTROM RESOLUTION AND REFINED MODEL OF THE PHOTOSYNTHETIC REACTION-CENTER FROM RHODOPSEUDOMONAS-VIRIDIS. *Journal of Molecular Biology* 246:429-457.

Faulkner, C. J., S. Lees, P. N. Ciesielski, D. E. Cliffel, and G. K. Jennings. 2008. Rapid assembly of photosystem I monolayers on gold electrodes. *Langmuir* 24:8409-8412.

Frolov, L., Y. Rosenwaks, C. Carmeli, and I. Carmeli. 2005. Fabrication of a photoelectronic device by direct chemical binding of the photosynthetic reaction center protein to metal surfaces. *Advanced Materials* 17:2434.

Frolov, L., Y. Rosenwaks, S. Richter, C. Carmeli, and I. Carmeli. 2008. Photoelectric junctions between GaAs and photosynthetic reaction center protein. *Journal of Physical Chemistry C* 112:13426-13430.

Giardi, M. T., V. Scognamiglio, G. Rea, G. Rodio, A. Antonacci, M. Lambreva, G. Pezzotti, and U. Johanningmeier. 2009. Optical biosensors for environmental monitoring based on computational and biotechnological tools for engineering the photosynthetic D1 protein of Chlamydomonas reinhardtii. *Biosensors & Bioelectronics* 25:294-300.

Govorov, A. O. and I. Carmeli. 2007. Hybrid structures composed of photosynthetic system and metal nanoparticles: Plasmon enhancement effect. *Nano Letters* 7:620-625.

Guidelli, R. 2001. New directions and challenges in electrochemistry: bioelectrochemistry at metal-water interfaces. *Journal of Electroanalytical Chemistry* 504:1-28.

Haas, A. S., D. L. Pilloud, K. S. Reddy, G. T. Babcock, C. C. Moser, J. K. Blasie, and P. L. Dutton. 2001. Cytochrome c and cytochrome c oxidase: Monolayer assemblies and catalysis. *Journal of Physical Chemistry B* 105:11351-11362.

Ham, M. H., J. H. Choi, A. A. Boghossian, E. S. Jeng, R. A. Graff, D. A. Heller, A. C. Chang, A. Mattis, T. H. Bayhurt, Y. V. Grinkova, A. S. Zeiger, K. J. Van Vliet, E. K. Hobbie, S. G. Sligar, C. A. Wraight, and M. S. Strano. 2010. Photoelectrochemical complexes for solar energy conversion that chemically and autonomously regenerate. *Nature Chemistry* 2:929-936.

Heathcote, P., P. K. Fyfe, and M. R. Jones. 2002. Reaction centres: the structure and evolution of biological solar power. *Trends in Biochemical Sciences* 27:79-87.

Heering, H. A., F. G. M. Wiertz, C. Dekker, and S. de Vries. 2004. Direct immobilization of native yeast Iso-1 cytochrome c on bare gold: Fast electron relay to redox enzymes and zeptomole protein-film voltammetry. *Journal of the American Chemical Society* 126:11103-11112.

Hu, X. C., T. Ritz, A. Damjanovic, F. Autenrieth, and K. Schulten. 2002. Photosynthetic apparatus of purple bacteria. *Quarterly Reviews of Biophysics* 35:1-62.

Janzen, A. F. and M. Seibert. 1980. PHOTOELECTROCHEMICAL CONVERSION USING REACTION-CENTER ELECTRODES. *Nature* 286:584-585.

Jones, M. R. 2009. The petite purple photosynthetic powerpack. *Biochemical Society Transactions* 37:400-407.

Kaniber, S. M., F. C. Simmel, A. W. Holleitner, and I. Carmeli. 2009. The optoelectronic properties of a photosystem I-carbon nanotube hybrid system. *Nanotechnology* 20.

Katz, E. 1994. APPLICATION OF BIFUNCTIONAL REAGENTS FOR IMMOBILIZATION OF PROTEINS ON A CARBON ELECTRODE SURFACE - ORIENTED IMMOBILIZATION OF PHOTOSYNTHETIC REACTION CENTERS. *Journal of Electroanalytical Chemistry* 365:157-164.

Kondo, M., Y. Nakamura, K. Fuji, M. Nagata, Y. Suemori, T. Dewa, K. Lida, A. T. Gardiner, R. J. Cogdell, and M. Nango. 2007. Self-assembled monolayer of light-harvesting core complexes from photosynthetic bacteria on a gold electrode modified with alkanethiols. *Biomacromolecules* 8:2457-2463.

Krassen, H., A. Schwarze, B. Friedrich, K. Ataka, O. Lenz, and J. Heberle. 2009. Photosynthetic Hydrogen Production by a Hybrid Complex of Photosystem I and [NiFe]-Hydrogenase. *Acs Nano* 3:4055-4061.

Lakowicz, J. R. 2001. Radiative decay engineering: Biophysical and biomedical applications. *Analytical Biochemistry* 298:1-24.

Lebedev, N., S. A. Trammell, A. Spano, E. Lukashev, I. Griva, and J. Schnur. 2006. Conductive wiring of immobilized photosynthetic reaction center to electrode by cytochrome c. *Journal of the American Chemical Society* 128:12044-12045.

Lu, Y., J. Xu, B. Liu, and J. Kong. 2007. Photosynthetic reaction center functionalized nano-composite films: effective strategies for probing and exploiting the photo-induced electron transfer of photosensitive membrane protein. *Biosensors & Bioelectronics* 22:1173-1185.

Lu, Y. D., M. J. Yuan, Y. Liu, B. Tu, C. H. Xu, B. H. Liu, D. Y. Zhao, and J. L. Kong. 2005. Photoelectric performance of bacteria photosynthetic proteins entrapped on tailored mesoporous WO3-TiO2 films. *Langmuir* 21:4071-4076.

Lukashev, E. P., V. A. Nadtochenko, E. P. Permenova, O. M. Sarkisov, and A. B. Rubin. 2007. Electron phototransfer between photosynthetic reaction centers of the bacteria Rhodobacter sphaeroides and semiconductor mesoporous TiO2 films. *Doklady Biochemistry and Biophysics* 415:211-216.

Magis, J. G., M.-J. den Hollander, W. G. Onderwaater, J. D. Olsen, C. N. Hunter, T. J. Aartsma, and R. N. Frese. 2010. Light harvesting, energy transfer and electron cycling of a native

photosynthetic membrane adsorbed onto a gold surface. *Biochimica et Biophysica Acta* 1798:637-645.

Maly, J., J. Krejci, M. Ilie, L. Jakubka, J. Masojidek, R. Pilloton, K. Sameh, P. Steffan, Z. Stryhall, and M. Sugiura. 2005. Monolayers of photosystem II on gold electrodes with enhanced sensor response - effect of porosity and protein layer arrangement. *Analytical and Bioanalytical Chemistry* 381:1558-1567.

Matsuura, K. and K. Shimada. 1986. CYTOCHROMES FUNCTIONALLY ASSOCIATED TO PHOTOCHEMICAL-REACTION CENTERS IN RHODOPSEUDOMONAS-PALUSTRIS AND RHODOPSEUDOMONAS-ACIDOPHILA. *Biochimica et Biophysica Acta* 852:9-18.

McAuley-Hecht, K. E., P. K. Fyfe, J. P. Ridge, S. M. Prince, C. N. Hunter, N. W. Isaacs, R. J. Cogdell, and M. R. Jones. 1998. Structural studies of wild-type and mutant reaction centers from an antenna-deficient strain of Rhodobacter sphaeroides: Monitoring the optical properties of the complex from bacterial cell to crystal. *Biochemistry* 37:4740-4750.

Nakamura, C., M. Hasegawa, Y. Yasuda, and J. Miyake. 2000. Self-assembling photosynthetic reaction centers on electrodes for current generation. *Biochemistry and Biotechnology* 84:401-408.

Nakamura, H. and I. Karube. 2003. Current research activity in biosensors. *Analytical and Bioanalytical Chemistry* 377:446-468.

Nogi, T., I. Fathir, M. Kobayashi, T. Nozawa, and K. Miki. 2000. Crystal structures of photosynthetic reaction center and high-potential iron-sulfur protein from Thermochromatium tepidum: Thermostability and electron transfer. *Proceedings of the National Academy of Sciences of the United States of America* 97:13561-13566.

Ogawa, M., K. Shinohara, Y. Nakamura, Y. Suemori, M. Nagata, K. Iida, A. T. Gardiner, R. J. Cogdell, and M. Nango. 2004. Self-assembled monolayer of light-harvesting 1 and reaction center (LH1-RC) complexes isolated from Rhodospirillum rubrum on an amino-terminated ITO electrode. *Chemistry Letters* 33:772-773.

Pogorelov, T. V., F. Autenrieth, E. Roberts, and Z. A. Luthey-Schulten. 2007. Cytochrome c(2) exit strategy: Dissociation studies and evolutionary implications. *Journal of Physical Chemistry B* 111:618-634.

Qian, P., P. A. Bullough, and C. N. Hunter. 2008. Three-dimensional reconstruction of a membrane-bending complex - The RC-LH1-PufX core dimer of Rhodobacter sphaeroides. *Journal of Biological Chemistry* 283:14002-14011.

Rea, G., F. Polticelli, A. Antonacci, V. Scognamiglio, P. Katiyar, S. A. Kulkami, U. Johanningmeier, and M. T. Giardi. 2009. Structure-based design of novel Chlamydomonas reinhardtii D1-D2 photosynthetic proteins for herbicide monitoring. *Protein Science* 18:2139-2151.

Reiss, B. D., D. K. Hanson, and M. A. Firestone. 2007. Evaluation of the photosynthetic reaction center protein for potential use as a bioelectronic circuit element. *Biotechnology Progress* 23:985-989.

Roszak, A. W., T. D. Howard, J. Southall, A. T. Gardiner, C. J. Law, N. W. Isaacs, and R. J. Cogdell. 2003. Crystal structure of the RC-LH1 core complex from Rhodopseudomonas palustris. *Science* 302:1969-1972.

Sanders, C. A., M. Rodriguez, and E. Greenbaum. 2001. Stand-off tissue-based biosensors for the detection of chemical warfare agents using photosynthetic fluorescence induction. *Biosensors & Bioelectronics* 16:439-446.

Sepunaru, L., I. Tsimberov, L. Forolov, C. Carmeli, I. Carmeli, and Y. Rosenwaks. 2009. Picosecond Electron Transfer from Photosynthetic Reaction Center Protein to GaAs. *Nano Letters* 9:2751-2755.

Solovev, A. A., F. Y. Katz, V. A. Shuvalov, and Y. E. Erokhin. 1991. PHOTOELECTROCHEMICAL EFFECTS FOR CHEMICALLY MODIFIED PLATINUM-

ELECTRODES WITH IMMOBILIZED REACTION CENTERS FROM RHODOBACTER-SPHAEROIDES R-26. *Bioelectrochemistry and Bioenergetics* 26:29-41.

Suemori, Y. and et al. 2006. Self-assembled monolayer of light-harvesting core complexes of photosynthetic bacteria on an amino-terminated ITO electrode. *Photosynthesis Research* 90:17-21.

Suemori, Y., K. Fujii, M. Ogawa, Y. Nakamura, K. Shinohara, K. Nakagawa, M. Nagata, K. Iida, T. Dewa, K. Yamashita, and M. Nango. 2007. Molecular assembly of artificial photosynthetic antenna core complex on an amino-terminated ITO electrode. *Colloids and Surfaces B-Biointerfaces* 56:182-187.

Tauschel, H. D. and J. F. Hoeniger. 1974. FINE-STRUCTURE OF RHODOPSEUDOMONAS-ACIDOPHILA. *Canadian Journal of Microbiology* 20:13.

Terasaki, N., M. Iwai, N. Yamamoto, T. Hiraga, S. Yamada, and Y. Inoue. 2008. Photocurrent generation properties of Histag-photosystem II immobilized on nanostructured gold electrode. *Thin Solid Films* 516:2553-2557.

Terasaki, N., N. Yamamoto, T. Hiraga, Y. Yamanoi, T. Yonezawa, H. Nishihara, T. Ohmori, M. Sakai, M. Fujii, A. Tohri, M. Iwai, Y. Inoue, S. Yoneyama, M. Minakata, and I. Enami. 2009. Plugging a Molecular Wire into Photosystem I: Reconstitution of the Photoelectric Conversion System on a Gold Electrode. *Angewandte Chemie-International Edition* 48:1585-1587.

Terasaki, N., N. Yamamoto, K. Tamada, M. Hattori, T. Hiraga, A. Tohri, I. Sato, M. Iwai, S. Taguchi, I. Enami, Y. Inoue, Y. Yamanoi, T. Yonezawa, K. Mizuno, M. Murata, H. Nishihara, S. Yoneyama, M. Minakata, T. Ohmori, M. Sakai, and M. Fujii. 2007. Bio-photo sensor: Cyanobacterial photosystem I coupled with transistor via molecular wire. *Biochimica et Biophysica Acta-Bioenergetics* 1767:653-659.

Trammell, S. A., I. Griva, A. Spano, S. Tsoi, L. M. Tender, J. Schnur, and N. Lebedev. 2007. Effects of distance and driving force on photoinduced electron transfer between photosynthetic reaction centers and gold electrodes. *Journal of Physical Chemistry C* 111:17122-17130.

Trammell, S. A., A. Spano, R. Price, and N. Lebedev. 2006. Effect of protein orientation on electron transfer between photosynthetic reaction centers and carbon electrodes. *Biosensors & Bioelectronics* 21:1023-1028.

Trammell, S. A., Y. Wang, J. M. Zullo, R. Shashidhar, and N. Lebedev. 2004. Orientated binding of photosynthetic reaction centers on gold using Ni-NTA self-assembled monolayers. *Biosensors & Bioelectronics* 19:1649-1655.

Ventrella, A., L. Catucci, and A. Agostiano. 2010. Herbicides affect fluorescence and electron transfer activity of spinach chloroplasts, thylakoid membranes and isolated Photosystem II. *Bioelectrochemistry* 79:43-49.

Xu, J. J., Y. D. Lu, B. H. Liu, C. H. Xu, and J. L. Kong. 2007. Sensitively probing the cofactor redox species and photo-induced electron transfer of wild-type and pheophytin-replaced photosynthetic proteins reconstituted in self-assembled monolayers. *Journal of Solid State Electrochemistry* 11:1689-1695.

Yehezkeh, O., O. I. Wilner, R. Tel-Vered, D. Roizman-Sasde, R. Nechushtai, and I. Willner. 2010. Generation of Photocurrents by Bis-aniline-Cross-Linked Pt Nanoparticle/Photosystem I Composites on Electrodes. *Journal of Physical Chemistry B* 114:14383-14388.

Zhao, J. Q., N. Ma, B. H. Liu, Y. L. Zhou, C. H. Xu, and J. L. Kong. 2002a. Photoelectrochemistry of photosynthetic reaction centers embedded in Al2O3 gel. *Journal of Photochemistry and Photobiology A-Chemistry* 152:53-60.

Zhao, J. Q., Y. L. Zou, B. H. Liu, C. H. Xu, and J. L. Kong. 2002b. Differentiating the orientations of photosynthetic reaction centers on Au electrodes linked by different bifunctional reagents. *Biosensors & Bioelectronics* 17:711-718.

Zinth, W. and J. Wachtveitl. 2005. The first picoseconds in bacterial photosynthesis - Ultrafast electron transfer for the efficient conversion of light energy. *Chemphyschem* 6:871-880.

Chapter 4

Use of engineered unique cysteine residues to facilitate oriented coupling of proteins directly to a gold substrate.

Abstract

A pre-requisite for any 'lab on a chip' device that utilizes an electrical signal from the sensor protein is the ability to attach the protein in a specific orientation onto a conducting substrate. Here, we demonstrate the covalent attachment to a gold surface of light-harvesting membrane proteins, from *Rhodobacter sphaeroides*, via cysteine residues engineered on either the cytoplasmic or periplasmic face. This simple directed attachment is superior in its ability to retain light-harvesting complex function, when compared to a similar attachment procedure utilizing a self-assembled monolayer on gold. Light-harvesting complex 1 has previously been observed to have superior photostability over light-harvesting complex 2 (Magis et al., 2010); this characteristic is maintained even with the introduction of cysteine residues.

The contents of this chapter has been published in:

Gerhard J. Magis, John D. Olsen, Nicholas P. Reynolds, Graham J. Leggett, C. Neil Hunter, Thijs J. Aartsma, and Raoul N. Frese. 2011. Use of engineered unique cysteine residues to facilitate oriented coupling of proteins directly to a gold substrate. *Photochemistry and Photobiology* 87:1050-1057

4.1 Introduction

There is considerable interest in utilizing the wide array of naturally occurring sensor proteins, particularly redox sensitive proteins, to manufacture highly sensitive detector chips (e.g. Wang (Wang, 2005)). The use of engineered cysteine (Cys) residues as a means to selectively immobilize soluble proteins, mostly enzymes, has been extensively reviewed by Hernandez & Fernandez-Lafuente (Hernandez and Fernandez-Lafuente, 2011), and the soluble bacterial cytochrome b_{562} has been immobilized on gold (Della Pia et al., 2011). Gold has also been used as a crosslinking substrate for an analog of the human myc tag peptide to a microcantilever to monitor antibody-peptide interaction (Kim et al., 2003). Several crosslinking chemistries have been trialed on the model integral membrane proteins, light-harvesting complexes (LHC) and reaction centers (RC), from photosynthetic bacteria, as these are readily available and can be easily tested for surface-bound functionality by spectroscopy (Reynolds et al., 2007;Trammell et al., 2004;Trammell et al., 2006). However, in order to exert control over protein orientation on the substrate most of these techniques have relied either upon indigenous residues in a fortuitous location or upon an engineered polyhistidine tag at the exposed terminus of a polypeptide.

Reynolds et al. (Reynolds et al., 2007) attached the WT LH2 complex of *Rhodobacter sphaeroides* (*Rba. sphaeroides*) to a patterned self assembled monolayer (SAM) on gold and tested the resultant hybrid structure for functionality by fluorescence emission spectroscopy, successfully demonstrating energy transfer from the B800 absorbing bacteriochlorophylls (BChl) to the emitting B850 BChls. If the protein structure of the LHC was badly distorted by the attachment chemistry or proximity to the SAM surface, this would have resulted in a misalignment of the BChls in the complex, affecting energy transfer. Thus the fluorescence emission signal would have been impaired or distorted, which was not the case. Directed binding of the LHC was obtained by crosslinking cytoplasmically exposed lysine (Lys) residues (see figure 2) to the SAM. In other work, a combination of site-directed mutagenesis, nanoimprint lithography and host-guest interactions was used to attach LH2 complexes engineered with cysteine residues to a glass substrate (Escalante et al., 2008).

In this work we have utilized the LH1 and LH2 complexes of the same purple bacterium, *Rba. sphaeroides*, see figure 1A for surface-rendered structures, but we have used an established mutagenesis and complementation system to generate unique Cys residues in the α polypeptide of each LHC (Jones et al., 1992), which are capable of directing the orientation of the complex on a gold surface. The use of engineered Cys residues for the site-specific immobilization of proteins to solid supports presents a number of advantages

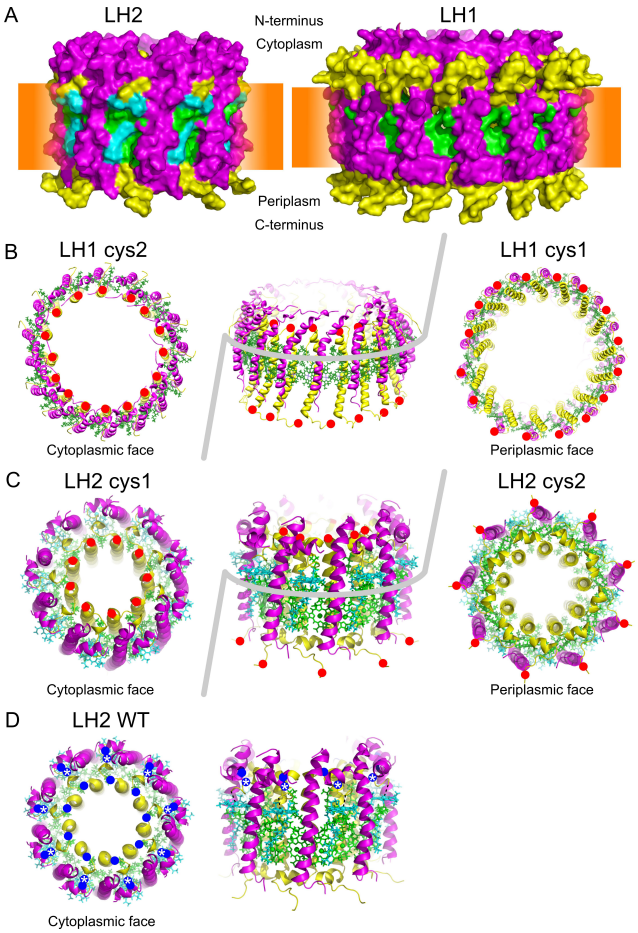


Figure 1.

(A) A surface-rendered atomic structure of the nine-fold symmetric LH2 and model structure of the sixteen-fold symmetric LH1, each showing their native orientation and position in the native membrane bilayer (orange). The α polypeptides are colored yellow and the β polypeptides are colored magenta in both complexes, the B800 BChls are colored cyan and the B850 BChls in green in the LH2 structure and the B875 BChls green in the LH1 model, the structures are not to scale. This color scheme is used in panels B, C and D.

(B) A cartoon representation of a model LH1 structure showing the positions of the Cys residues (red discs) in the cys1 and cys2 mutants on the periplasmic and cytoplasmic faces of the complex, respectively. The central view shows only some of the Cys locations for clarity.

(C) A cartoon representation of the LH2 structure showing the positions of the Cys residues (red discs) in the cys1 and cys2 mutants on the cytoplasmic and periplasmic faces of the complex, respectively. The central view shows only some of the Cys locations for clarity.

(D) A cartoon representation of the WT LH2 showing the locations of the native Lys residues (blue discs, αLys -26 denoted by *) on the cytoplasmic face and in the membrane plane; parts of the complex have been omitted for clarity. The dashed lines indicate the ligand between the N-terminal Met residue and the central magnesium of the BChl *a*.

over other immobilization techniques: (1) The simplicity and mildness of the Cys labeling protocol enables strong and stable biomolecule attachment, (2) the mutation of the protein by the replacement of single residues near to the N and C terminals of the proteins are unlikely to affect the protein structure, (3) the binding occurs via the thiol side chain of the Cys group to the gold surface, therefore it is only the SH group of the Cys that is involved. However, there are some potential problems with using Cys residues that must be carefully considered: (1) Using multiple Cys residues in order to increase binding strength may begin to affect the structure of the protein, (2) The location of the Cys residues is known to affect their redox-stability, possibly leading to oxidation of the SH groups to form disulfide bridges resulting in protein aggregation.

Recent work by Hoefling et al. (Hoefling et al., 2010) has predicted that certain amino acid residues have a strong tendency to bind to a gold surface non-specifically; their calculated binding energies can be summarized as aromatic < sulfur < positive < polar < aliphatic ~ negative. This conjecture has implications for our results when using the LH1 complex as the extrinsic regions are rich in aromatic and positive amino acids when compared to the LH2 complex.

The purple bacterial LHCs are multimeric proteins, which leads to the presence of nine Cys residues on the *Rba. sphaeroides* LH2 complex, see figure 1C, and sixteen Cys residues on the LH1 complex (one Cys per α polypeptide in each complex), see figure 1B, providing multiple/additive very strong covalent links between the complex and the gold substrate. We have measured the fluorescence excitation spectra of the attached complexes as this technique not only demonstrates that the LHCs remain functional but also highlights any defects in the internal energy transfer between the B800 and B850 BChls of the LH2 complex that could arise from distortions of the complex upon successful attachment to the surface. Our results show that both LH1 and LH2 complexes can be attached to gold substrates and remain functional, as indicated by their fluorescence excitation and emission spectra as compared to the equivalent solution spectra, thus demonstrating that engineered Cys residues can be used for the directed attachment of membrane proteins to a gold substrate.

Although our measurements were routinely conducted *in vacuo* to prevent oxidative photodamage, exposure to air allowed us to monitor the stability and function of immobilized LHCs. In the presence of molecular oxygen, LH2 complexes rapidly lost their fluorescence signal. In contrast we observed the same remarkable photostability for LH1 complexes as reported by Magis et al. (Magis et al., 2010).

4.2 Materials and Methods

4.2.1 Site-directed mutagenesis

Unique Cys residues were engineered into the LH1 and LH2 genes of *Rba. sphaeroides* by PCR mutagenesis (Olsen et al., 2003) at the following protein sequence positions for LH1: αCys+27 (LH1 cys1), αAsp-20→Cys (LH1 cys2) where α denotes the α polypeptide of LH1, and for LH2: αThr-19→Cys (LH2 cys1), αAla+22→Cys (LH2 cys2), where α and β are the polypeptides of LH2. The numbering system follows that of Loach et al. (Loach et al., 1994), where the central conserved His residue is denoted as 0, all + numbers are towards the C-terminus and all – numbers are towards the N-terminus of the polypeptide.

4.2.2 Preparation of samples

The mutated genes were introduced by conjugative mating into the *Rba. sphaeroides* deletion strains DD13 and DD13/G, which express primarily spheroidenone and neurosporene, respectively (Jones et al., 1992). The transconjugant strains containing the mutated LH genes were grown chemoheterotrophically in the dark under oxygen-limited conditions and membranes were prepared as described previously (Olsen et al., 1994). Purified protein was prepared as outlined in Olsen et al. (Olsen et al., 2003), with the modification of using the detergent β-DDM for preparing the LH1 protein at a final concentration of 1% w/v during solubilization and at 0.03% for all subsequent steps.

4.2.3 Preparation of surfaces

Gold

Freshly cleaved mica was sputter coated with a 1 nm adhesion layer of molybdenum germanium (MoGe) using an ATC-1800 magnetron sputtering system with a deposition rate of 1.32 nm per minute (10 mTorr Argon environment). Then, 20 nm thick gold films were sputtered with a deposition rate of 9.2 nm per minute (5 mTorr environment composed of a mixture of Argon with 1% oxygen). This resulted in gold films with a typical RMS roughness of 0.3 nm as deduced from atomic force microscopy images of the bare gold surfaces.

(3- aminopropyl) – triethoxysilane SAMs on glass

Glass microscope slides (Chance Proper no. 2 thickness, size 22 mm x 64 mm) were cleaned using Piranha solution (70% sulfuric acid (>95%) (Fisher Scientific, Loughborough, UK) 30% hydrogen peroxide 100 vol. (Sigma Chemical Company) and then treated with RCA solution (20% hydrogen peroxide 100 vol., 20% ammonium hydroxide (>95%) (Sigma Chemical Company) for one hour at 80 °C in order to create a

homogenous hydroxyl surface. The surfaces were rinsed in copious de-ionized water (18.2 MΩ) and dried. The cleaned substrates were immersed in a 5mM solution of (3-aminopropyl)-triethoxysilane in anhydrous tetrahydrofuran (>99%) (THF) (Sigma Chemical Company) for 90 minutes in an anhydrous nitrogen atmosphere. The SAMs were then rinsed in THF and HPLC grade ethanol (Sigma Chemical Company) and sonicated for 15 minutes in THF in order to remove any aggregates that may have formed on the surface. Finally the SAMs were placed in a vacuum oven at 120 °C (Fistreem International, Loughborough, UK), for one hour in order to remove any solvent remaining on the surface.

Mercaptoundecanoic Acid SAMs on gold films

SAMs of mercaptoundecanoic acid (99%) (MUA) (Sigma Chemical Company, Poole, UK) were prepared on gold covered glass microscope slides (Chance Proper no. 2 thickness, size 22 mm x 64 mm), which were cleaned using Piranha solution. The surfaces were rinsed in copious de-ionized water (18.2 MΩ) and dried. The cleaned substrates were immersed in a 2 mM solution of MUA in HPLC grade ethanol (Sigma Chemical Company) for 18 hours, then rinsed and stored in ethanol until use.

4.2.4 Protein immobilization

Attachment of wild type (WT) LH2 to (3-aminopropyl)-triethoxysilane SAMs on glass was achieved by exposure to solutions of LH2 (6.5 μg mL^{-1} in a buffer containing 10 mM HEPES [pH 7.5], 1% β-OG (n-octyl β-D-glucopyranoside; Glycon Biochemicals) and 150mM NaCl) for 15-30 min. The sample was rinsed with buffer (10 mM HEPES [pH 7.5] and 1% β-OG) to remove any unbound LH2. For covalent attachment the glass was silanized and immersed in a solution of 10% glutaraldehyde (Sigma) in de-ionized water (18.2 MΩ) for 30 minutes before rinsing in de-ionized water.

Attachment of WT LH2 to MUA SAMs on gold films was achieved by activation of the carboxylic acid terminated SAM (MUA in figure 2) to form a carboxylic ester which is converted to a surface-bound N-hydroxysuccinimidyl ester by exposure of the SAM to an aqueous solution of 1-ethyl-3,3, dimethyl carbodiimide, EDC, (Sigma) (20 mM) and N-hydroxysuccinimide, NHS, (Sigma) (20 mM) for 30 min and rinsing with de-ionized water (for a schematic of the reactions see figure 2). A solution of LH2 (6.5 μg mL^{-1} in a buffer containing 10 mM HEPES [pH 7.5], 1% β-OG and 150mM NaCl) was then applied for 15-30 min, and the sample rinsed with buffer (10mM HEPES [pH 7.5] and 1% β-OG) to remove any unbound LH2. The method used for attachment of WT LH1 is identical to this

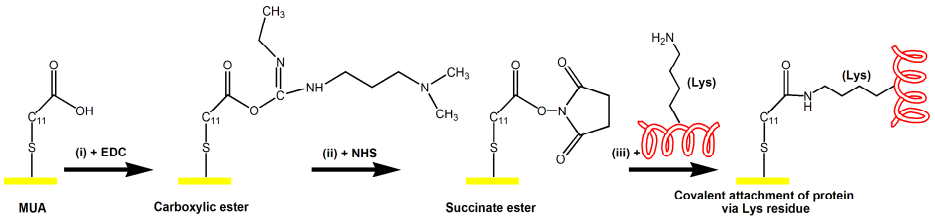


Figure 2. A schematic pathway of the chemical activation of the MUA SAM and subsequent crosslinking to WT LH2 complexes purified from *Rba. sphaeroides*. (i) Activation of 1-Ethyl-3-(3-dimethylaminopropyl)carbodiimide (EDC) with MUA to form carboxylic ester; (ii) reaction of the carboxylic ester with N-hydroxysuccinimide (NHS) to form succinate ester (more stable intermediate, reacts with primary amines at physiological pH); (iii) reaction of exposed side chain of a lysine residue on the surface of the light-harvesting complex with the succinate ester, resulting in the covalent attachment of the protein.

protocol, except for the use of the detergent β-DDM (Sigma Aldrich) (0.03%) at a pH of 8.0.

Attachment of LH2 cys1 and cys2 complexes directly to gold was achieved by loading 25 µL of the bulk protein solution (OD_{850} 2-3 in a buffer containing 10 mM HEPES [pH 7.5], 1% β-OG, 150 mM NaCl and 10 mM DTT) diluted with 175 µL buffer (10 mM HEPES [pH 7.5] and 1% β-OG) onto the gold surface. After 15 min incubation the sample was rinsed with 1 ml of buffer to remove non-covalently bound proteins. This loading and rinsing was repeated 2 times after which the surface was gently blown dry under a mild stream of nitrogen-gas. The protocol for the direct attachment of LH1 cys1 and LH1 cys2 onto gold is identical, except for the use of the detergent β-DDM (0.03%) and a pH of 8.0.

4.2.5 Spectroscopy of surface-immobilized proteins

Fluorescence experiments were performed at room temperature with a home-built confocal microscope setup with the objective mounted inside a cryostat. The latter enables measuring in an oxygen-free environment by pumping the cryostat to vacuum. Homogeneity of the sample distribution on the surface was checked by confocal fluorescence imaging of the sample by scanning the laser over a wide-range (> 100 µm) at a fixed wavelength (800 or 850 nm for LH2, 870 nm for LH1) and monitoring the fluorescence-signal using an avalanche photodiode (APD, Perkin-Elmer SPCM-AQR-16).

Fluorescence emission spectra were recorded by directing the emitted fluorescence via a series of long-passfilters with a transmission between 815 and 1015 nm (Hugo Anders, Germany), towards a blazed grating (Richardson Gratings) that disperses the collimated fluorescence. A lens is finally used to project the diffracted beam onto a liquid-nitrogen-cooled CCD camera (Roper Scientific, USA). The excitation intensity used to record an

emission spectrum was typically 200 W cm^{-2}, with an integration time of 60 seconds. The recorded spectra were all corrected for the sensitivity of the CCD camera.
Fluorescence excitation spectra were recorded in vacuum at room temperature. A series of three identical interference bandpass filters was employed in the detection path to remove most of the stray light. Two sets of filters were used depending on the sample under investigation, one with a transmission between 875 and 910 nm for LH2 and the other with a transmission between 905 and 940 nm for LH1. This allows the detection with the APD of the red part of the fluorescence for both LH2 and LH1. Excitation spectra were then recorded by scanning the wavelength of the titanium sapphire (TiSa) laser from 790 nm (lower limit of the laser) to either 870 or 900 nm, depending on which filter-set is used. In all cases linearly polarized light was used. All fluorescence excitation spectra were corrected for both the sensitivity of the APD and the wavelength dependence of the excitation-intensity.

4.2.6 Photostability assessment of immobilized proteins

To study the photostability of LH1 assemblies on a surface, we utilized the fluorescence emission spectroscopy setup already described but replaced the long-pass filters with a series of 3 identical interference bandpass filters with transmission between 905 and 940 nm. For all photostability measurements, the sample was illuminated with an intensity of 75 W cm^{-2} at a wavelength of 870 nm. The detected fluorescence signal was integrated for 60 seconds to improve the signal-to-noise ratio.

4.2.7 Atomic Force Microscopy

Atomic Force Microscopy (AFM) images of the samples were obtained using a commercial AFM (Nanoscope IIIa, Veeco, Santa Barbara, CA, USA). Tapping mode images in air were acquired with an E-scanner (14 μm range) and using Si probes with a resonance frequency of 75 kHz and a nominal spring constant of 2.8 N m^{-1}.

4.3 Results and Discussion

The use of unique Cys residues as a method not only to direct the orientation of the protein but also to form a covalent bond to a gold substrate establishes this technique as a viable way to attach integral membrane proteins to conducting substrates. Moreover our use of the LH1 and LH2 complexes of *Rba. sphaeroides* has allowed us to determine whether the attachment chemistry is detrimental to the protein function as the bound chromophores of the LH complexes are very sensitive to the structural integrity of the protein. Evidence for this sensitivity was shown by point mutation studies (Fowler et al., 1993;Fowler et al.,

1997;Olsen, 1994;Sturgis et al., 1997), also by high pressure treatment (Gall et al., 1997;Reddy et al., 1996;Wu et al., 1998).

In order to gain insight into the surface coverage of the LHCs on gold surfaces we utilized topographical AFM under ambient conditions operating in tapping mode. Figure 3 shows a representative image of single LH2 cys1 complexes attached to a flat gold surface at a concentration of 25 μL of protein solution (OD_{850} 2-3) in 175 μL buffer. The brighter points have the expected height for such a complex, as seen in the section (figure 3, lower panel). All of the complexes in this image are well separated from their nearest neighbors therefore we can be confident that in subsequent figures we are observing only spectral changes that are brought about by the attachment of the protein to the gold and not from any aggregation effects. The size of the features seen in figure 3 suggests that protein aggregates arising from the formation of disulfide bridges between the Cys residues were not present. This was expected as disulfide bridges are formed by the oxidation of deprotonated thiol groups (cysteine thiolates) (Bulaj, 2005). The standard pKa value of such Cys residues is 9.1 (Harris and Turner, 2002) so at pH 7.5 it was expected that the fraction of deprotonated thiol groups will be small. The pKa of Cys residues can be significantly reduced due to its surrounding chemical environment. The proximity of the thiol to the N-terminus of α-helical structures due to helix dipole interactions, hydrogen bonding to neighboring residues or electrostatic interactions with positively charged residues are all known to reduce the pKa (Wang et al., 2001). LH1 cys2 is close to two Arg residues but as it occurs where there is likely to be a helix-turn-helix structure in the polypeptide the potential for hydrogen bonding and electrostatic interactions is probably small. LH1 cys1 is at the C-terminus of the α polypeptide where the nearest positive residue, Arg, is 5 residues away and this region is likely to be isolated from the other α C-terminal helices, see figure 1B, so again is presumed to be free of interactions that would lower the pKa. LH2 cys1 is analogous to LH1 cys1 in that it is in a helix-turn-helix structure with a Lys one residue distant while LH2 cys2 has no Lys or Arg residues anywhere in its proximity.

The LH2 Cys mutant complexes used in this study show little or a small perturbation of their fluorescence excitation spectra when attached to gold; similarly the WT LH2 complex when adhered to silanized glass shows minimal disturbance of the B800 and B850 excitation bands, whereas the WT LH2, when attached to an MUA-SAM, shows an almost complete loss of the B800 band, see figure 4. This discrepancy may stem from the glutaraldehyde used to crosslink the WT LH2 to the silanized surface. It is known that aqueous solutions of glutaraldehyde form polymeric species under basic conditions

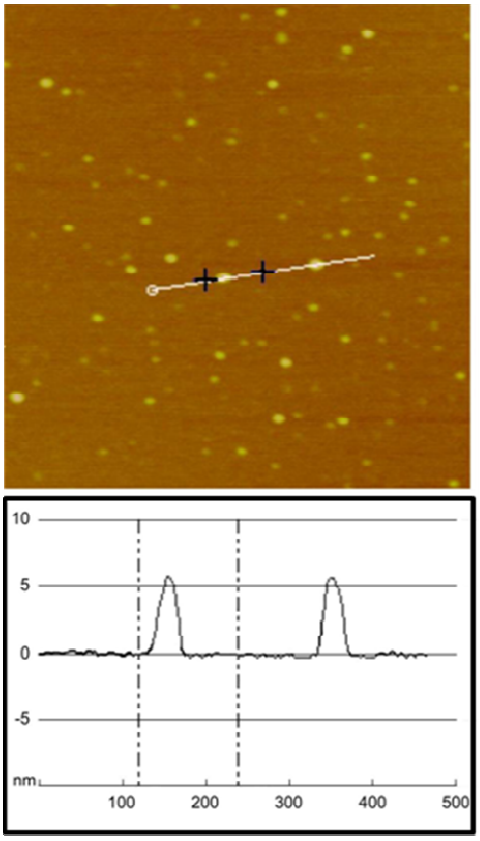


Figure 3. A topographical AFM image (tapping mode in air) of isolated LH2 cys1 complexes on a flat gold surface. The section shows that the heights of some of the particles are over 5 nm, which is consistent with the expected dimensions of an oriented LH2 complex. The scan area is 1 μm x 1 μm, full z = 12 nm.

(Migneault et al., 2004). Our attachment regime, which uses a buffer at pH 7.5, could promote the formation of flexible poly-glutaraldehyde linkers which allow a separation between the cytoplasmic face of the complex and the glass surface; such a separation could avoid alteration or deformation of the labile B800 binding site (Clayton and Clayton, 1981), which is known to be close to the cytoplasmic face of the LH2 complex. The near complete absence of the B800 band, when using an MUA-SAM and EDC NHS cross-linking chemistry, indicates a probable loss of some of the B800 BChls. This procedure also utilizes native Lys residues; the single β Lys residue and two α Lys residues are marked as blue discs in figure 1D, although we do not know which of these Lys residues is

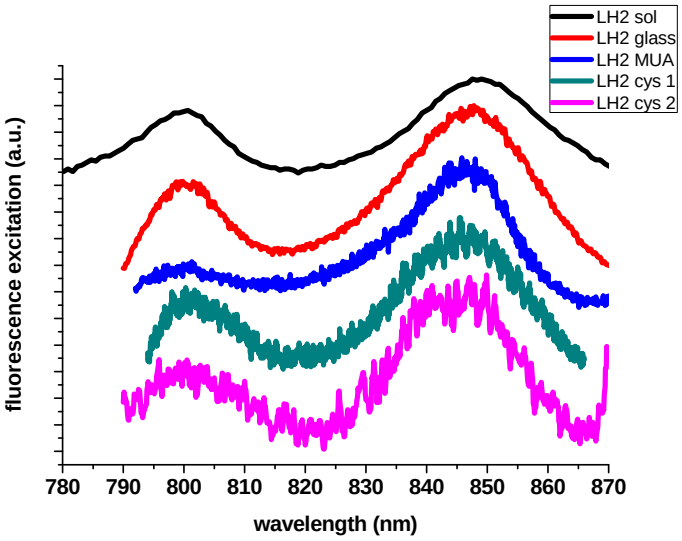


Figure 4. Fluorescence excitation spectra of the WT and cys1 and cys2 mutants of LH2 attached to glass, an MUA-SAM on gold or directly to the gold surface; see insert for details of the samples. The emission was measured with an APD and filters transmitting between 875 and 910 nm. For comparison we included the solution absorption spectrum of WT LH2.

involved in crosslinking to the MUA-SAM. The nature of the chemistry leads to a very restrictive linkage between the carboxyl moiety of the MUA and the free amino group of the Lys residue, tethering the residue very close to the SAM surface and thus likely distorting the LH2 structure. Indeed, if the crosslink is formed to the Lys residue closest to the B800 binding site, αLys-26 (marked with * in figure 1D), which is a part of the N-terminus of the α polypeptide that provides the N-terminal Met ligand to the BChl, then any perturbation of this region is highly likely to disturb the B800 binding site (Clayton and Clayton, 1981;Gall et al., 1997).

The LH2 cys1 mutant shows minimal alteration of the excitation spectrum (figure 4) indicating that even though the B800 BChl is brought into close proximity with the gold surface this is not deleterious to energy transfer from B800 to B850 BChls. The B800 excitation maximum for the LH2 cys2 sample, although attenuated slightly, shows that B800 to B850 energy transfer is also retained in this mutant. There is a broadening of the B850 excitation band and a small shift towards the blue; the Cys residue in the LH2 cys2 mutant is on the periplasmic face of the complex, which would direct that attachment of the C-terminal end of the α polypeptide to the gold surface. The α polypeptide is known to form two H-bonds, one to the α-bound B850 BChl and the other to the β-bound B850 BChl (Clayton and Clayton, 1981;Fowler et al., 1994;Gall and Robert, 1999;McDermott et al.,

1995), thus any disturbance of the C-terminal region of the α polypeptide is likely to perturb one or both of these H-bonds, leading to a blue shift of the maximum. We conclude that the use of Cys residues to directly attach the LH2 complex of *Rba. sphaeroides* to a gold surface with a known orientation does not cause significant protein denaturation.

Although the silanized glass provides a minimally deleterious attachment regime for the attachment of the WT LH2 complex, the orientation for the majority of proteins is likely to be unknown. This unpredictable orientation renders this chemistry unsatisfactory when directed orientation is our primary goal.

The WT LH1 complex was not removed by the washing regime that successfully removed the WT LH2 from the gold surface. We believe this is due to a set of circumstances that are unique to the LH1 complex and that it does not invalidate our presumption of oriented binding of the LH2 cys1 and cys2 mutants. Hoefling et al. (Hoefling et al., 2010) calculated the adsorption free energies of individual amino acids with an Au (111) surface and found a surprising variation in energies. The hierarchy can be broadly summarized as aromatic < sulfur < positive < polar < aliphatic ~ negative. Analyzing the extrinsic regions of the α and β polypeptides of both LH1 and LH2 we can see a very marked difference in the numbers of amino acids from the top three groupings of this hierarchy for the N and C-terminal regions. In the N-terminal regions of an LH1 αβ polypeptide pair (the LH1 complexes comprises 16 such pairs) there are 12 amino acids potentially involved in surface adsorption (aromatic, sulfur, positive) whereas LH2 only has 6 in the equivalent region; this pattern is repeated for the C-terminal regions where LH1 has 9 highly interacting amino acids and LH2 only 4. However only the positively charged residues Arg and Lys may be exposed to the aqueous phase and thus able to interact with the gold surface; Met, like Trp, Tyr and Phe, are hydrophobic and thus likely to be inaccessible. Under these conditions the number of potentially interacting amino acids for an LH1 αβ polypeptide pair at the N-terminus is 5 (3 Lys + 2 Arg) and for LH2 is 3 (3 Lys), whilst at the C-terminus LH1 has 3 such amino acids (1 Lys, 2 Arg) and LH2 has none. If we take the arithmetic sum of the calculated interaction energies, which are 30.0 kJ mol^{-1} for a Lys residue and 36.3 kJ mol^{-1} for an Arg residue (Hoefling et al., 2010), the maximal accessible residues for the N-terminus of a single LH1 αβ pair has a theoretical binding energy of 162.6 kJ mol^{-1} which is the same order of magnitude as a Au-S bond, *ca* 200 kJ mol^{-1} (Hoefling et al., 2010). The differences between LH1 and LH2 are even more marked when the oligomeric state of the complexes (16 LH1 αβ polypeptide pairs per circular complex, and 9 LH2 αβ polypeptide pairs per LH2) are taken into account. We stress that the binding

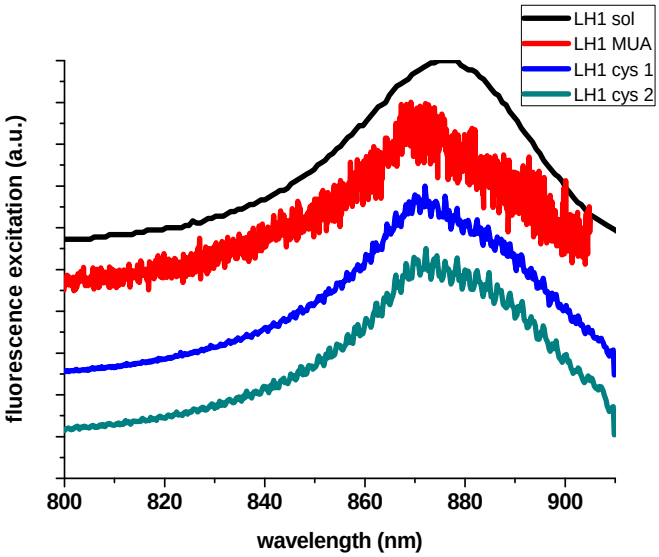


Figure 5. Fluorescence excitation spectra of WT and cys1 and cys2 mutants of LH1 attached to MUA-SAM and gold, see insert for details. The emission was measured with an APD and filters transmitting between 905 and 940 nm. For comparison we included the solution absorption spectrum of WT LH1.

energies for LH complexes based upon theoretical calculations for individual amino acids are an upper limit though. Most likely, several residues in the LH1 complexes are within an α-helical conformation and are not available for bond formation with the gold surface. Given the competing forces mentioned above for binding the N-terminus of LH1 to gold through Arg and Lys residues Cys residues in the LH1-cys1 mutant may be insufficient to direct binding to gold solely at the C-terminus.

The results for the LH1 Cys mutants, cys1 (cytoplasmic face) and cys2 (periplasmic face), on gold and the WT LH1 on an MUA-SAM all show a distinct blue shift of the fluorescence excitation maximum in comparison with the spectrum of the WT LH1 complex in solution (figure 5). However due to the level of noise in the LH1 WT on the MUA SAM, which is a function of the low coverage of monodisperse complexes, it is difficult to comment upon any underlying differences. It is clear that the cys1 and cys2 mutants have very similar line shapes and widths, maybe indicating that the attachment of the LH1-cys mutants is not directed solely by cysteines, but also by other residues such as Arg and Lys, as mentioned above. The changes in line shape with respect to the WT LH1 solution spectrum may in part be due to the more flexible nature of the LH1 complex, which is a sixteen-fold repeating ring-shaped assembly of two transmembrane polypeptides

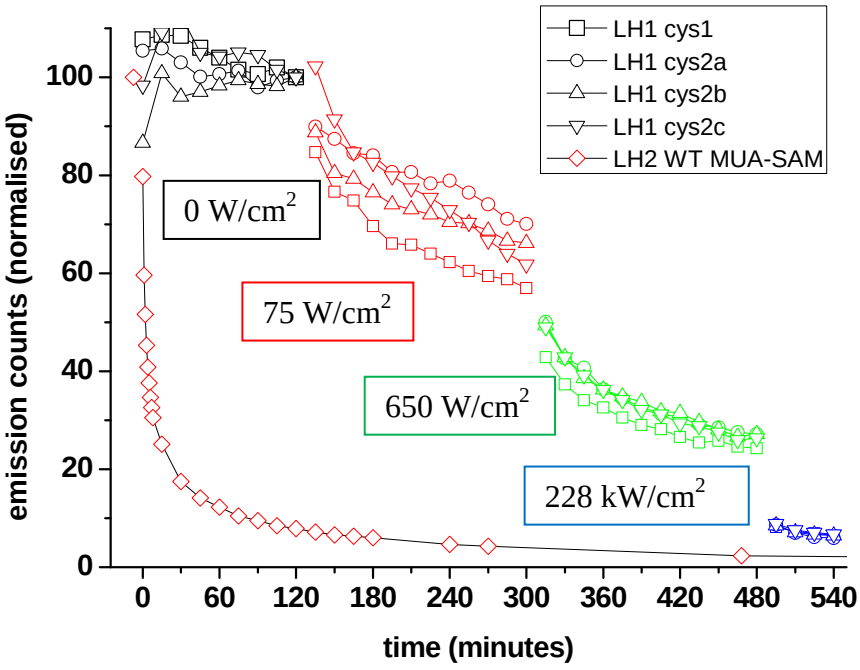


Figure 6. Fluorescence emission counts as a function of time for WT LH2 and LH1 cys1 and 2 mutants on gold, excited at 870 nm, and exposed to air. See insert for details of the samples. The emission was measured with and APD and 3 identical interference bandpass filters with transmission between 905 and 940 nm.

(the α polypeptide, yellow, and the β polypeptide, magenta, in figure 1A & B) that non-covalently bind carotenoid and bacteriochlorophyll pigment molecules and which normally surrounds the reaction centre within the photosynthetic membrane. The flexibility of the LH1 complex is well illustrated by the AFM study of 2D crystals of these complexes by Bahatyrova et al. (Bahatyrova et al., 2004) who observed circular, elliptical and even polygonal structures. The gold surfaces used in this work, both for SAM formation and direct binding of Cys residues, have a roughness of 0.3 nm RMS (see figure 3), which is highly likely to distort the LH1 ring structure in the z plane as each pair of polypeptides carries a Cys residue and the αβ pairs of polypeptides are only bound to their neighbors by hydrogen bonds and hydrophobic interactions.

Whilst tolerance of molecular oxygen is not a requirement for all proteins that may be attached to gold surfaces for nanotechnology applications it is of interest to those wishing

to utilize natural light-harvesting proteins. At the conclusion of the primary experiments we therefore exposed the attached complexes to air, whilst maintaining the illumination, in order to gauge their photostability. The data shown in figure 6 show the most remarkable result whereby the LH1 complex withstood progressively higher illumination levels whereas the WT LH2 complex on the MUA-SAM had effectively 'died' after less than 30 minutes. The LH1 cys mutants still showed significant activity, measured as fluorescence emission, after 480 minutes, the last 180 minutes being with 650 W cm^{-2} irradiation. It should be noted that the LH2 cys mutants on gold lost all activity in less than two minutes when exposed to irradiation in the presence of oxygen (data not shown). This photostability rivals that of WT LH1 complexes adsorbed onto a gold surface by Magis et al. (Magis et al., 2010), who speculated that it was a function of the specific association of BChls and carotenoids in the LH1 structure.

4.4 Conclusion

We have demonstrated that unique engineered Cys residues can provide a reliable means to direct specifically oriented attachment of membrane proteins to a gold surface that causes minimal perturbation to the protein thus preserving its function. We therefore propose that this technique could be used for attachment, with specific orientation, of any other membrane proteins such as channel or sensory transduction proteins to a conducting substrate such as gold. Competitive binding via intrinsic protein residues should be considered. Protocols described here applied to the attachment of a variety of light harvesting complexes from different species will allow a better understanding of protein binding onto gold.

We have also observed that the LH1 complex of *Rba. sphaeroides* with introduced cysteine linkers can withstand high levels of illumination in the presence of molecular oxygen making this model protein a potential candidate for a hybrid light-harvesting photovoltaic panel.

References

Bahatyrova, S., R. N. Frese, K. O. van der Werf, C. Otto, C. N. Hunter, and J. D. Olsen. 2004. Flexibility and size heterogeneity of the LH1 light harvesting complex revealed by atomic force microscopy - Functional significance for bacterial photosynthesis. *Journal of Biological Chemistry* 279:21327-21333.

Bulaj, G. 2005. Formation of disulfide bonds in proteins and peptides. *Biotechnology Advances* 23:87-92.

Clayton, R. K. and B. J. Clayton. 1981. B850 Pigment-Protein Complex of Rhodopseudomonas-Sphaeroides - Extinction Coefficients, Circular-Dichroism, and the Reversible Binding of Bacteriochlorophyll. *Proceedings of the National Academy of Sciences of the United States of America-Biological Sciences* 78:5583-5587.

Della Pia, E. A., Q. Chi, D. D. Jones, J. E. Macdonal, J. Ulstrup, and M. Elliott. 2011. Single-molecule mapping of long-range electron transport for a cytochrome b562 variant. *Nano Lett.* 11:176-182.

Escalante, M., Y. Zhao, M. J. W. Ludden, R. Vermeij, J. D. Olsen, E. Berenschot, C. N. Hunter, J. S. V. Huskens, and C. Otto. 2008. Nanometer arrays of functional light harvesting antenna complexes by nanoimprint lithography and host-guest interactions. *Journal of the American Chemical Society* 130:8892-8893.

Fowler, G. J. S., W. Crielaard, R. W. Visschers, R. van Grondelle, and C. N. Hunter. 1993. Site-directed mutagenesis of the LH2 light-harvesting complex of *Rhodobacter-sphaeroides* - changing beta-lys23 to gln results in a shift in the 850 nm absorption peak. *Photochemistry and Photobiology* 57:2-5.

Fowler, G. J. S., S. Hess, T. Pullerits, V. Sundstrom, and C. N. Hunter. 1997. The role of beta Arg(-10) in the B800 bacteriochlorophyll and carotenoid pigment environment within the light-harvesting LH2 complex of Rhodobacter sphaeroides. *Biochemistry* 36:11282-11291.

Fowler, G. J. S., G. D. Sockalingum, B. Robert, and C. N. Hunter. 1994. Blue shifts in bacteriochlorophyll absorbence correlate with changed hydrogen bonding patterns in light-harvesting 2 mutants of *Rhodobacter sphaeroides* with alterations at α-Tyr-44 and α-Tyr-45. *Biochem. J.* 299:695-700.

Gall, A., G. J. S. Fowler, C. N. Hunter, and B. Robert. 1997. Influence of the protein binding site on the absorption properties of the monomeric bacteriochlorophyll in Rhodobacter sphaeroides LH2 complex. *Biochemistry* 36:16282-16287.

Gall, A. and B. Robert. 1999. Characterization of the different peripheral light-harvesting complexes from high- and low-light grown cells from *Rhodopseudomonas palustris*. *Biochemistry* 38:5185-5190.

Harris, T. K. and G. J. Turner. 2002. Structural basis of perturbed pKa values of catalytic groups in enzyme active sites. *Iubmb Life* 53:85-98.

Hernandez, K. and R. Fernandez-Lafuente. 2011. Coupling immobilization and site directed mutagenesis to improve biocatalyst or biosensor performance. *Enzyme and Microbial Technology* 48:107-122.

Hoefling, M., F. Iori, S. Corni, and K.-E. Gottschalk. 2010. Interaction of amino acids with the Au(III) surface: Adsorption free energies from molecular dynamics simulations. *Langmuir* 26:8347-8351.

Jones, M. R., G. J. S. Fowler, L. C. D. Gibson, G. G. Grief, J. D. Olsen, W. Crielaard, and C. N. Hunter. 1992. Mutants of Rhodobacter-Sphaeroides Lacking One Or More Pigment Protein Complexes and Complementation with Reaction-Center, Lh1, and Lh2 Genes. *Molecular Microbiology* 6:1173-1184.

Kim, B. H., O. Mader, U. Weimar, R. Brock, and D. P. Kern. 2003. Detection of antibody peptide interaction using microcantilevers as surface stress sensors. *Journal of Vacuum Science and Technology B* 21:1472-1475.

Loach, P. A., P. S. Parkesloach, C. M. Davis, and B. A. Heller. 1994. Probing Protein Structural Requirements for Formation of the Core Light-Harvesting Complex of Photosynthetic Bacteria Using Hybrid Reconstitution Methodology. *Photosynthesis Research* 40:231-245.

Magis, J. G., M.-J. den Hollander, W. G. Onderwaater, J. D. Olsen, C. N. Hunter, T. J. Aartsma, and R. N. Frese. 2010. Light harvesting, energy transfer and electron cycling of a native photosynthetic membrane adsorbed onto a gold surface. *Biochimica et Biophysica Acta* 1798:637-645.

McDermott, G., S. M. Prince, A. A. Freer, A. M. HawthornthwaiteLawless, M. Z. Papiz, R. J. Cogdell, and N. W. Isaacs. 1995. Crystal-Structure of An Integral Membrane Light-Harvesting Complex from Photosynthetic Bacteria. *Nature* 374:517-521.

Migneault, I., C. Dartiguenave, M. J. Bertrand, and K. C. Waldron. 2004. Glutaraldehyde:behaviour in aqueous solution, reaction with proteins, and application to enzyme crosslinking. *Biotechniques* 37:790-802.

Olsen, J. D. 1994. The role of highly conserved amino-acid residues in the light-harvesting 1 complex of *Rhodobacter sphaeroides*. *University of Sheffield. Thesis/Dissertation*.

Olsen, J. D., B. Robert, C. A. Siebert, P. A. Bullough, and C. N. Hunter. 2003. Role of the C-terminal extrinsic region of the α polypeptide of the light-harvesting 2 complex of *Rhodobacter sphaeroides*: A domain swap study. *Biochemistry* 42:15114-15123.

Olsen, J. D., G. D. Sockalingum, B. Robert, and C. N. Hunter. 1994. Modification of A Hydrogen-Bond to A Bacteriochlorophyll-A Molecule in the Light-Harvesting 1-Antenna of Rhodobacter-Sphaeroides. *Proceedings of the National Academy of Sciences of the United States of America* 91:7124-7128.

Reddy, N. R. S., H. M. Wu, R. Jankowiak, R. Picorel, R. J. Cogdell, and G. J. Small. 1996. High pressure studies of energy transfer and strongly coupled bacteriochlorophyll dimers in photosynthetic protein complexes. *Photosynthesis Research* 48:277-289.

Reynolds, N., S. Janusz, M. Escalante-Marun, J. Timney, R. E. Ducker, J. D. Olsen, C. Otto, V. Subramaniam, G. J. Legget, and C. N. Hunter. 2007. Directed Formation of Micro-and Nanoscale Patterns of Functional Light-Harvesting LH2 Complexes. *Journal of the American Chemical Society* 129:14625-14631.

Sturgis, J. N., J. D. Olsen, B. Robert, and C. N. Hunter. 1997. Functions of Conserved Tryptophan Residues of the Core Light-Harvesting Complex of *Rhodobacter sphaeroides*. *Biochemistry* 36:2772-2778.

Trammell, S. A., A. Spano, R. Price, and N. Lebedev. 2006. Effect of protein orientation on electron transfer between photosynthetic reaction centers and carbon electrodes. *Biosensors & Bioelectronics* 21:1023-1028.

Trammell, S. A., Y. Wang, J. M. Zullo, R. Shashidhar, and N. Lebedev. 2004. Orientated binding of photosynthetic reaction centers on gold using Ni-NTA self-assembled monolayers. *Biosensors & Bioelectronics* 19:1649-1655.

Wang, J. 2005. Carbon-nanotube based electrochemical biosensors: A review. *Electroanalysis* 17:7-14.

Wang, P.-F., M. J. McLeish, M. M. Kneen, G. Lee, and G. L. Kenyon. 2001. An unusually low pKa for Cys282 in the active site of human muscle creatine kinase. *Biochemistry* 40:11698-11705.

Wu, H. M., M. Ratsep, R. Jankowiak, R. J. Cogdell, and G. J. Small. 1998. Hole-burning and absorption studies of the LH1 antenna complex of purple bacteria: Effects of pressure and temperature. *Journal of Physical Chemistry B* 102:4023-4034.

Summary

The interfacing of biomolecules to nanostructures, electrode surfaces and/or optical components constitutes the new discipline of bioelectronics. It is based on electron transfer between a protein and an electrode, and can be monitored by amperometric techniques. The integration of biomolecules with electronics has strong potential for applications in a variety of functional devices, ranging from biosensors to solar cells.

Typically, a bio-electronic device consists of an assembly of redox-active proteins on a conducting electrode such that the electron transfer process can be transformed into a measurable output signal by electronic transduction. Direct coupling of the protein to an electrode by surface assembly offers important advantages from a technological point of view in terms of efficiency, reactivity, specificity, selectivity and sensitivity. Important factors to consider are: optimization of the electrical contact, biocompatibility of the interface, and control over alignment and orientation of the surface-assembled biomolecules. These issues can be addressed by the development and optimization of protocols for immobilization and mono-layer formation of biomolecules on electrode surfaces. Furthermore, it may be advantageous to engineer a linker or an electron-relay unit between the electrode and the biomolecules as a conduit for electrons in order to improve the electrical contact.

In this thesis we explore the possibilities of constructing a bio-electronic device for solar energy conversion by surface-assembly of photosynthetic pigment-protein complexes on a gold electrode. Optical excitation of the photosynthetic pigments gives rise to charge separation in the so-called reaction center complex. Energy conversion is completed by subsequent electron transfer to the electrode, generating a light-induced electric current.

Such a device allows us to address a number of questions that are directly related to bio-inspired solar energy conversion:

- How can biological systems be interfaced with electronic, mechanical and optical instruments?
- Specifically, what is the energy conversion efficiency of such an optimized device?
- Does the intrinsic photostability of photosynthetic systems lead to enhanced performance?
- Can general design criteria for bio-inspired energy conversion be derived or tested?

In Chapter 2 we report a functional characterization of native and untreated membrane fragments of *Rhodobacter sphaeroides* adsorbed onto a gold surface. Employing fluorescence confocal spectroscopy and light-induced amperometry we show that adsorbed membranes maintain their energy and electron transferring functionality. Gold-adsorbed membranes are shown to generate a high photocurrent density of 10 $\mu A\ cm^{-2}$ for several minutes, and to maintain activity for up to three days while continuously illuminated. The surface-adsorbed membranes exhibit a remarkable functional stability under aerobic conditions, even when exposed to light intensities well above that of direct solar irradiation. These findings present a major advancement, facilitating the characterization of supramolecular biological and artificial energy transducing mechanisms.

In Chapter 3 we describe our efforts to maximize photocurrent generation by bacterial photosynthetic reaction center pigment-protein complexes (RCs) interfaced with a metal electrode. By direct adsorption of RCs to a bare gold electrode we obtained substantial photocurrents despite the absence of coating layers on the electrode, or engineered linkers to achieve oriented deposition of RCs on the surface. A comparison with the effect of self-assembled monolayers on gold electrodes suggests that the high photocurrent densities on bare electrodes presumably are the consequence of the absence of an insulating layer between the photoactive pigments and the metal. Utilizing RCs surrounded by the Light-Harvesting 1 (LH1) complex resulted in even higher photocurrents, most probably due to the better surface coverage of uniformly oriented RC-LH1 complexes. Introduction of cytochrome-*c* (cyt-*c*) as a molecular relay resulted in a further increase of the photo-current, probably by intercalation of cyt-*c* between the adhered RCs or RC-LH1 complexes and the electrode, thus mediating electron transfer. The maximum current density achieved with RC-LH1 complexes was of the order of 25 $\mu A\ cm^{-2}$, a value which was limited by the available illumination intensity. High currents could be generated constinuously for several hours or days, under ambient conditions.

In Chapter 4 we demonstrate the covalent attachment to a gold surface of light-harvesting membrane proteins, from *Rhodobacter sphaeroides*, via cysteine residues engineered on either the cytoplasmic or periplasmic face. This simple directed attachment is superior in its ability to retain light-harvesting complex function, when compared to a similar attachment procedure utilizing a self-assembled monolayer on gold. Light-harvesting complex 1 has previously been observed to have superior photostability over light-harvesting complex 2 (see Chapter 2); this characteristic is retained with the introduction of cysteine residues.

The data shows that light-harvesting complexes can be immobilized directly on a gold surface and on various SAM surfaces whilst retaining their full optical functionality. All energy transferring reactions still take place and are similar to those observed for the detergent-solubilized proteins. Furthermore it is shown that LH1 complexes exhibit a remarkable photostability, even under ambient conditions. These findings demonstrate the possibility of interfacing a fully functional energy transferring protein complex to a conducting substrate in the presence of oxygen, with the capacity of converting light into electrical energy.

Samenvatting

Het koppelen van biomoleculen aan nanostructuren, elektrode oppervlakken en/of optische componenten vormt het nieuwe vakgebied van de bio-elektronica. Dit onderzoeksveld is gebaseerd op de elektronoverdracht tussen een eiwit en een elektrode, een proces dat kan worden gevolgd met behulp van amperometrische technieken. De integratie van biomoleculen met elektronica heeft potentie voor toepassingen in een verscheidenheid van functionele apparaten, variërend van biosensoren tot zonnecellen.

Gewoonlijk bestaat een bio-elektronisch instrument uit een verzameling redox-actieve eiwitten op een geleidende elektrode, zodanig dat het proces van elektronoverdracht door elektronische transductie omgezet kan worden in een meetbaar uitgangssignaal. De directe koppeling van het eiwit aan een elektrode door middel van oppervlakte assemblage biedt, vanuit technologisch oogpunt, belangrijke voordelen in termen van efficiëntie, reactiviteit, specificiteit, selectiviteit en gevoeligheid. Belangrijke overwegingen hierbij zijn: de optimalisatie van elektronisch contact, de biocompatibiliteit van het oppervlak, en controle over de ordening en oriëntatie van de aan het oppervlak bevestigde biomoleculen. Om in dit vakgebied succesvol te kunnen zijn is het noodzakelijk te werken met goede protocollen voor immobilisatie en vorming van monolagen van biomoleculen op elektrode-oppervlakken. Bovendien kan het voordelig zijn om het biomolecuul specifiek te verankeren op de elektrode, bijvoorbeeld via een geschikt molecuul dat een verbinding kan aangaan met zowel het biomolecuul als de elektrode. Zo'n moleculair anker kan tevens functioneren als een 'electron-relay' om het elektronisch contact te verbeteren.

In dit proefschrift onderzoeken we de mogelijkheden om bio-elektronische componenten te ontwikkelen voor de conversie van zonne-energie, die gebaseerd zijn op oppervlakte-assemblage van fotosynthetische pigment-eiwit complexen op een goud-elektrode. Optische excitatie van de pigmenten resulteert in een ladingsscheiding in het zogenaamde reactie centrum (RC) complex. Deze stap wordt gevolgd door elektronoverdracht naar de elektrode, waarbij een licht-geïnduceerde elektrische stroom wordt gegenereerd.

Op deze manier wordt een gefunctionaliseerde elektrode gemaakt die ons in staat stelt om een aantal fundamentele vragen aan de orde te stellen die direct verband houden met bio-geïnspireerde conversie van zonne-energie:

- Hoe kunnen biologische materialen worden gekoppeld met elektronische, mechanische en optische systemen?

- Wat is de efficiëntie van de energie-conversie van een dergelijk geoptimaliseerd apparaat?
- Leidt de intrinsieke fotostabiliteit van fotosynthetische systemen tot betere prestaties?
- Kunnen algemene ontwerp criteria voor bio-geïnspireerde energie-conversie worden afgeleid of getest?

In hoofdstuk 2 wordt een functionele karakterisering gepresenteerd van onbehandelde membraan fragmenten van *Rhodobacter Sphaeroides*, die geadsorbeerd zijn op een goud-substraat. Gebruik makend van confocale fluorescentie spectroscopie en licht-geïnduceerde amperometrie laten we zien dat de geadsorbeerde membranen hun functionaliteit wat betreft energie- en elektron-overdracht behouden. Deze goud-geadsorbeerde membranen genereren in eerste instantie een stabiele hoge fotostroom dichtheid van 10 $\mu A\ cm^{-2}$ die in de tijd geleidelijk afneemt. Ze behouden hun activiteit gedurende drie dagen onder continue belichting. De geadsorbeerde membranen vertonen een opmerkelijke functionele stabiliteit, zelfs onder aërobe omstandigheden en bij blootstelling aan licht-intensiteiten hoger dan die van directe zonnestraling. Deze bevindingen vormen een belangrijke stap voorwaarts in de karakterisering van mechanismen voor supramoleculaire biologische en kunstmatige energietransductie.

In hoofdstuk 3 worden methodes beschreven om de foto-geïnduceerde stroom te maximaliseren van bacteriële RCs die gekoppeld zijn aan een goud-elektrode. Door directe adsorptie van RCs aan een kale goud-elektrode worden fotostromen opgewekt die aanzienlijk groter zijn dan in het geval waar de elektrode bedekt is met een tussenlaag in de vorm van een zelf-assemblerende monolaag (SAM) van alkaanthiol-molekulen. Gebruik van RCs omringd door het LH1 complex (RC-LH1, waarbij LH staat voor het Engelse 'Light Harvesting') resulteert in nog hogere fotostromen, verrassend genoeg niet vanwege de verbeterde lichtabsorptie, maar waarschijnlijk door een betere oppervlaktedekking van gelijkmatig georiënteerde RC-LH1 complexen. Introductie van cytochroom-*c* (cyt-*c*) als een moleculair 'relay' resulteert in een verdere toename van de fotostroom, waarschijnlijk door intercalatie van cyt-*c* tussen de gebonden RCs of RC-LH1 complexen en de elektrode, resulterend in een nog efficiëntere elektronoverdracht. De maximale stroomdichtheid die werd bereikt met deze RC-LH1 complexen was in de orde van 25 $\mu A\ cm^{-2}$ en werd beperkt door de beschikbare lichtintensiteit. Dergelijk hoge stromen konden worden gegenereerd gedurende enkele uren of dagen, onder continue belichting bij kamertemperatuur en onder aërobe omstandigheden.

In hoofdstuk 4 wordt beschreven hoe de licht-oogstende membraan-eiwitten van *Rhodobacter sphaeroides* covalent kunnen worden gebonden aan een goud-substraat via cysteine residuen die in het eiwit zijn ingebouwd ofwel aan de cytoplasmatische ofwel aan de periplasmatische kant. In vergelijking met andere hechtingstechnieken die gebaseerd zijn op adsorptie is deze specifieke binding superieur als het er om gaat om de functie van het licht-absorberende complex te behouden. De complexen vormen zo een stabiele monolaag met een hoge oppervlaktedichtheid. We hebben eerder aangetoond dat het LH1-complex een veel grotere fotostabiliteit heeft dan het LH2-complex (zie hoofdstuk 2); deze eigenschap blijft gehandhaafd, zelfs bij introductie van cysteine-residuen.

De resultaten laten zien dat licht-oogstende, fotosynthetische eiwitcomplexen rechtstreeks geïmmobiliseerd kunnen worden op een goud-substraat en op verschillende SAM oppervlakken met behoud van hun volledige optische functionaliteit en reactiviteit. De energie- en elektron-overdragende reacties vinden nog steeds plaats in deze eiwitten en zijn vergelijkbaar met die welke optreden zowel in oplossing als onder natuurlijke omstandigheden. Een opvallend resultaat is de opmerkelijke fotostabiliteit van het LH1 complex. Dit onderzoek toont aan dat het mogelijk is om een fotosynthetisch pigment-eiwitcomplex aan een geleidend substraat te koppelen waardoor dit systeem in staat is om licht om te zetten in elektrische energie, zelfs in de aanwezigheid van zuurstof.

Curriculum Vitae

Gerhard Magis werd op 22 juni 1978 geboren in Winterswijk. In 1997 behaalde hij zijn VWO diploma aan het Christelijk College Schaersvoorde te Aalten, waarna hij natuurkunde ging studeren aan de Universiteit Leiden. Na het afleggen van het doctoraalexamen in 2003 begon hij aan zijn promotieonderzoek aan de Universiteit Leiden in de vakgroep biofysica. Het onderzoek richtte zich op het assembleren van photosynthetische eiwitten op geleidende oppervlakken en de effecten hiervan op de functionele rol van het eiwit. De resultaten van dit onderzoek werden gepresenteerd op verschillende nationale en internationale conferenties.

In november 2008 is hij gaan werken als junior trader / strategist bij IMC Financial Markets. Sinds 1 juli 2010 is hij werkzaam als business analist bij de divisie Zorg & Gezondheid van Achmea.

Nawoord

Veel mensen hebben, direct of indirect, bijgedragen aan de totstandkoming van dit proefschrift. Zonder de schijn te willen wekken van een volledig overzicht wil ik een aantal van hen in het bijzonder bedanken: Raoul Frese wiens inbreng essentieel was, Ward de Ruijter, John van Egmond, Willem Versluys, Dre de Wit, John Olsen, Nicholas Reynolds, Mike Jones, Neil Hunter, Razvan Stan, Harjo Lobeek, François Karstens, Eveline van Steenpaal, Jante Salverda en John van Noort.

Verder wil ik mijn familie (met name mijn ouders die mij altijd op alle vlakken gesteund hebben), vrienden en schoonfamilie bedanken voor al hun betrokkenheid en relativeringsvermogen. Met name in die periodes waarin het onderzoek iets minder voortvarend ging was het fijn om te merken hoe bijzonder sommige vriendschappen en relaties zijn.

Een promotieonderzoek is een aaneenschakeling van hoogtepunten en dieptepunten. In terugblik vallen die allemaal in het niet bij het mooiste dat mij in deze periode is overkomen. Lieve Karin, bedankt voor al jouw liefde, begrip en steun.

ISBN 978-90-8593-112-6
Casimir PhD series 2012-1